Hong Kong Journal of Radiology

Hong Kong Journal of Radiology

HKJR

香港放射科醫學雜誌

VOLUME 26 · NUMBER 4 · 2023

ISSN 2223-6619

Highlights of this issue:

- Effects of Different Liver Diseases on Metabolic Reference in ^{18}F-Fluorodeoxyglucose Positron Emission Tomography/Computed Tomography
- Treatment Outcomes and Toxicities of Stereotactic Body Radiotherapy for Oligoprogressive Metastatic Non–Small-Cell Lung Cancer
- Breast Ductography: A Hidden Diagnostic Gem for Patients with Abnormal Nipple Discharge

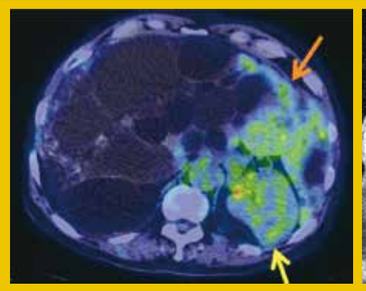

In the article “Effects of Different Liver Diseases on Metabolic Reference in ^{18}F-Fluorodeoxyglucose Positron Emission Tomography/Computed Tomography”. The ^{18}F-fluorodeoxyglucose positron emission tomography/computed tomography axial image shows a patient suffering from polycystic liver disease (arrows).

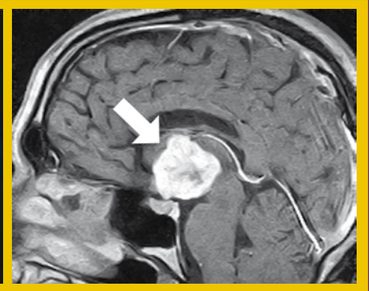

In the article “Mimics of Pituitary and Pineal Germ Cell Tumours on Imaging: A Pictorial Essay”. Contrast-enhanced T1-weighted sagittal image shows a glial cell tumour at the suprasellar retrochiasmatic region (arrow).

Vol. 26 No. 4, 2023 Pages 237-296

Official Publication of
Hong Kong College of Radiologists

HKAM PRESS

HKJR

COVER IMAGES

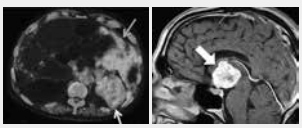

..... SEE PAGES 245 & 285

Hong Kong Journal of Radiology

Hong Kong Journal of Radiology is a continuation of the *Journal of the Hong Kong College of Radiologists*. This journal is dedicated to publish all aspects of clinical oncology, diagnostic radiology, and nuclear medicine.

VOLUME 26 • NUMBER 4 • DECEMBER 2023

Original Articles

Perspective

Case Report

Pictorial Essays

ePub-only Articles

The following ePub-only articles can be found on the HKJR website <http://www.hkjr.org>.

When citing this journal, abbreviate as ***Hong Kong J Radiol***.

INFORMATION FOR SUBSCRIBERS

Hong Kong Journal of Radiology (**香港放射科醫學雜誌**) is the official peer-reviewed publication of the Hong Kong College of Radiologists and is published by the Hong Kong Academy of Medicine Press.

Frequency
Quarterly, 1 volume a year.

Correspondence concerning subscriptions should be addressed to:

Executive Assistant
Hong Kong Journal of Radiology
Room 909, 9/F, Hong Kong Academy of Medicine Jockey Club Building
99 Wong Chuk Hang Road, Aberdeen, Hong Kong
Tel: (852) 2871 8788; Fax: (852) 2554 0739
Email: hkjr@hkcr.org

Annual subscription rate

Hong Kong delivery:	HK$400 per volume.
Overseas delivery (by airmail):	US$100* per volume.
	* Bank charges shall be borne by the subscriber.

- Rates are the same for individuals and institutions.
- Renewals should be promptly received to avoid a break in journal delivery. The Hong Kong College of Radiologists does not guarantee to supply back issues on late renewals.

Change of address
The College must be notified 60 days in advance. Journals undeliverable because of an incorrect address will be destroyed. Send address changes to:

Hong Kong Journal of Radiology
Room 909, 9/F, Hong Kong Academy of Medicine Jockey Club Building
99 Wong Chuk Hang Road, Aberdeen, Hong Kong

Please return your Subscription Order Form to:

Hong Kong Journal of Radiology
Room 909, 9/F, Hong Kong Academy of Medicine Jockey Club Building
99 Wong Chuk Hang Road, Aberdeen, Hong Kong

I enclose payment (US$/HK$) _____
Please make bank draft, cheque, or cashier's order payable to **"Hong Kong College of Radiologists"**

Name (in English): _____

Address: _____

_____

Tel: _____ Fax: _____ Email: _____

Please (✓) accordingly
I would like to subscribe to the *Hong Kong Journal of Radiology*

❒ Hong Kong delivery: HK$400/volume
❒ Overseas delivery: US$100/volume*
(Postage charge included)
*Bank charges shall be borne by the subscriber.

❒ 3 volumes ❒ 2 volumes ❒ 1 volume

Subscription period: From Volume _____ to Volume _____

Hong Kong Journal of Radiology

Aims and Editorial Policy

Hong Kong Journal of Radiology **香港放射科醫學雜誌** is the official peer-reviewed academic journal of Hong Kong College of Radiologists, a founder College of the Hong Kong Academy of Medicine. The Journal is published quarterly and is indexed in EMBASE/*Excerpta Medica*, SCOPUS, Emerging Sources Citation Index, and Index Copernicus. Papers are published on all aspects of diagnostic imaging, clinical oncology, and nuclear medicine, including original research, editorials, review articles, and case reports. Papers on radiological protection, quality assurance, audit in radiology, and matters related to radiological training or education are included.

All papers submitted are subject to peer review, and the Editorial Board reserves the right to edit papers in preparation for publication in the Journal. Authors are asked to refer to the *Information for Authors* published in each issue of the Journal, regarding the style and presentation of their articles. Failure to do so may result in rejection of their papers by the Editorial Board.

Manuscripts should be submitted online via the HKAMedTrack <www.hkamedtrack.org/hkjr>. Correspondence should be sent to:

Managing Editor, HKJR Editorial Office
c/o Hong Kong Academy of Medicine Press
10/F, Hong Kong Academy of Medicine Jockey Club Building
99 Wong Chuk Hang Road, Aberdeen, Hong Kong
Tel: (852) 2871 8809; Fax: (852) 2515 9061
Email: hkjr@hkam.org.hk

Advertisements

Correspondence concerning advertisements should be addressed to:

Executive Assistant
Hong Kong College of Radiologists
Room 909, 9/F Hong Kong Academy of Medicine Jockey Club Building
99 Wong Chuk Hang Road, Aberdeen, Hong Kong.
Tel: (852) 2871 8788; Fax: (852) 2554 0739
Email: hkjr@hkcr.org

Reprints

Reprints of individual articles are available to authors only. Reprints in large quantities (non-authors), for commercial or academic use, may be purchased from the publisher. For information and prices, please send an email to: hkjr@hkam.org.hk.

Copyright

On acceptance of an article by the Journal, the corresponding author will be asked to transfer copyright of the article to the College. The Copyright Transfer Assignment Form will be sent to the author at the time of acceptance.

Disclaimer

Hong Kong Journal of Radiology and the publisher do not guarantee, directly or indirectly, the quality or efficacy of any product or service described in the advertisements or other material which is commercial in nature in this issue. All articles published, including editorials and letters, represent the opinions of the authors and do not reflect the official policy of the Journal, Hong Kong College of Radiologists, the publisher, or the institution with which the author is affiliated, unless this is clearly specified.

Hong Kong Journal of Radiology
ISSN 2223-6619 (Print)
ISSN 2307-4620 (Online)

Hong Kong J Radiol. 2023;26:240-7. Epub 11 Dec 2023 | https://doi.org/10.12809/hkjr2217526

ORIGINAL ARTICLE **CME**

Effects of Different Liver Diseases on Metabolic Reference in ^{18}F-Fluorodeoxyglucose Positron Emission Tomography/Computed Tomography

KS Ng, KK Ng, KS Chu, BT Kung, TK Au Yong

Nuclear Medicine Unit, Queen Elizabeth Hospital, Hong Kong SAR, China

ABSTRACT

Introduction: *In addition to visual assessment, measuring standardised uptake values (SUVs) in ^{18}F-fluorodeoxyglucose positron emission tomography/computed tomography (^{18}F-FDG PET/CT) for extrahepatic lesion characterisation often uses comparisons with normal liver and blood pool uptake as metabolic references. However, the effects of liver diseases on these metabolic references are not well understood. This study therefore aimed to investigate how different liver diseases affect ^{18}F-FDG uptake in the liver and the blood pool.*

Methods: *A total of 168 patients who underwent ^{18}F-FDG PET/CT in our institution were retrospectively evaluated. The mean SUVs in the liver and blood pool were measured. Based on their clinical history and investigation results, patients were categorised into the following five groups: normal liver, hyperbilirubinaemia, cirrhosis, steatosis, and polycystic liver disease. The mean liver-to–blood pool SUV ratios of the different groups were statistically analysed using t tests and linear regression.*

Results: *Compared with the control group, patients with hyperbilirubinaemia were associated with a higher mean lesion SUV, while those with cirrhosis, steatosis, and polycystic liver disease had lower ratios. Increasing severity of steatosis correlated with decreasing SUV. All results were statistically significant.*

Conclusion: *This study demonstrates that liver diseases can affect lesion SUV in proportion to their severity. Radiologists should review the underlying hepatic conditions of patients before using liver and blood pool as references for ^{18}F-FDG measurements.*

Key Words: *Fluorodeoxyglucose F18; Liver; Positron-emission tomography*

Correspondence: *Dr KS Ng, Nuclear Medicine Unit, Queen Elizabeth Hospital, Hong Kong SAR, China*
Email: nks176@ha.org.hk

Submitted: 13 Jan 2022; Accepted: 10 May 2022.

Contributors: KSN designed the study, acquired the data, analysed the data and drafted the manuscript. KKN, KSC, BTK and TKAY critically revised the manuscript for important intellectual content. All authors had full access to the data, contributed to the study, approved the final version for publication, and take responsibility for its accuracy and integrity.

Conflicts of Interest: As editors of the journal, KSN and TKAY were not involved in the peer review process. Other authors have disclosed no conflicts of interest.

Funding/Support: This research received no specific grant from any funding agency in the public, commercial, or not-for-profit sectors.

Data Availability: All data generated or analysed during the present study are available from the corresponding author on reasonable request.

Ethics Approval: The study was approved by the Queen Elizabeth Hospital Research Ethics Committee of Hospital Authority, Hong Kong (Ref No.: KC/KE-19-0048-ER-4). Informed patient consent was waived by the Committee due to the retrospective nature of the study.

中文摘要

不同肝臟疾病對^{18}F-氟脫氧葡萄糖正子斷層掃描／電腦斷層掃描代謝參考的影響

吳國勝、吳官橋、朱競新、龔本霆、歐陽定勤

簡介：除了視覺評估之外，測量^{18}F-氟脫氧葡萄糖正子斷層掃描／電腦斷層掃描（^{18}F-FDG PET/CT）中的標準化攝取值（SUV）來表徵肝外病變特徵通常使用與正常肝臟和血池攝取的比較作為代謝參考。然而，肝臟疾病對這些代謝參考的影響尚不清楚。因此，本研究旨在調查不同的肝臟疾病如何影響肝臟和血池中^{18}F-FDG的攝取。

方法：本研究對在本院接受^{18}F-FDG PET/CT檢查的168位患者進行回顧性分析，並測量其肝臟和血池中的平均SUV。根據患者的臨床病史和檢查結果，我們將患者分為以下五組：正常肝臟、高膽紅素血症、肝硬化、脂肪變性和多囊性肝病。我們使用t檢定和線性迴歸對不同組別的平均肝臟與血池SUV比率進行統計分析。

結果：與對照組相比，高膽紅素血症患者的平均病變SUV值較高，而肝硬化、脂肪變性和多囊性肝患者的平均病變SUV值較低。脂肪變性嚴重程度的增加與 SUV的減少有關。所有結果均具有統計意義。

結論：本研究表明，肝臟疾病對病變SUV的影響與其嚴重程度成正比。在使用肝臟和血池作為^{18}F-FDG測量的參考之前，放射科醫生應檢查患者的潛在肝臟狀況。

INTRODUCTION

Both semiquantitative assessment and qualitative visual interpretation are applied in ^{18}F-fluorodeoxyglucose positron emission tomography/computed tomography (^{18}F-FDG PET/CT) for lesion characterisation.[1] In the semiquantitative approach, the maximum standardised uptake value (SUV_{max}) is calculated, but this depends on multiple factors, including injection time, uptake period, and blood glucose level.[2] Thus, it is difficult to compare the absolute SUV_{max} between different PET/CT systems.[2] For qualitative visual interpretation, the ^{18}F-FDG uptake of a lesion is typically graded with respect to mean blood pool and liver uptake of a patient (e.g., score 1: no uptake; 2: less than or equal to blood pool; 3: between blood pool and liver; 4: moderately more than liver; and 5: markedly more than liver[3]). This approach is useful in lesion delineation: a lesion is generally regarded as genuine (i.e., the lesion is true instead of false positive) if its uptake is higher than that of liver and not genuine if its uptake is less than or equal to that of blood pool. This is also useful in treatment response assessment (e.g., a disease is likely deteriorating if the score increases in interval scan). Visual interpretation is the recommended method in different guidelines, including the Deauville criteria for high-grade lymphoma,[3] PERCIST (Positron Emission Tomography Response Criteria in Solid Tumors) 1.0 for solid tumours proposed by the Society of Nuclear Medicine and Molecular Imaging,[4,5] as well as for vasculitis assessment developed by the European Association of Nuclear Medicine and the Society of Nuclear Medicine and Molecular Imaging.[6] Ideally, blood pool and liver uptake should have minimal variability such that they can be utilised as reliable metabolic references. There are existing procedural protocols standardising patient preparation and acquisition techniques.[7] The aim of this study was to evaluate the liver and blood pool uptake in different liver diseases (hyperbilirubinaemia, cirrhosis, steatosis, and polycystic liver disease) and their potential effect on lesion assessment. Focal liver diseases (e.g., hepatocellular carcinoma and liver metastasis) were not included here as their effects have already been covered in the literature,[8] and we believe that general hepatic metabolism is likely more dependent on systemic liver diseases than focal liver pathologies. Throughout this research, the ratio between the mean SUV of the liver and that of the blood pool (SUV_{liver}/$SUV_{blood\ pool}$ ratio) instead of absolute SUV was evaluated because the ratio was more relevant to the grading. Mean SUV (SUV_{mean}), instead of SUV_{max}, of liver and blood pool was investigated as an analogue of visual interpretation.

METHODS

Patient Recruitment

Cases of patients who underwent whole-body ^{18}F-FDG PET/CT in our centre from 1 January 2011 to 31 December 2015 were retrospectively reviewed. The clinical background and investigation results were reviewed, including drinking history, blood test results, radiological images, and endoscopic findings. Continuous data were reported as mean ± standard deviation. Subjects were excluded if: (1) liver malignancy had been diagnosed histologically; or (2) liver malignancy was suspected radiologically (e.g., by ^{18}F-FDG PET/CT, ultrasound, CT or magnetic resonance imaging) within 12 weeks of ^{18}F-FDG PET/CT imaging; or (3) no liver function tests were available within 2 weeks of ^{18}F-FDG PET/CT imaging; or (4) blood glucose level was > 11 mmol/L before ^{18}F-FDG PET/CT acquisition.

A total of 168 adult patients (56.5% male, 43.5% female) with a mean age of 62.3 ± 13.4 years were included. The majority had undergone ^{18}F-FDG PET/CT for oncological indications: lung (23.2%), lymphoma (14.8%), breast (12.5%), biliary (9.5%), colon (8.3%), renal (6.0%), and other (12.6%) cancers. Some of the subjects (13.1%) showed no evidence of malignancy after thorough workup. Each case was then assigned to one of the following five groups (Table 1):

(1) The control group (n = 50): liver function (i.e., serum bilirubin, alanine aminotransferase, aspartate aminotransferase and alkaline phosphatase levels) was normal, and there was no evidence of cirrhosis, steatosis or polycystic liver disease;
(2) the hyperbilirubinaemia group (n = 29): the serum bilirubin level was greater than or equal to the upper limit of the normal level (21 μmol/L) within 2 weeks of ^{18}F-FDG PET/CT acquisition, and there was no evidence of cirrhosis, steatosis or polycystic liver disease;
(3) the cirrhosis group (n = 27): features of cirrhosis had been documented by means of imaging (e.g., ultrasound, CT or magnetic resonance imaging) or oesophagogastroduodenoscopy. Liver function was normal, and there was no evidence of steatosis or polycystic liver disease;
(4) the steatosis group (n = 52): the mean liver density in Hounsfield units (HU_{liver}) on CT was lower than that of the spleen (HU_{spleen}). As SUV measurement is potentially dependent on the distribution of steatosis (e.g., diffuse, focal, multinodular, etc.), this study focused on the patients with diffuse steatosis. Liver function was normal, and there was no evidence of cirrhosis or polycystic liver disease; and
(5) the polycystic liver disease group (n = 10): the liver contained > 20 cysts as defined in the literature.[9] Liver function was normal, and there was no evidence of cirrhosis or steatosis.

Technical Aspects

All ^{18}F-FDG FDG PET-CT examinations were performed with the same PET/CT scanner (Discovery 710; General Electric, Milwaukee [WI], United States). The mean ^{18}F-FDG activity administered was 407.0 ± 45.5 MBq. After a mean uptake time of 59.8 ± 6.21 minutes, PET data were acquired from skull vertex to mid thighs in seven to eight bed positions (3 minutes per bed position) with mean axial bed coverage of 15.2 cm per bed and 9-slice bed overlap in two-dimensional acquisition mode. Reconstruction using Optimization of Ordered Subset Expectation Maximization was performed with 4.2-mm section thickness in a 128 × 128 matrix and processed through a standard filter. Non-contrast CT data were acquired for anatomical correlation and attenuation correction.

Measurements and Statistical Analyses

The SUV is defined as the activity measured in a volume of interest (VOI) divided by the injected ^{18}F-FDG dose, based on body weight[10]:

$$SUV = \frac{Activity_{VOI}\ (MBq/mL)}{Dose_{injection}\ (MBq/kg)}$$

SUV_{liver} was measured in a 3-cm–diameter spherical VOI over the right lobe of the liver as recommended in the PERCIST 1.0 criteria.[4,5] No observable lesion was included in the liver VOI, except for the unavoidable multiple cysts in polycystic liver disease. $SUV_{blood\ pool}$ was measured in another spherical VOI with diameter > 2 cm in the descending thoracic aorta. Atherosclerotic plaque was avoided in the blood pool VOI as the diseased vessel wall was often ^{18}F-FDG–avid.[4,5] The mean HU of the liver and the spleen were recorded in two-dimensional circular regions of interest with diameters > 3 cm. The body weight was routinely recorded on the same day of the ^{18}F-FDG PET/CT acquisition, with mean weight of 63.4 ± 11.7 kg. Statistical analyses, including two-sided *t* tests and linear regression, were performed with SPSS (Windows version 20.0; IBM Corp, Armonk [NY], United States). The results were regarded as statistically significant if the corresponding p values were < 0.05.

RESULTS

Figure 1a shows a representative maximum intensity projection (MIP) of a control case. The ^{18}F-FDG uptake in the liver (orange arrow) was homogeneous without discernible hypermetabolic lesions. The degree of uptake was normal and greater than that in the mediastinal blood pool (purple arrow), i.e., $SUV_{liver}/SUV_{blood\ pool}$ ratio > 1, and in the spleen. All of the 50 control cases had $SUV_{liver}/SUV_{blood\ pool}$ ratios > 1, with a mean SUV ratio of 1.39 (Table 1).

In the hyperbilirubinaemia group, the serum bilirubin level ranged from 23 to 667 μmol/L (mean = 107). Four cases had elevated aspartate aminotransferase level (> 47 IU/L), four had elevated alkaline phosphatase level (> 140 IU/L), and 18 had both enzymes elevated. Thus, 26 subjects (89.7%) had elevated liver enzyme(s) in addition to the increased serum bilirubin level. The hyperbilirubinaemia cases had a mean SUV ratio of 1.49, which was greater than that of the controls. A two-sided *t* test showed that the difference in mean SUV ratios achieved statistical significance (p = 0.0053; Table 1). A representative MIP of the hyperbilirubinaemia cases demonstrates the higher degree of contrast between

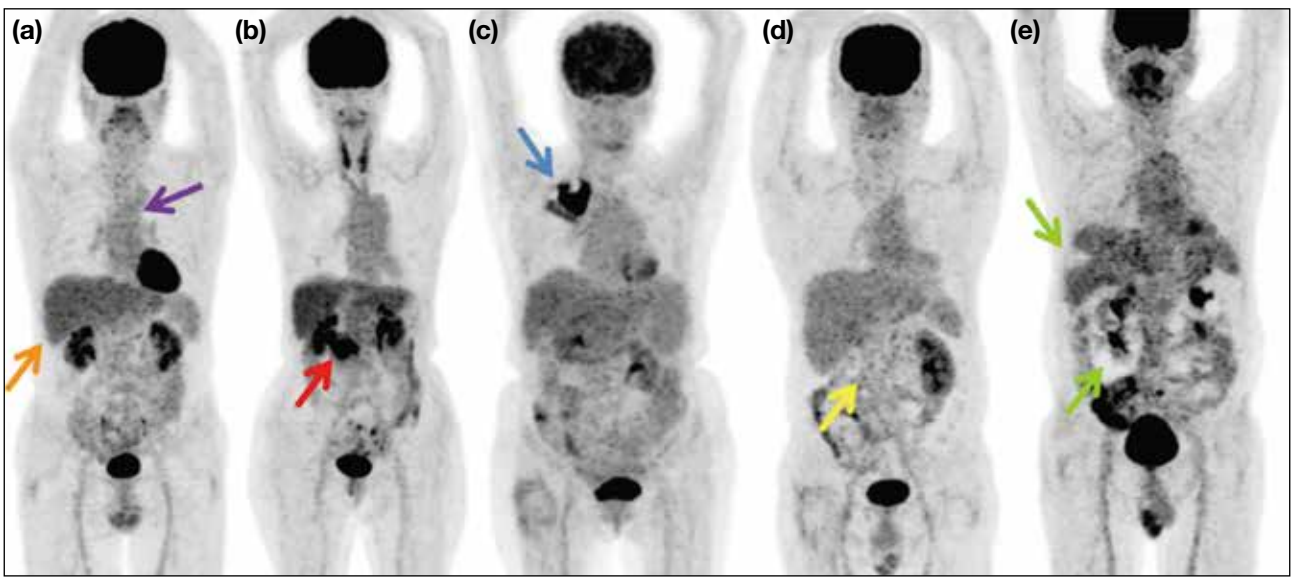

Figure 1. Maximum intensity projections of representative subjects of the five groups. (a) A control case showing liver uptake (orange arrow) is normally greater than that in the mediastinal blood pool (purple arrow) [standardised uptake value (SUV) ratio = 1.41]; (b) a hyperbilirubinaemia case with gallbladder tumour causing biliary obstruction (red arrow) [SUV ratio = 1.86]; (c) a cirrhosis case with right lung tumour (blue arrow) [SUV ratio = 1.24]; (d) a steatosis case with prior right nephrectomy for renal cell carcinoma (yellow arrow) [SUV ratio = 1.02]; and (e) a polycystic liver disease case with cold defects in liver and kidneys (green arrows) corresponding to cysts [SUV ratio = 0.79].

Table 1. Characteristics of the five groups (n = 168).

	Controls (n = 50)	Hyperbilirubinaemia (n = 29)	Cirrhosis (n = 27)	Steatosis (n = 52)	Polycystic liver disease (n = 10)
Definition	Normal liver	Bilirubin level ≥21 μmol/L	Cirrhotic features in US/CT/MRI/OGD	$HU_{liver} < HU_{spleen}$	No. of cysts > 20
Serum bilirubin, μmol/L	< 21	≥ 21	< 21	< 21	< 21
Steatosis	No	No	No	Yes	No
Cirrhosis	No	No	Yes	No	No
No. of cysts	≤ 20	≤ 20	≤ 20	≤ 20	> 20
SUV ratio (mean ± standard deviation)	1.39 ± 0.12	1.49 ± 0.19	1.29 ± 0.10	1.28 ± 0.15	0.75 ± 0.44
p Value*	N/A	0.0053	0.0003	0.0002	< 0.0001

Abbreviations: CT = computed tomography; HU_{liver} = density of the liver in Hounsfield units; HU_{spleen} = density of the spleen in Hounsfield units; MRI = magnetic resonance imaging; N/A = not applicable; OGD = oesophagogastroduodenoscopy; SUV = standardised uptake value; US = ultrasound.

* Two-sided *t* test.

hepatic and blood pool uptake compared with that of the controls (Figure 1b). The cause of hyperbilirubinaemia in Figure 1b was biliary obstruction secondary to a gallbladder tumour (red arrow). To investigate the correlation between bilirubin level and the SUV ratio, linear regression analysis was performed. Figure 2 shows that the SUV ratio was higher with increasing serum bilirubin level (black circles, bottom x-axis), with a corresponding slope of 0.0008 L/μmol and a correlation coefficient of 0.438. The relationship between serum bilirubin level and the SUV ratio was further examined by subdividing the hyperbilirubinaemia cases into two groups: mild (serum bilirubin level: 21-63 μmol/L, i.e., grade 1 to 2 hyperbilirubinaemia as defined by the Common Terminology Criteria for Adverse Events version 5.0[11]) and severe (serum bilirubin level > 63 μmol/L, i.e., grade 3 to 4 hyperbilirubinaemia). Table 2 shows that the mild hyperbilirubinaemia cases had a mean SUV ratio of 1.44, while the severe hyperbilirubinaemia cases had a mean SUV ratio of 1.59 (p = 0.0359).

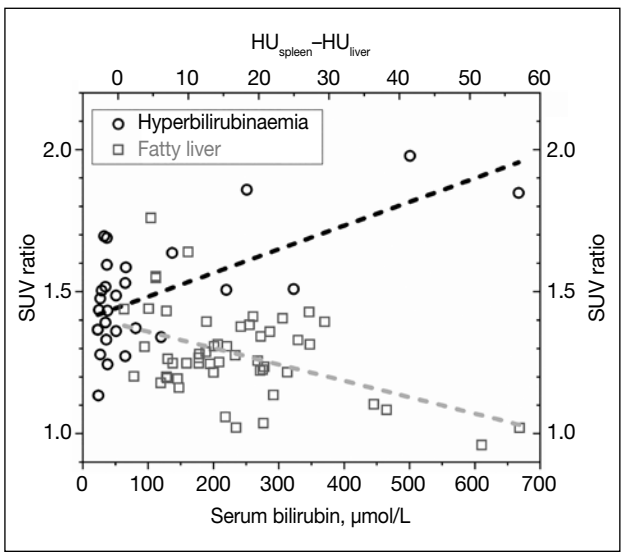

Figure 2. Linear regression plots of liver-to–blood pool standardised uptake value (SUV) ratio against the serum bilirubin level for the hyperbilirubinaemia cases (black circles, bottom x-axis) and the difference between the density of the spleen and the liver in Hounsfield units (HU_{spleen}–HU_{liver}) for the steatosis cases (grey squares, top x-axis). The hyperbilirubinaemia cases had a corresponding slope of 0.0008 L/μmoL and a correlation coefficient of 0.438. The steatosis cases had a corresponding slope of -0.0062 and a correlation coefficient of 0.209.

In the cirrhosis cases, 16 out of the 27 (59.3%) subjects had cirrhotic features documented by more than one modality (e.g., ultrasound, CT and oesophagogastroduodenoscopy). Twenty-three (85.2%) subjects had identifiable causes of cirrhosis (chronic hepatitis B: 51.9%, hepatitis C: 14.8%, chronic alcoholism: 18.5%). The cirrhosis cases had a mean SUV ratio of 1.29, which was less than that of the controls (p = 0.0003; Table 1). A representative MIP of a cirrhosis subject in Figure 1c shows that the visual contrast between liver and blood pool uptake was less than that of the control cases.

In the steatosis group, the HU_{liver} ranged from 5.5 to 55.2 (mean = 37.2) and the difference between HU_{spleen} and HU_{liver} (HU_{spleen}–HU_{liver}) ranged from 1 to 57 (mean = 16.6). The steatosis cases had a mean SUV ratio of 1.28, which was less than that of the controls (p = 0.0002; Table 1). The mean SUV ratio was still > 1, implying that liver had greater uptake than the blood pool. However, individuals with severe steatosis could have liver uptake as low as that of the blood pool, as illustrated in Figure 1d. To study if the SUV ratio depended on the severity of the steatosis, linear regression analysis was performed. The SUV ratios of the subjects with steatosis are plotted against the HU_{spleen}–HU_{liver} in Figure 2. It was observed that the SUV ratios decreased with increasing HU_{spleen}–HU_{liver} (grey squares, top x-axis). The corresponding slope in linear regression analysis was -0.0062 and the correlation coefficient was 0.209. The relationship between the steatosis severity and the SUV

Table 2. Subgroup analyses of hyperbilirubinaemia and steatosis groups.

	Hyperbilirubinaemia (n = 29)		Steatosis (n = 52)	
Subgroup	Mild (n = 19)	Severe (n = 10)	Mild (n = 17)	Moderate-to-severe (n = 35)
Criterion	Bilirubin level: 21-63 μmol/L	Bilirubin level > 63 μmol/L	HU_{spleen}–HU_{liver} ≤ 10	HU_{spleen}–HU_{liver} > 10
SUV ratio (mean ± standard deviation)	1.44 ± 0.14	1.59 ± 0.24	1.35 ± 0.18	1.25 ± 0.13
p Value*	0.0359		0.0201	

Abbreviations: HU_{liver} = density of the liver in Hounsfield units; HU_{spleen} = density of the spleen in Hounsfield units; SUV = standardised uptake value.
* Two-sided *t* test.

ratio was further evaluated by subdividing the subjects into mild (HU_{spleen}–$HU_{liver} \leq 10$) and moderate-to-severe (HU_{spleen}–$HU_{liver} > 10$) steatosis cases in accordance with Jacobs et al's study.[12] The mild steatosis cases had a higher mean SUV ratio of 1.35, while the moderate-to-severe steatosis cases had a lower mean SUV ratio of 1.25 ($p = 0.0201$; Table 2).

In the polycystic liver disease group, the mean SUV ratio was 0.75. This implies that unlike all the other cases which had mean ratios ≥ 1, the uptake in polycystic liver was generally less than that in the blood pool (Table 1). Figure 1e shows the MIP of a case of polycystic liver disease. The liver uptake was heterogeneous with a cold spot corresponding to a large hepatic cyst (upper green arrow). Table 1 shows that the SUV ratio of the polycystic liver disease cases had the greatest standard deviation (0.44) among all the cases (control group: 0.12, hyperbilirubinaemia group: 0.19, cirrhosis group: 0.10, steatosis group: 0.15) due to the variabilities in size, number and distribution of hepatic cysts with no uptake. Figure 3 shows another subject who had larger and more cysts compared with Figure 1e. The MIP and hybrid images in Figure 3 demonstrate almost no uptake in the right lobe of the liver and the corresponding SUV ratio was 0.12, while the left lobe of the liver (orange arrow in Figure 3b), with fewer and smaller cysts, demonstrated uptake similar to that of the blood pool and the spleen (yellow arrow in Figure 3b). Although the right hepatic lobe is commonly recommended as the standard metabolic reference in many international guidelines,[3-6] Figure 3 clearly illustrates that the right lobe is less appropriate for reference compared with the left lobe when the right lobe is more diseased.

DISCUSSION

^{18}F-FDG visual interpretation is advocated for oncological[3-5,13-15] and inflammatory[6,14] conditions, using liver and blood pool as metabolic references. While the PERCIST 1.0 criteria recommend that diseased liver is generally unsuitable for visual reference, the precise effects of different hepatic diseases on ^{18}F-FDG uptake have not been entirely elucidated.[4] The current study included a spectrum of liver diseases ranging from biochemical abnormality (hyperbilirubinaemia) to various structural changes (cirrhosis, steatosis, and polycystic liver disease) that can either increase or decrease the SUV ratio. They can be ranked in terms of their mean SUV ratios in descending order of hyperbilirubinaemia, control, cirrhosis and steatosis, and

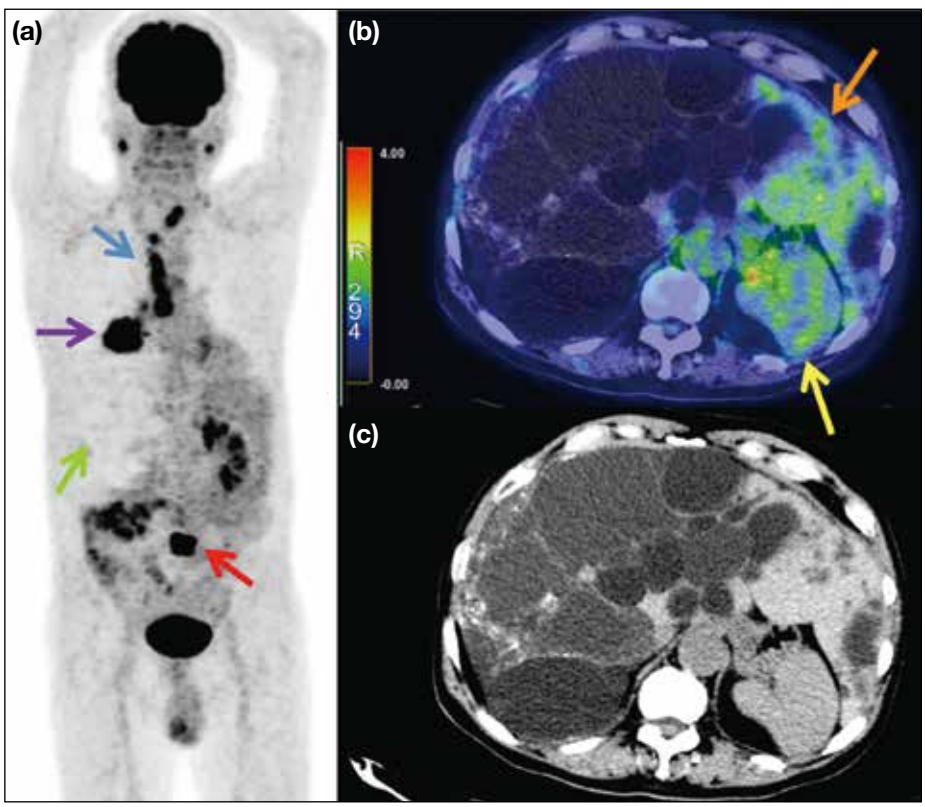

Figure 3. (a) Maximum intensity projection (MIP), (b) ^{18}F-fluorodeoxyglucose positron emission tomography/computed tomography, and (c) computed tomography images of a patient suffering from polycystic liver disease. The right hepatic region in MIP has no uptake (green arrow in [a]) because of numerous large liver cysts, with a corresponding standardised uptake value ratio of 0.12. The left hepatic lobe (orange arrow in [b]) has uptake similar to that of the spleen (yellow arrow in [b]) because of smaller and fewer cysts compared to the right lobe. A hypermetabolic right lung tumour (purple arrow in [a]) with metastases to lymph nodes (blue arrow in [a]) and the L5 level (red arrow in [a]) are seen.

polycystic liver disease.

The hyperbilirubinaemia cases showed higher SUV ratios than the controls. This is likely because jaundice implies hepatitis, and inflammation generally leads to increased ^{18}F-FDG uptake.[15] This hypothesis is supported by our findings that higher serum bilirubin levels were associated with higher SUV ratios (Figure 2). High SUV ratio raises the concern for increasing false negative rate in lesion delineation, particularly if the lesion is only mildly ^{18}F-FDG–avid. Clinical scenarios of hyperbilirubinaemia, due to biliary obstruction or acute hepatitis, are commonly encountered in oncology practice. In this study, hyperbilirubinaemia was used as an indicator of abnormal liver function and hepatitis. While serum bilirubin can be hepatic or haemolytic in origin, 89.7% of the hyperbilirubinaemia cases in this study exhibited elevated levels of other liver enzyme(s). This finding supports the hypothesis that the observed hyperbilirubinaemia was primarily hepatic in nature.

The cirrhosis cases had lower mean SUV ratios compared with the controls, probably as a result of the impaired glucose metabolism in liver fibrosis. Although liver biopsy is the gold standard for the diagnosis of cirrhosis, the procedure is invasive and not commonly employed. The cirrhosis subjects in this study were therefore selected based on radiological and endoscopic findings. For radiological findings, the sensitivity varies from 77% to 82% and the specificity ranges from 68% to 80%.[16] In this study, most cirrhotic cases (85.2%) had identifiable aetiologies of the cirrhosis. The majority (59.3%) also had cirrhotic features documented in more than one investigation.

The steatosis cases had lower SUV ratios than the control cases, consistent with previous observations.[17] We demonstrated that a more significant reduction in the SUV ratio can be expected in livers with higher degrees of steatosis. These results can be explained by the lower ^{18}F-FDG uptake in fat content compared with normal liver parenchyma and the impaired glucose metabolism in steatosis. Abele and Fung's study[18] showed that the SUV_{mean} in steatotic patients was lower than that of the controls (2.18 vs. 2.03). While this difference did not achieve statistical significance, the authors suggested that the limited power of their study might not have been sufficient to detect a true difference between the cases (i.e., type II error). The different sample sizes between Abele and Fung's study (n = 23)[18] and the current report (n = 52) may offer an explanation of this discrepancy. On the other hand, Keramida et al[19] demonstrated no difference in SUV_{mean} between steatosis cases and the controls; however, their SUV_{mean} had a complicated adjustment for hepatic fat content and the potential effect of such adjustment on the original SUV magnitude is still unclear. Most clinical scenarios and research studies, including our investigation, had no adjustment. The current study excluded any subject with biochemical or structural abnormality of steatotic livers, while previous studies did not specifically elaborate the biochemical or structural properties.[17-19] Most importantly, the current study emphasises the $SUV_{liver}/SUV_{blood\ pool}$ ratio instead of absolute SUV, because the ratio is more relevant to visual interpretation.

A simple cyst is defined as a thin-walled sac containing serous fluid.[20] Therefore, it has lower ^{18}F-FDG uptake compared with normal hepatic parenchyma. This explains why the mean SUV ratio observed in polycystic liver cases was the lowest among all the cases. While polycystic liver is not considered a reliable metabolic reference, its SUV was still evaluated in a 3-cm–diameter fixed-sized spherical VOI in accordance with the PERCIST 1.0 criteria for equivalent comparison with other cases.[4,5] The minimum SUV ratio among the polycystic liver cases was 0.12, which is clearly unsuitable as metabolic reference (Figure 3). This report further demonstrates that the hepatic uptake in polycystic liver disease depends on the size, number, and distribution of the cysts. The heterogeneous and variable uptake in the polycystic liver prohibits its application as a reliable metabolic reference.

Steatosis, cirrhosis and polycystic liver disease cases showed lower SUV ratios than those in the control cases. Their hepatic uptake could be similar to or even lower than blood pool or splenic uptake. This observation was distinct from the observation in the controls, in which normal liver uptake was always greater than blood pool and splenic uptake. A previous study of high-grade lymphoma indeed has suggested that lymphomatous involvement in spleen should be suspected if the spleen has greater uptake than the liver.[21] Therefore, the deceptively low liver-to–blood pool SUV ratio observed in steatosis, cirrhosis, and polycystic liver disease can potentially lead to higher false positive rates in lesion detection.

All disease cases had mean SUV ratios different from the controls and the differences were statistically significant in two-sided *t* tests. However, such quantitative

differences may not always appear conspicuous in the qualitative visual interpretation. For example, the visual contrast between liver/blood pool uptake in the cirrhosis cases was slightly less than that in the control cases. The visual differences between the mild hyperbilirubinaemia/steatosis cases and the controls were also subtle. On the other hand, in severe hyperbilirubinaemia, severe steatosis and polycystic liver disease cases, their visual contrast between liver/blood pool uptake was obviously different from that in the controls. Thus, severe liver diseases can have significant quantitative and qualitative effects on the liver/blood pool references. This can eventually affect the diagnostic accuracy of visual interpretation.

Limitations

The current study had some limitations. First, subtle hepatic tumour or metastasis may be present. To minimise this pitfall, subjects with a histological diagnosis or radiological suspicion of liver malignancy were excluded from this study. Second, the number of cases of polycystic liver disease (10 patients) was lower compared to other groups because of its inherently low prevalence. Third, the liver function tests were obtained within 2 weeks, rather than on the same day, of ^{18}F-FDG PET/CT acquisition. Fourth, this study demonstrated that all disease cases had SUV ratios different from that of the controls in quantitative aspect. Future study is required to determine if this quantitative difference can be translated to significant changes in qualitative visual interpretation.

CONCLUSION

Liver/blood pool uptake in ^{18}F-FDG PET/CT can be influenced by various liver conditions, including hyperbilirubinaemia, cirrhosis, steatosis, and polycystic liver disease. As liver diseases progress in severity, their impact on liver/blood pool uptake becomes more prominent. Therefore, radiologists should exercise great caution in the utilisation of liver/blood pool uptake as metabolic references in cases of significant hepatic disease. Clinical history, biochemical function and imaging findings should be thoroughly reviewed before visual interpretation.

REFERENCES

1. Ziai P, Hayeri MR, Salei A, Salavati A, Houshmand S, Alavi A, et al. Role of optimal quantification of FDG PET imaging in the clinical practice of radiology. Radiographics. 2016;36:481-96.
2. Boellaard R. Standards for PET image acquisition and quantitative data analysis. J Nucl Med. 2009;50 Suppl 1:11S-20S.
3. Barrington SF, Mikhaeel NG, Kostakoglu L, Meignan M, Hutchings M, Müeller SP, et al. Role of imaging in the staging and response assessment of lymphoma: consensus of the International Conference on Malignant Lymphomas Imaging Working Group. J Clin Oncol. 2014;32:3048-58.
4. Wahl RL, Jacene H, Kasamon Y, Lodge MA. From RECIST to PERCIST: evolving considerations for PET response criteria in solid tumors. J Nucl Med. 2009;50 Suppl 1:122S-50S.
5. O JH, Lodge MA, Wahl RL. Practical PERCIST: a simplified guide to PET Response Criteria in Solid Tumors 1.0. Radiology. 2016;280:576-84.
6. Jamar F, Buscombe J, Chiti A, Christian PE, Delbeke D, Donohoe KJ, et al. EANM/SNMMI guideline for ^{18}F-FDG use in inflammation and infection. J Nucl Med. 2013;54:647-58.
7. Boellaard R, O'Doherty MJ, Weber WA, Mottaghy FM, Lonsdale MN, Stroobants SG, et al. FDG PET and PET/CT: EANM procedure guidelines for tumour PET imaging: version 1.0. Eur J Nucl Med Mol Imaging. 2010;37:181-200.
8. Park JW, Kim JH, Kim SK, Kang KW, Park KW, Choi JI, et al. A prospective evaluation of ^{18}F-FDG and ^{11}C-acetate PET/CT for detection of primary and metastatic hepatocellular carcinoma. J Nucl Med. 2008;49:1912-21.
9. Gevers TJ, Drenth JP. Diagnosis and management of polycystic liver disease. Nat Rev Gastroenterol Hepatol. 2013;10:101-8.
10. Nabi HA, Zubeldia JM. Clinical applications of ^{18}F-FDG in oncology. J Nucl Med Technol. 2002;30:3-9.
11. US Department of Health and Human Services. Common Terminology Criteria for Adverse Events (CTCAE) version 5.0. 2017. Available from: https://ctep.cancer.gov/protocoldevelopment/electronic_applications/docs/ctcae_v5_quick_reference_5x7.pdf. Accessed 9 Oct 2023.
12. Jacobs JE, Birnbaum B, Shapiro MA, Langlotz CP, Slosman F, Rubesin SE, et al. Diagnostic criteria for fatty infiltration of the liver on contrast-enhanced helical CT. AJR Am J Roentgenol. 1998;171:659-64.
13. Barrington SF, Kluge R. FDG PET for therapy monitoring in Hodgkin and non-Hodgkin lymphomas. Eur J Nucl Med Mol Imaging. 2017;44:97-110.
14. Soussan M, Nicolas P, Schramm C, Katsahian S, Pop G, Fain O, et al. Management of large-vessel vasculitis with FDG-PET: a systematic literature review and meta-analysis. Medicine (Baltimore). 2015;94:e622.
15. Love C, Tomas MB, Tronco GG, Palestro CJ. FDG PET of infection and inflammation. Radiographics. 2005;25:1357-68.
16. Kudo M, Zheng RQ, Kim SR, Okabe Y, Osaki Y, Iijima H, et al. Diagnostic accuracy of imaging for liver cirrhosis compared to histologically proven liver cirrhosis. A multicenter collaborative study. Intervirology. 2008;51 Suppl 1:17-26.
17. Lin CY, Lin WY, Lin CC, Shih CM, Jeng LB, Kao CH. The negative impact of fatty liver on maximum standard uptake value of liver on FDG PET. Clin Imaging. 2011;35:437-41.
18. Abele JT, Fung CI. Effect of hepatic steatosis on liver FDG uptake measured in mean standard uptake values. Radiology. 2010;254:917-24.
19. Keramida G, Potts J, Bush J, Verma S, Dizdarevic S, Peters AM. Accumulation of ^{18}F-FDG in the liver in hepatic steatosis. AJR Am J Roentgenol. 2014;203:643-8.
20. Vachha B, Sun MR, Siewert B, Eisenberg RL. Cystic lesions of the liver. AJR Am J Roentgenol. 2011;196:W355-66.
21. Rini JN, Leonidas JC, Tomas MB, Palestro CJ. ^{18}F-FDG PET versus CT for evaluating the spleen during initial staging of lymphoma. J Nucl Med. 2003;44:1072-4.

Hong Kong J Radiol. 2023;26:248-54. Epub 23 Nov 2023 | https://doi.org/10.12809/hkjr2217647

ORIGINAL ARTICLE **CME**

Treatment Outcomes and Toxicities of Stereotactic Body Radiotherapy for Oligoprogressive Metastatic Non–Small-Cell Lung Cancer

KKS Wong, TY Kam, MW Yeung, SI Soong

Department of Clinical Oncology, Pamela Youde Nethersole Eastern Hospital, Hong Kong SAR, China

ABSTRACT

Introduction: *This study reviewed the toxicities and outcomes of stereotactic body radiotherapy (SBRT) for oligoprogressive metastatic non–small-cell lung cancer (NSCLC).*

Methods: *The cases of patients with oligoprogressive NSCLC receiving SBRT from 2015 to 2020 were reviewed retrospectively. Demographics were analysed by descriptive statistics. Important treatment outcomes including local control and survival were analysed by the Kaplan-Meier method. Simple and multivariable Cox regression analyses were carried out to investigate prognostic factors. Toxicities were reported using the Common Terminology Criteria for Adverse Event version 4.0.*

Results: *Forty-one cases with 51 oligoprogressive sites were included. The median age of the cohort was 65 years. The most commonly ablated sites were the lung (68.6%) and bone metastasis (17.6%). The most common driver mutation was the epithelial growth factor receptor mutation (82.9%). SBRT doses ranged from 30 to 60 Gy in 3 to 10 fractions. Median follow-up time was 64 weeks. SBRT achieved a 1-year local control rate of 85%. Median progression-free survival (PFS) after SBRT was 8.8 months and median time from SBRT to the next line of systemic treatment was 9 months. A robust response to pre-SBRT systemic treatment was significantly associated with longer PFS after SBRT. Median overall survival was 58 months. There was one case of grade 3 pneumonitis (2%) and one case of rib fracture (2%).*

Conclusion: *SBRT for oligoprogression in NSCLC is an effective strategy to prolong the time to the next systemic treatment with minimal toxicities.*

Key Words: *Carcinoma, non-small-cell lung; Radiation oncology; Radiosurgery; Stereotactic body radiotherapy; Treatment outcome*

Correspondence: *Dr KKS Wong, Department of Clinical Oncology, Pamela Youde Nethersole Eastern Hospital, Hong Kong SAR, China*
Email: wks447@ha.org.hk

Submitted: 9 Oct 2022; Accepted: 20 Jan 2023.

Contributors: All authors designed the study. KKSW and TYK acquired and analysed the data. All authors drafted the manuscript and critically revised the manuscript for important intellectual content. All authors had full access to the data, contributed to the study, approved the final version for publication, and take responsibility for its accuracy and integrity.

Conflicts of Interest: All authors have disclosed no conflict of interest.

Funding/Support: This research received no specific grant from any funding agency in the public, commercial, or not-for-profit sectors.

Data Availability: All data generated or analysed during the present study are available from the corresponding author on reasonable request.

Ethics Approval: This research was approved by the Hong Kong East Cluster Research Committee of Hospital Authority, Hong Kong (Ref No.: HKECREC2022032). Informed consent was waived by the Committee due to the retrospective nature of the study.

中文摘要

寡進展轉移性非小細胞肺癌體部立體定向放射治療的療效及毒性

黃嘉誠、甘子揚、楊美雲、宋崧

簡介：本研究回顧寡進展轉移性非小細胞肺癌體部立體定向放射治療（SBRT）的毒性及結果。

方法：本研究回顧2015至2020年間接受SBRT的寡進展非小細胞肺癌患者個案。我們對患者的人口統計資料進行描述性統計，並使用Kaplan-Meier法分析重要的治療結果（包括局部控制及存活）以及簡單及多變量Cox迴歸分析研究預後因素。我們使用常見毒性標準（CTCAE）第4.0版本報告毒性。

結果：本研究包括了41例共51個寡進展部位。患者年齡中位數為65歲，最常見的消融部位是肺部（68.6%）及骨轉移（17.6%）。最常見的驅動基因突變是表皮生長因子受體突變（82.9%）。SBRT劑量介乎30至60 Gy，分3至10次。隨訪時間中位數為64星期。SBRT的一年局部控制率達85%。接受SBRT後的無惡化存活期中位數為8.8個月，而接受SBRT後至下次全身性治療的中位數時間則為9個月。接受SBRT前的全身性治療的顯著反應與較長的接受SBRT後的無惡化存活期顯著相關。整體存活期中位數為58個月。有一例3級肺炎（2%）及一例肋骨骨折（2%）。

結論：寡進展轉移性非小細胞肺癌SBRT在毒性減到最低的情況下能有效延長患者接受下次全身性治療前的存活期。

INTRODUCTION

Stereotactic body radiotherapy (SBRT) is a radiation technique that delivers a high dose of radiation to a small tumour target using highly conformal techniques.[1] It is widely used to treat early-stage non–small-cell lung cancer (NSCLC) with durable local control (LC) and a high cure rate.[2] Oligoprogressive disease (OPD) is defined as a clinical scenario in which there is initial polymetastatic disease that responds to systemic treatment until there is development of new subclones with drug resistance.[3] It refers to a limited number of new metastases with different authors quoting a range from a maximum of three to five sites of progression.[4,5] SBRT can be used to ablate these resistant clones before they proliferate and metastasise. Here we report the treatment outcomes and toxicities of SBRT for oligoprogressive metastatic NSCLC in our institution.

METHODS

We conducted a retrospective review of 41 patients who received SBRT for oligoprogressive NSCLC from 1 January 2015 to 31 December 2020. Only patients who had ≤ 3 foci of radiological progression during systemic therapy (excluding central nervous system progression) were included. Demographics were analysed by descriptive statistics using SPSS (Window version 23.0; IBM Corp, Armonk [NY], United States). Planning target volumes (PTVs) were generated by the Eclipse Treatment Planning System (Varian Inc, Palo Alto [CA], United States). Important treatment outcomes including LC and survival were analysed by the Kaplan-Meier method. Univariate and multivariate analysis were used to investigate prognostic factors. Toxicities were reported using the Common Terminology Criteria for Adverse Event version 4.0. Treatment response was monitored by interval computed tomography (CT) or positron emission tomography/computed tomography (PET/CT) scan at intervals determined by the patients' physicians and was reported by the RECIST (Response Evaluation Criteria in Solid Tumours) version 1.1 criteria. Progression-free survival (PFS) was defined as the time interval from date of initiation of SBRT to any progression or death. PFS from the previous systemic treatment (PFS1) was defined by the time from the start of the previous systemic treatment to the initiation of SBRT. Overall survival (OS) was defined as the time interval from the start of systemic treatment to the date of death from any cause. Complete follow-up data were available at the time of analysis. The study adhered to the STROBE (Strengthening the Reporting of Observational Studies in Epidemiology) reporting guidelines.

Our radiotherapy treatment protocol followed the Radiation Therapy Oncology Group trials protocol,[6,7]

the United Kingdom Stereotactic Ablative Radiotherapy Consortium guidelines,[8] and the American Association of Physicists in Medicine Task Group 101 report.[9] The details of treatment simulation scan, image co-registration, and PTV margins are described in Table 1. For lung lesions, three-dimensional CT with breath-hold was used for lower lobe tumours, while four-dimensional CT was used for upper lobe tumours. Contouring was performed on different respiratory phases and maximum intensity projection. Regarding spinal metastases, planning CT images were co-registered with diagnostic MRI. For liver and adrenal metastases, we used three-dimensional CT with breath-hold technique if possible. When PET/CT was available, it was registered to the planning CT to assist in gross tumour volume contouring, which was performed before treatment in 94.1% of our cases. For spinal metastases, we followed the International Spine Radiosurgery Consortium consensus guidelines[10] to contour different parts of the vertebra as our clinical target volume. For lung, liver, adrenal, and non-spinal bone metastasis cases, there was no margin expansion to form the clinical target volume. Treatment was prescribed at the 60% to 90% isodose line. The treatment aim was that 95% of the PTVs should receive at least the prescribed dose and 99% of the PTVs should receive at least 90% of prescribed dose. Positioning was verified with cone beam CT before each fraction. Treatment was delivered using intensity-modulated radiotherapy or volumetric modulated arc therapy, depending on the radiotherapists' preference.

RESULTS

A total of 51 SBRT sites were included. All patients had Eastern Cooperative Oncology Group performance status ≤ 2. There were 33 cases with a single site of OPD and 8 cases with > 1 site of OPD. Thirty-five cases had developed OPD during targeted therapy, and 6 cases had developed OPD during chemotherapy. The baseline demographics and SBRT treatment sites are depicted in Table 2.

The median age of the cohort was 65 years. Epithelial growth factor receptor (EGFR) mutation was the most common driver mutation (82.9%). The most commonly ablated site was the lung (68.6%), followed by bone metastasis (17.6%) as shown in Table 2. The SBRT dose and fractionation ranged from 30 to 60 Gy in 3 to 10 fractions depended on the location of the metastasis. Fractionation details are described in Table 2. Most treatments were given every 2 days and completed within

Table 1. Summary of planning images and planning target volume (PTV) margins.

	Lung	Spine	Liver	Adrenal
3DCT	Exhale breath-hold if tolerated for lower lobe tumour	Normal breathing	Exhale breath-hold, acquired in venous phase for GTV contour	Exhale breath-hold for GTV contour
4DCT	Using different respiratory phases and MIPs for contouring tumour, AVIP for contouring OARs and dose calculation	-	-	✓
		Co-registration		
MRI	-	T1-weighted gadolinium-enhanced and T2-weighted axial and sagittal sequences	Selected cases	-
PET/CT	✓	✓	✓	✓
		PTV margins		
	Lung	Spinal bone	Non-spinal bone	Liver and adrenal
3DCT with breath-hold	PTV = CTV + 8 mm	-	-	PTV = CTV + 5 mm in axial direction and + 8 mm in superior-inferior direction
4DCT	PTV = CTV + 5 mm	-	-	-
3DCT with normal breathing	-	PTV = CTV + 2 mm	PTV = CTV + 5 mm	-

Abbreviations: 3DCT = three-dimensional computed tomography; 4DCT = four-dimensional computed tomography; AVIP = average intensity projection; CTV = clinical target volume; GTV = gross tumour volume; MIP = maximum intensity projection; MRI = magnetic resonance imaging; OAR = organ at risk; PET/CT = positron emission tomography/computed tomography.

Table 2. Patient demographics (n = 41), treatment sites, dose and fractionations, and planning target volume (PTV) in different sites of metastases.*

Age at SBRT, y	
Median (range)	65 (31-87)
Sex, No. (%)	
Male	20 (48.8%)
Female	21 (51.2%)
Histology, No. (%)	
Adenocarcinoma	39 (95.1%)
Adenocarcinoma with neuroendocrine features	1 (2.4%)
Adeno-squamous carcinoma	1 (2.4%)
Driver mutations, No. (%)	
EGFR	34 (82.9%)
Anaplastic lymphoma kinase	2 (4.9%)
ROS-1 receptor tyrosine kinase	2 (4.9%)
RET fusion	1 (2.4%)
No mutations	2 (4.9%)
Types of EGFR mutations, No. (%) [n = 34]	
Exon 19 deletion	17 (50.0%)
L858R mutation	14 (41.2%)
L861Q mutation	2 (5.9%)
Exon 19 insertion	1 (2.9%)
Type of systemic treatment before SBRT, No. (%)	
Chemotherapy	6 (14.6%)
Targeted therapy	35 (85.4%)
SBRT target sites (n = 51)	
Adrenal	4 (7.8%)
Liver	3 (5.9%)
Lung	35 (68.6%)
Pelvis	4 (7.8%)
Rib	1 (2.0%)
Spine	4 (7.8%)
SBRT sites	Dose and fractionations†
Lung	Central lesion: 50 Gy/5 fr; 60 Gy/8 fr; 35 Gy/5 fr; 50 Gy/10 fr Peripheral lesion: 54 Gy/3 fr
Spine	35 Gy/5 fr; 30 Gy/5 fr
Rib	50 Gy/5 fr
Pelvis	35 Gy/5 fr
Liver	50 Gy/5 fr
Adrenal	40 Gy/5 fr
PTV, median (range), cm^3	
Lung	35.2 (11.3-102.2)
Adrenal	53.3 (31-95.5)
Spinal bone metastasis	34.4 (30.7-231.1)
Non-spinal bone metastasis	51.7 (40.9-101.4)
Liver	145.8 (114.6-230)

Abbreviations: EGFR = epithelial growth factor receptor; fr = fractions; RET = rearranged during transfection; SBRT = stereotactic body radiotherapy.

* Data are shown as No. (%), unless otherwise specified.

† Depend on the lesion location and surrounding organs at risk, where the choice is bounded by the guidelines quoted in the article (please refer to references 8 to 10).

2 weeks, except in peripheral lung lesions using 54 Gy over 3 fractions, in which treatments were separated by 4 days and completed within 2 weeks. Volume details of PTV in different SBRT sites are also reported in Table 2.

For the treatment outcome, 20 out of 41 patients (48.8%) were alive at last follow-up. With a median follow-up time of 64 weeks, a total of 7 out of 51 sites (13.7%) developed local failure. The 1-year LC rate was 85%. The median PFS after SBRT, which was defined by the time interval from date of initiation of SBRT to any progression or death, was 8.8 months. The median time from SBRT to the next line of systemic treatment was 9 months. The median OS was 58 months (Figure).

Possible prognosticators affecting PFS are assessed in Table 3. In simple Cox regression analysis, deeper response to previous systemic treatment and longer PFS1 (≥ 12 months) were significantly associated with longer PFS. In multivariable analysis, only PFS1 ≥ 12 months remained statistically significant. Meanwhile, sex, driver mutation type, lung or non-lung metastases, number of SBRT sites, degree of response to previous systemic treatment, and biological equivalent dose > 100 Gy did not significantly affect PFS.

We demonstrated a significant association between a better response to pre-SBRT systemic treatment (either partial response or complete response) and a longer PFS following SBRT. A longer PFS1 was also significantly associated with longer PFS after SBRT (Table 3).

For treatment-related toxicities, only one patient (2.4%) developed grade 3 pneumonitis, and one patient (2.4%) developed a rib fracture. There were no grade 4 to 5 toxicities. The patient who developed symptomatic pneumonitis had radiographic features of pneumonitis on CT scan. Pneumonitis was treated with a course of empirical antibiotics and a tapering course of steroids. EGFR tyrosine kinase inhibitor was temporarily suspended during management of pneumonitis. The patient was still alive at last follow-up and required 2 L/min of long-term oxygen therapy. For the rib fracture in our study, it was detected by follow-up PET/CT scan and the patient was asymptomatic without the need of analgesic.

DISCUSSION

Targeted therapy in NSCLC significantly changes the treatment landscape of metastatic NSCLC. However, disease progression is inevitable when a drug-resistant

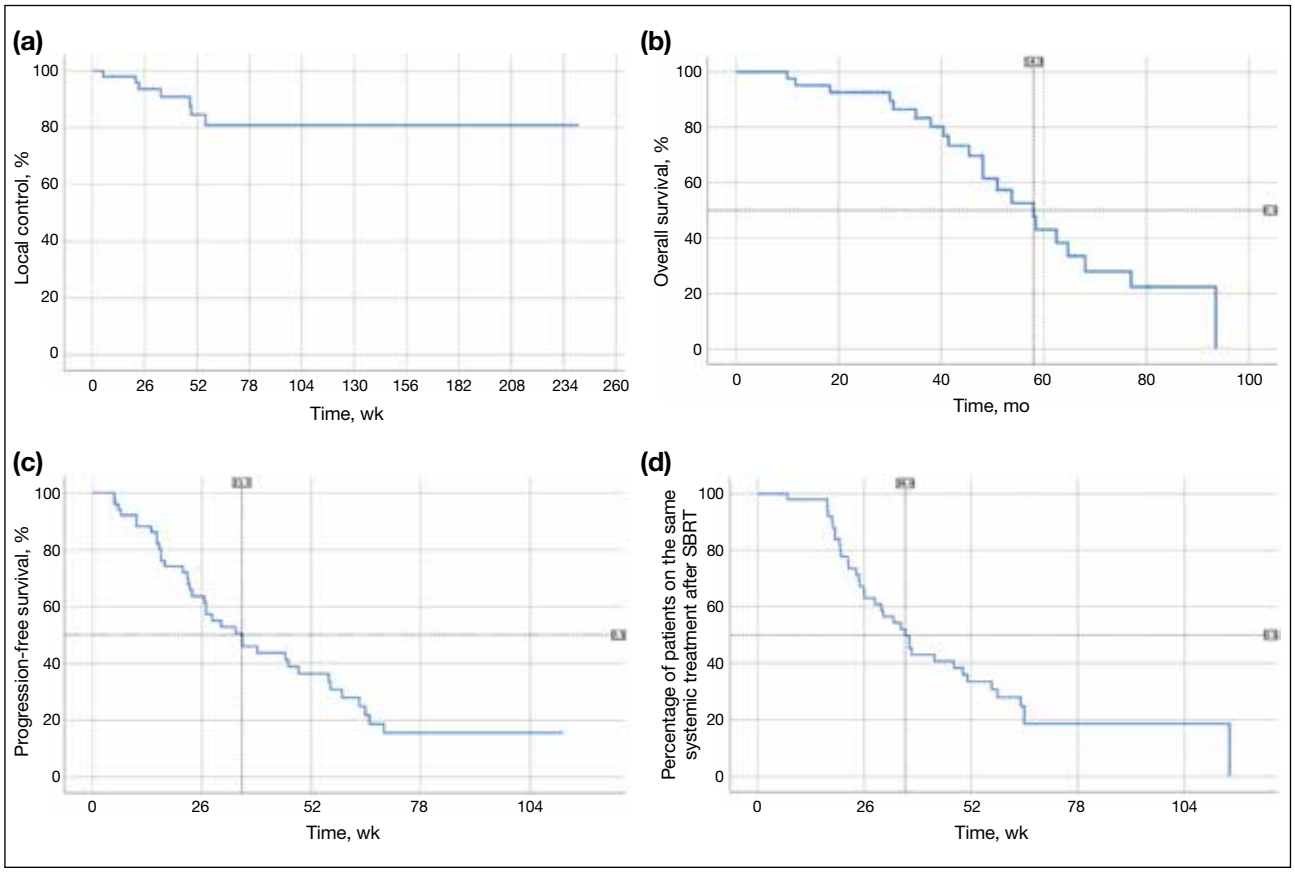

Figure. Kaplan-Meier estimates for the survival functions of (a) local control, (b) overall survival, (c) progression-free survival, and (d) time from stereotactic body radiotherapy (SBRT) to next line of systemic treatment.

Table 3. Cox regression analyses for progression-free survival.

Univariable analysis Variable	Hazard ratio (95% CI)	p Value (log-rank)
Sex (female vs. male)	0.941 (0.492-1.800)	0.855
L858R mutation vs. Exon 19 deletion	0.867 (0.453-1.661)	0.668
Lung vs. non-lung SBRT site	0.577 (0.291-1.143)	0.115
No. of SBRT sites = 1 vs. > 1	0.621 (0.320-1.204)	0.158
Response to previous systemic treatment (SD/PD vs. PR/CR)	3.343 (1.448-7.720)	0.005
BED < 100 Gy vs. ≥ 100 Gy	1.278 (0.581-2.812)	0.542
PFS1 < 12 mo vs. ≥ 12 mo	3.683 (1.784-7.603)	< 0.001
Multivariable analysis Variable	**Hazard ratio (95% CI)**	**p Value (log-rank)**
Sex (female vs. male)	0.681 (0.284-1.636)	0.391
L858R mutation vs. exon 19 deletion	1.158 (0.451-2.040)	0.913
Lung vs. non-lung SBRT site	0.431 (0.147-1.262)	0.125
No. of SBRT sites = 1 vs. > 1	0.414 (0.164-1.044)	0.062
Response to previous systemic treatment (SD/PD vs. PR/CR)	2.560 (0.531-12.351)	0.242
BED < 100 Gy vs. ≥ 100 Gy	0.570 (0.157-2.064)	0.392
PFS1 < 12 mo vs. ≥ 12 mo	3.906 (1.431-10.663)	0.008

Abbreviations: BED = biological equivalent dose; CI = confidence interval; CR = complete response; PD = progressive disease; PFS1 = progression-free survival from the previous systemic treatment; PR = partial response; SBRT = stereotactic body radiotherapy; SD = stable disease.

clone develops and proliferates. Oligoprogression is a distinct clinical entity which specifies a state where the number of progression sites is limited to ≤ 5.[4,5] A strategy for OPD is not yet well defined. Theoretically, eradicating the resistant subclone by SBRT will potentially prolong the use of tyrosine kinase inhibitors upon progression.

The benefits of SBRT in OPD have yet to be explored in prospective studies and current data mostly came from phase II studies. Most of the studies were retrospective in nature and they included a heterogeneous group of patients with different molecular profiles. Different local ablative therapies other than SBRT were included in some studies. Several retrospective studies of patients with EGFR or anaplastic lymphoma kinase–mutated NSCLC treated with local ablative therapy and continued treatment with EGFR- or anaplastic lymphoma kinase–targeted therapy resulted in improved PFS (Table 4),[11-14] with reported magnitudes of PFS ranging from 3.3 to 7 months.

Our data showed that SBRT delivers reasonably good LC at the metastatic sites, and our LC rate of 85% is on par with other different case series.[11-14] Also, our findings revealed that SBRT to OPD brings a benefit of PFS of 8.8 months, which is in line with the existing literature. This benefit is not only demonstrated on follow-up imaging, but it is also clinically meaningful in a sense that it can be translated into a delay in the use of the next systemic treatment by 9 months. With these data, the magnitude of benefit from SBRT in OPD can be quantified. Therefore, opening up the option of SBRT at the first appearance of OPD could potentially forestall the use of cytotoxic chemotherapy, and hence preserve the quality of life of patients for a longer period.

To maximise the benefit of SBRT, selecting the correct patients is crucial. Significant prognostic factors associated with longer PFS after SBRT include longer PFS1 and better radiological response to previous systemic treatment. These two factors constitute a favourable profile of tumours which are likely to derive sustained systemic response after SBRT for OPD. Hence, they can potentially serve as criteria when selecting suitable patients to receive SBRT and hence maximise the survival benefit.

Oligoprogression should also be well defined by sensitive imaging such as PET/CT before delivering SBRT. Treatment should be limited to a maximum of three to five sites of disease progression according to the literature.[4,5] However, we could not demonstrate a significantly shorter PFS for > 1 SBRT site in our study, probably due to the limitation of the small number of cases.

Merino Lara et al[14] reported 108 patients with metastatic NSCLC treated with extracranial SBRT, and revealed an incidence of grade ≥ 3 pneumonitis within 1 year of treatment of approximately 2%; SBRT-induced bone fracture was reported in 3% of the patients, and there were no grade 4 or 5 toxicities. Similar to their findings, the toxicities observed in our retrospective cohort aligned with these reported ranges.

Limitations

Our study has several limitations. First, the retrospective nature and small sample size (41 patients with 51 treatment sites) may lead to underreporting of toxicities and inadequate statistical power to detect significant differences. Also, retrospective studies are prone to selection and sampling bias. Second, our cohort predominantly consisted of patients who developed OPD during targeted therapy treatment. Therefore, we need to be cautious about the limitation when generalising the data on other patients who have OPD during non–targeted therapy treatment. As interval imaging post-SBRT is based on the clinician's discretion, the regular imaging to document local failure or progression is not as strict as in randomised trials. There is no randomisation and no control arm comparing the benefits of SBRT and changing systemic treatment at the first appearance of

Table 4. Summary of current data on stereotactic body radiotherapy (SBRT) in oligoprogressive non–small-cell lung cancer.

	Our study	Chan et al[11]	Weickhardt et al[12]	Qiu et al[13]	Merino Lara et al[14]
No. of patients	41	25	25	46 (only 8 on SBRT)	20
1-year local control rate	85%	76%	N/A	2-year OS: 65.2%	84.4%
Median PFS, mo	8.8	7	6.2	7	3.3
Grade ≥ 3 toxicity	Pneumonitis, 2.4%	Oesophagitis, 4%	Fatigue, 8%	Pneumonitis, 4.3%	Pneumonitis, 2%

Abbreviations: N/A = not available; OS = overall survival; PFS = progression-free survival.

OPD. Hence, the clinical question whether SBRT is better than changing systemic treatment at the discovery of OPD remains unanswered. Moreover, measuring the time from SBRT to the next systemic treatment as a surrogate of clinical benefit may be affected by the patient's decision and choice of treatment, instead of objective assessment using radiographic progression. Lastly, patients with limited metastases may have intrinsic biology that allows them to have a longer survival independent of the success of local or systemic therapies.

CONCLUSION

Our data concur with existing literature that SBRT to OPD in NSCLC is an effective and safe strategy to prolong the time to next systemic treatment with minimal toxicities. Further studies including the HALT study (Stereotactic Body Radiotherapy for the Treatment of OPD)[15] and the STOP trial [Randomized Study of Stereotactic Body Radiation Therapy (SBRT) in Patients With Oligoprogressive Metastatic Cancers of the Breast and Lung][16] will provide prospective data on PFS and OS for SBRT in the setting of OPD.

REFERENCES

1. Timmerman RD, Herman J, Cho LC. Emergence of stereotactic body radiation therapy and its impact on current and future clinical practice. J Clin Oncol. 2014;32:2847-54.
2. Ball D, Mai GT, Vinod S, Babington S, Ruben J, Kron T, et al. Stereotactic ablative radiotherapy versus standard radiotherapy in stage 1 non–small-cell lung cancer (TROG 09.02 CHISEL): a phase 3, open-label, randomised controlled trial. Lancet Oncol. 2019;20:494-503.
3. Guckenberger M, Lievens Y, Bouma AB, Collette L, Dekker A, deSouza NM, et al. Characterisation and classification of oligometastatic disease: a European Society for Radiotherapy and Oncology and European Organisation for Research and Treatment of Cancer consensus recommendation. Lancet Oncol. 2020;21:e18-28.
4. Hellman S, Weichselbaum RR. Oligometastases. J Clin Oncol. 1995;13:8-10.
5. Patel PH, Palma D, McDonald F, Tree AC. The dandelion dilemma revisited for oligoprogression: treat the whole lawn or weed selectively? Clin Oncol (R Coll Radiol). 2019;31:824-33.
6. Timmerman R, Paulus R, Galvin J, Michalski J, Straube W, Bradley J, et al. Stereotactic body radiation therapy for inoperable early stage lung cancer. JAMA. 2010;303:1070-6.
7. Bezjak A, Paulus R, Gaspar LE, Timmerman RD, Straube WL, Ryan WF, et al. Safety and efficacy of a five-fraction stereotactic body radiotherapy schedule for centrally located non–small-cell lung cancer: NRG Oncology/RTOG 0813 Trial. J Clin Oncol. 2019;37:1316-25.
8. Faculty of Clinical Oncology, The Royal College of Radiologists. Stereotactic ablative body radiation therapy (SABR): a resource. Version 6.1. Available from: https://www.sabr.org.uk/wp-content/uploads/2019/04/SABRconsortium-guidelines-2019-v6.1.0.pdf. Accessed 13 Nov 2023.
9. American Association of Physicists in Medicine. Report No. 101 – Stereotactic body radiation therapy: the report of AAPM Task Group 101 (2010). Available from: https://www.aapm.org/pubs/reports/detail.asp?docid=102. Accessed 13 Nov 2023.
10. Cox BW, Spratt DE, Lovelock M, Bilsky MH, Lis E, Ryu S, et al. International Spine Radiosurgery Consortium consensus guidelines for target volume definition in spinal stereotactic radiosurgery. Int J Radiat Oncol Biol Phys. 2012;83:e597-605.
11. Chan OS, Lee VH, Mok TS, Mo F, Chang AT, Yeung RM. The role of radiotherapy in epidermal growth factor receptor mutation–positive patients with oligoprogression: a matched-cohort analysis. Clin Oncol (R Coll Radiol). 2017;29:568-75.
12. Weickhardt AJ, Scheier B, Burke JM, Gan G, Lu X, Bunn PA Jr, et al. Local ablative therapy of oligoprogressive disease prolongs disease control by tyrosine kinase inhibitors in oncogene-addicted non–small-cell lung cancer. J Thorac Oncol. 2012;7:1807-14.
13. Qiu B, Liang Y, Li Q, Liu G, Wang F, Chen Z, et al. Local therapy for oligoprogressive disease in patients with advanced stage non–small-cell lung cancer harboring epidermal growth factor receptor mutation. Clin Lung Cancer. 2017;18:e369-73.
14. Merino Lara T, Helou J, Poon I, Sahgal A, Chung HT, Chu W, et al. Multisite stereotactic body radiotherapy for metastatic non–small-cell lung cancer: delaying the need to start or change systemic therapy? Lung Cancer. 2018;124:219-26.
15. ClinicalTrials.gov, US National Library of Medicine. Stereotactic Body Radiotherapy for the Treatment of OPD (HALT). Available from: https://clinicaltrials.gov/study/NCT03256981. Accessed 31 Oct 2023.
16. ClinicalTrials.gov, US National Library of Medicine. Randomized Study of Stereotactic Body Radiation Therapy (SBRT) in Patients With Oligoprogressive Metastatic Cancers of the Breast and Lung. Available from: https://www.clinicaltrials.gov/study/NCT03808662. Accessed 31 Oct 2023.

Hong Kong J Radiol. 2023;26:255-9. Epub 18 Dec 2023 | https://doi.org/10.12809/hkjr2217570

ORIGINAL ARTICLE

The Value of Arterial Sheath Placement Prior to Caesarean Section for Major Placenta Praevia

W Shu[1], AHC Wong[2], LW Chan[1]

[1]Obstetrics and Gynaecology Clinic, Gleneagles Hospital Hong Kong, Hong Kong SAR, China
[2]Department of Radiology, Pamela Youde Nethersole Eastern Hospital, Hong Kong SAR, China

ABSTRACT

Introduction: *This study aims to assess the value of non-urgent femoral sheath placement in women with major placenta praevia by analysing its utilisation rate and associated outcome measures.*

Methods: *We performed a 10-year retrospective cohort analysis of cases of women who underwent elective Caesarean section for major placenta praevia in a single obstetric unit. We compared outcomes between those with preoperative femoral sheath placement to those not receiving a sheath.*

Results: *One hundred and forty-five women with major placenta praevia were enrolled. Femoral sheaths were placed in 70 cases, and 7.1% experienced successful uterine artery embolisation. The complication rate of femoral sheath placement was low (1.4%). The odds of receiving additional uterotonics were higher in the femoral sheath placement group (odds ratio = 5.44; p = 0.013). Femoral sheath placement was not associated with reduced blood loss, need for blood transfusion, operation duration, or the use of additional procedures to abate bleeding. The rate of intensive care unit admissions was comparable in both groups.*

Conclusion: *The placement of femoral arterial sheath prior to elective Caesarean section in cases of major placenta praevia may not be beneficial. It is time-consuming and does not improve maternal morbidity.*

Key Words: *Arterial; Caesarean section; Maternal mortality; Placenta praevia*

Correspondence: *Dr W Shu, Obstetrics and Gynaecology Clinic, Gleneagles Hospital Hong Kong, Hong Kong SAR, China*
Email: wendy.shu@gleneagles.hk

Submitted: 30 Apr 2022; Accepted: 25 Aug 2022.

Contributors: All authors designed the study, acquired and analysed the data, drafted the manuscript, and critically revised the manuscript for important intellectual content. All authors had full access to the data, contributed to the study, approved the final version for publication, and take responsibility for its accuracy and integrity.

Conflicts of interest: All authors have disclosed no conflicts of interest.

Funding/support: This research received no specific grant from any funding agency in the public, commercial, or not-for-profit sectors.

Data Availability: All data generated or analysed during the present study are available from the corresponding author on reasonable request.

Ethics Approval: The research was approved by the Hong Kong East Cluster Research Ethics Committee of Hospital Authority, Hong Kong (Ref No.: HKECREC-2020-136).

Acknowledgement: The authors thank Mr Steve LT Lee, senior radiographer of Pamela Youde Nethersole Eastern Hospital, for retrieving data of cases who had femoral sheath inserted at the radiology department of the institution, and Mr Robert Porsch for advising on statistical analysis.

中文摘要

剖腹產前放置動脈鞘對於嚴重前置胎盤的價值

舒敏欣、黃可澄、陳連偉

簡介：本研究透過分析使用率和相關結果指標，評估非緊急股動脈鞘放置對於嚴重前置胎盤孕產婦的價值。

方法：我們對一間產科因嚴重前置胎盤而接受擇期剖腹產的女性病例進行了10年回顧性隊列分析，並比較術前放置與未放置股動脈鞘患者的結果。

結果：共145名患有嚴重前置胎盤的女性納入研究，70例放置股動脈鞘，7.1%子宮動脈栓塞成功。股動脈鞘置入術的併發症發生率較低（1.4%）。股動脈鞘置入組接受額外子宮收縮劑子宮收縮的機率較高（優勢比 = 5.44；p = 0.013）。股動脈鞘放置與失血量減少、輸血需求、手術時間或使用其他方案來減少出血無關。兩組的加護病房入院率相若。

結論：對於嚴重前置胎盤的病例，在擇期剖腹產前放置股動脈鞘可能沒有好處。它耗時並且不會改善孕產婦發病率。

INTRODUCTION

The global prevalence of placenta praevia (PP) is approximately 5 per 1,000 pregnancies, with the highest prevalence reported in Asian women (12.2 per 1,000 pregnancies).[1] Delivery by Caesarean section in these cases are 12 times more likely to result in massive haemorrhage than Caesarean sections performed for other reasons.[2]

Preoperative measures in minimising haemorrhagic morbidities for these women can be achieved by closely liaising with blood bank specialists, haematologists, and interventional radiologists.[3] It has been suggested that interventional radiology with uterine artery embolisation (UAE), performed intraoperatively or postoperatively, has reduced the need for hysterectomy when pharmacological measures have failed.[4,5]

In 2017, Luo et al[6] advocated prophylactic intraoperative aortic balloon insertion with major PP, irrespective of the presence or absence of abnormal invasive placenta. However, a recent randomised controlled trial showed that prophylactic internal iliac artery balloon occlusion did not reduce postpartum haemorrhage (PPH) or have any effect on maternal or neonatal morbidity in this group of women.[7]

Prophylactic placement of femoral arterial catheters (or sheaths) for PP is becoming more widespread.[8] In our centre, femoral arterial sheath placement before Caesarean section for major PP is a common practice. We explored the value of femoral sheath placement in the management of PP.

METHODS

This was a 10-year retrospective observational analysis of all women with major PP delivered electively at our centre from January 2010 to December 2020. Anonymous data were collected from the Clinical Data Analysis and Reporting System, a computer-based administration database that records all the diagnostic and procedural coding of admitted patients, and cases were identified based on their diagnostic coding (10th edition of the International Classification of Diseases[9]). Missing data were retrieved manually from hard copies of the patients' records.

Major PP is defined by placenta covering the internal os either partially (grade III) or completely (grade IV).[10] The main bulk of the PP can be anterior, non-anterior, or complete (completely covering the internal os). The type of PP was determined by the most recent transvaginal ultrasound before delivery.

Elective Caesarean section was scheduled between 37 and 38 weeks of gestation by an obstetrician, who would arrange for femoral sheath placement by notifying a dedicated radiographer. A 5-Fr sheath (Lonyi Medicath, Shenzhen, China) [Figure] was inserted into the right common femoral artery before the elective Caesarean section in the radiology department. Techniques used to insert the sheath were by palpation, under fluoroscopy, or by ultrasonic guidance. Complications were categorised into bleeding, infection, and thrombosis. Femoral sheath placement was not performed when the delivery was urgent or in an emergency setting when the attending radiologist was otherwise occupied.

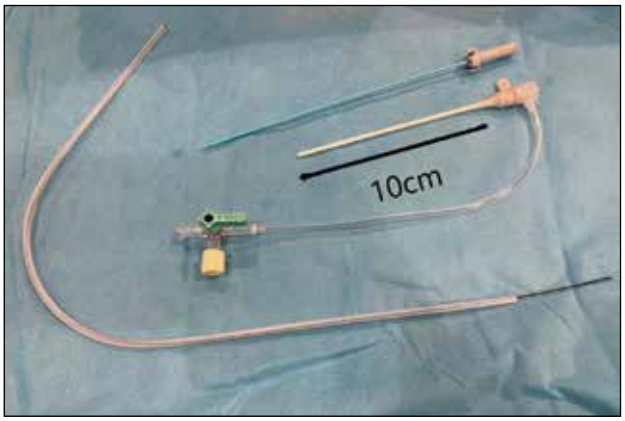

Figure. A 5-Fr femoral sheath set used in our institution.

Cases with major PP were divided into two groups, namely those with femoral sheath placement and those without. The primary outcome was the eventual need for UAE. Technically successful UAE was defined by successful embolisation of both uterine arteries. Secondary outcomes included estimated intraoperative blood loss; need for blood transfusion (units of packed red cells); operation duration; additional procedures to control bleeding, including compression sutures and Bakri balloon insertion; and additional uterotonics administered (medication other than the usual prophylactic oxytocin/ergometrine), including rectal misoprostol 800 to 1,000 mg, intramuscular carboprost 250 mcg, and infusion of concentrated oxytocin. PPH was defined by blood loss > 1,000 mL and the cause was categorised as active bleeding, concomitant placenta accreta, or uterine atony.

Simple differences between the two groups were analysed via Fisher's exact and correlation test for categorical and continuous variables, respectively. Continuous data were expressed as median (interquartile range) and were analysed with the Mann-Whitney *U* test. Multiple linear regression was performed to investigate the effects of femoral sheaths on estimated blood loss, need for blood transfusion, operation duration, and use of uterotonics/additional procedures after adjusting for possible confounders (i.e., age, gestation, parity, emergency Caesarean section, and antepartum haemorrhage). Poisson regression analysis was performed on units of blood transfused, while multiple linear regression analyses were performed to investigate the effects of femoral sheath on estimated blood loss and operation duration. Logistic regression analysis was performed on additional use of uterotonics, additional procedures, intensive care unit admissions, and hysterectomy. Analyses were carried out using R version 3.6.3. A p value < 0.05 was considered statistically significant.

RESULTS

One hundred and forty-five cases of major PP were enrolled. All patients were ethnically Chinese. Seventy-one (49%) were nulliparous. Seventy cases underwent Caesarean section with femoral sheath placement and 75 cases underwent Caesarean section without. The patient demographics and outcomes for the two groups are summarised in Table 1. The demographic and obstetric characteristics were similar in both groups, with the exception of the median gestational age at delivery, which was significantly lower in the cases not receiving femoral sheaths (36 vs. 37.1 weeks; $p < 0.0001$). The frequency of antepartum haemorrhage (84% vs. 61.4%) and need for emergency Caesarean section (82.7% vs. 30%) were higher in the group not receiving femoral sheaths %; (both $p < 0.0001$).

The eventual need for UAE was 4.0% for those not receiving femoral sheaths; it was 7.1% for the cases with femoral sheaths ($p = 0.48$). All UAEs were performed successfully in both groups. The majority (62.9%) of the femoral sheaths were inserted by ultrasonic guidance (Table 2). A single complication, a localised 6-cm haematoma, occurred in one case.

The overall incidence of PPH was 40.6%, mostly due to bleeding from the placental bed. The mean estimated intraoperative blood loss appears significantly greater in the cases receiving sheaths electively than in those undergoing emergent UAE (1,287 mL vs. 891 mL; $p = 0.018$) [Table 1]. However, the mean operation duration, blood transfusion rate, and use of additional procedures were comparable in both groups after adjusting for confounders (Table 3). Logistic regression analysis shows that the odds ratio for receiving additional uterotonics was higher in those receiving elective femoral sheaths (5.44, 95% confidence interval = 1.53-23.01; $p = 0.013$).

DISCUSSION

The current definition of PP is limited to placentas that cover the internal os.[10] Nonetheless, minor (grade I and II) and major (grade III and IV) PP are still in use to date.[10] The prevalence of PP in this study was 13.1 per 1,000 deliveries, higher than the rate of 5.2 per 1,000 pregnancies previously reported in 2013.[1] This can be contributed by raised awareness and screening of PP increasingly becoming a part of standard obstetric care. Iyasu et al[11] found that Asian women are twice more likely to develop PP compared to other ethnicities, hinting a genetic predisposition. All patients in this study are of Chinese ethnicity, which may have also contributed to the higher prevalence.

Table 1. Patient demographics and outcomes (n = 145).*

	Elective sheath (n = 70)	No elective sheath (n = 75)	p Value
Median age, y	34.9 (33.9-35.9)	35.2 (34.4-36.1)	0.66
Median parity	0 (0-1.0)	1 (0-1.0)	0.30
Twin pregnancy	4 (5.7%)	5 (6.7%)	1.0
Previous delivery method			0.079
Nulliparous	37 (52.9%)	34 (45.3%)	
Previous CS	22 (31.4%)	17 (22.7%)	
Previous vaginal delivery	11 (15.7%)	24 (32.0%)	
Median gestational age at delivery, wk	37.0 (37-38)	36.0 (33.5-37.0)	< 0.0001
Median gestation weight at delivery, g	2,902 (2,748-3,173)	2,675 (2,095-2,925)	< 0.0001
Major placenta praevia			0.69
Anterior	23 (32.9%)	25 (33.3%)	
Non-anterior	36 (51.4%)	42 (56.0%)	
Complete	11 (15.7%)	8 (10.7%)	
Antepartum haemorrhage	43 (61.4%)	63 (84.0%)	< 0.0001
Emergency CS	21 (30.0%)	62 (82.7%)	< 0.0001
UAE performed	5 (7.1%)	3 (4.0%)	0.48
PPH	34 (48.6%)	27 (36.0%)	0.177
Accreta	4 (5.7%)	3 (4.0%)	
Uterine atony	6 (8.6%)	9 (12.0%)	
Bleeders	23 (32.9%)	14 (18.7%)	
Unknown cause	1 (1.4%)	1 (1.3%)	
Mean estimated intraoperative blood loss, mL	1,287 ± 300	891 ± 141	0.018
Mean blood transfusion units	1.3 ± 0.6	0.79 ± 0.46	0.17
Mean operation duration, min	51.7 ± 4.4	46.5 ± 3.5	0.07
Additional procedures	14 (20.0%)	10 (13.3%)	0.38
Additional uterotonics	36 (51.4%)	19 (25.3%)	0.0019
ICU admission	7 (10.0%)	2 (2.7%)	0.089
Hysterectomy	2 (2.9%)	0	0.231

Abbreviations: CS = Caesarean section; ICU = intensive care unit; PPH = postpartum haemorrhage; UAE = uterine artery embolisation.
* Data are shown as No. (%), median (interquartile range) or mean ± standard deviation, unless otherwise specified.

Table 2. Techniques and complications of preoperative femoral sheath placement in placenta praevia (n = 70).*

Femoral sheath placement complication	1 (1.4%)
Haematoma	1 (1.4%)
Thrombosis	0
Infection	0
Techniques	
By palpation	17 (24.3%)
Under fluoroscopy	9 (12.9%)
By ultrasonic guidance	44 (62.9%)

* Data are shown as No. (%).

Unlike invasive coronary angiography in interventional cardiology,[12] to the best of our knowledge, femoral sheath placement in PP has not been previously studied. Femoral access can be technically difficult when circulation is compromised. Also, there is considerable variation in the anatomy of the femoral artery,[13] and its pulse may be nonpalpable in pregnant women with physiological oedema. Therefore, it was postulated that elective femoral arterial access prior to the procedure could facilitate UAE and reduce vascular complications when UAE is eventually needed. In this study, most of the femoral sheaths were inserted under ultrasonic guidance. Ultrasonic guidance is the preferred method by radiologists, with a success rate of 98.5% and reduced number of re-attempts.[14] Fluoroscopy, although safe, is the least preferred method because of concerns with radiation.[15]

The majority of the femoral sheaths were not used and were removed 24 hours postoperatively. Haematoma formation occurred in one case (1.4%) with preoperative femoral sheath insertion. Significant local haematoma can occur in 2% to 3% of the femoral sheath procedures, but these figures were derived from non-obstetric studies.[13,14] Thrombosis, potentiated by the inherent thrombogenic effect of pregnancy, was not observed in this study.

Other studies have shown that increased birth weight and greater gestational age were associated with more bleeding in major PP.[16,17] The cases receiving the sheath electively delivered at a greater gestational age, which was associated with more blood loss. Increased blood loss should not be attributed to the femoral sheath alone, as shown by multivariate analysis, which found that the

Table 3. Multiple regression analyses performed on outcome variables.

Factor	Coefficient level estimate	p Value	Odds ratio	95% Confidence interval
Estimated intraoperative blood loss	683.5	0.583	-	-19.8 to 517.97
Blood transfusion	0.21	0.28	1.23	0.85-1.79
Operative duration	4.39	0.144	-	1.52-10.30
Additional uterotonics	1.69	0.013	5.44	1.53-23.01
Additional procedures	0.12	0.84	1.13	0.35-3.71

femoral sheath is not associated with poorer outcome. The need for additional uterotonics was found in the cases receiving the sheath electively, however.

A large proportion of emergency Caesarean sections were performed without elective femoral sheath placement, because transport to the radiology department can be time-consuming and the radiologist may not be available. When UAE was needed in this group of women, the femoral access was uncomplicated, further arguing against the need for routine placement.

Limitations

Potential limitations of this study are due to its retrospective nature. Intraoperative blood loss was estimated since calibrated drapes and weighing of gauzes were not introduced yet at the time of this study. Long-term complications such as femoral artery aneurysm or arteriovenous fistula were not documented. In addition, explicit criteria were not applied when deciding which patients should receive a femoral sheath prior to delivery. This study also did not examine the role of femoral sheath in the placenta accreta spectrum, a rarer but significant cause of intractable intraoperative blood loss.

CONCLUSION

This 10-year retrospective analysis, focusing on the use of elective femoral sheath placement in cases of PP undergoing Caesarean section, did not confirm its theoretical advantage of facilitating subsequent UAE due to low usage. Furthermore, it may expose patients to unnecessary risks and discomfort. Future research should prioritise investigating the prophylactic use of femoral sheath in cases where UAE is more likely to be employed, such as placenta accreta spectrum.

REFERENCES

1. Cresswell JA, Ronsmans C, Calvert C, Filippi V. Prevalence of placenta praevia by world region: a systematic review and meta-analysis. Trop Med Int Health. 2013;18:712-24.
2. Royal College of Obstetricians and Gynaecologists. Blood Transfusions in Obstetrics. Green-top Guideline No. 47. London: RCOG; 2015.
3. Royal College of Obstetricians and Gynaecologists. Placenta Praevia and Placenta Accreta: Diagnosis and Management. Green-top Guideline No.27a. London: RCOG; 2018.
4. Vedantham S, Goodwin SC, McLucas B, Mohr G. Uterine artery embolization: an underused method of controlling pelvic hemorrhage. Am J Obstet Gynecol. 1997;176:938-48.
5. Mei J, Wang Y, Zou B, Hou Y, Ma T, Chen M, et al. Systematic review of uterus-preserving treatment modalities for abnormally invasive placenta. J Obstet Gynaecol. 2015;35:777-82.
6. Luo F, Xie L, Xie P, Liu S, Zhu Y. Intraoperative aortic balloon occlusion in patients with placenta previa and/or placenta accreta: a retrospective study. Taiwan J Obstet Gynaecol. 2017;56:147-52.
7. Yu SC, Cheng YK, Tse WT, Sahota DS, Chung MY, Wong SS, et al. Perioperative prophylactic internal iliac artery balloon occlusion in the prevention of postpartum hemorrhage in placenta previa: a randomized controlled trial. Am J Obstet Gynecol. 2020;223:117.e1-13.
8. Shevell T, Malone FD. Management of obstetric hemorrhage. Semin Perinatol. 2003;27:86-104.
9. National Center for Health Statistics, Centers for Disease Control and Prevention. ICD-10-CM International Classification of Diseases, Tenth Revision, Clinical Modification (ICD-10-CM). Available from: https://www.cdc.gov/nchs/icd/icd-10-cm.htm. Accessed 21 Nov 2023.
10. Jauniaux E, Alfirevic Z, Bhide AG, Belfort MA, Burton GJ, Collins SL, et al. Placenta praevia and placenta accreta: diagnosis and management: green-top guideline No. 27a. BJOG. 2019;126:e1-48.
11. Iyasu S, Saftlas AK, Rowley DL, Koonin LM, Lawson HW, Atrash HK. The epidemiology of placenta previa in the United States, 1979 through 1987. Am J Obstet Gynaecol. 1993;168:1424-9.
12. Castle EV, Rathod KS, Guttmann OP, Jenkins AM, McCarthy CD, Knight CJ, et al. Routine use of fluoroscopic guidance and up-front femoral angiography results in reduced femoral complications in patients undergoing coronary angiographic procedures: an observational study using an interrupted time-series analysis. Heart Vessels. 2019;34:419-26.
13. Abu-Fadel MS, Sparling JM, Zacharias SJ, Aston CE, Saucedo JF, Schechter E, et al. Fluoroscopy vs. traditional guided femoral arterial access and the use of closure devices: a randomized controlled trial. Catheter Cardiovasc Interv. 2009;74:533-9.
14. Kurisu K, Osanai T, Kazumata K, Nakayama N, Abumiya T, Shichinohe H, et al. Ultrasound-guided femoral artery access for minimally invasive neuro-intervention and risk factors for access site hematoma. Neurol Med Chir (Tokyo). 2016;56:745-52.
15. Stahl CM, Meisinger QC, Andre MP, Kinney TB, Newton IG. Radiation risk to the fluoroscopy operator and staff. AJR Am J Roentgenol. 2016;207:737-44.
16. Shinohara S, Okuda Y, Hirata S. Association between birth weight and massive haemorrhage in pregnancy with a low-lying placenta: a 9-year single-centre retrospective cohort study in Japan. J Obstet Gynaecol. 2019;39:22-6.
17. Boyle RK, Waters BA, O'Rourke PK. Blood transfusion for caesarean delivery complicated by placenta praevia. Aust N Z J Obstet Gynaecol. 2009;49:627-30.

Hong Kong J Radiol. 2023;26:260-5. Epub 12 Dec 2023 | https://doi.org/10.12809/hkjr2217565

PERSPECTIVE

Optimising Risk-based Breast Cancer Screening in Hong Kong

CPY Chien, G Ho, TPW Lam

Department of Radiology, Queen Mary Hospital, Hong Kong SAR, China

ABSTRACT

In Hong Kong, breast cancer is the most common cancer and the third leading cause of cancer mortality in women. The incidence has been increasing substantially over the past decades. In 2021, the Hong Kong Government launched a risk-based pilot screening programme with reference to the revised recommendations of the Cancer Expert Working Group on Cancer Prevention and Screening. The mortality rate reduction has yet to be assessed. This article provides an overview of breast cancer screening, briefly discusses the background and updated recommendations, and focuses on the supplementary screening tools and future directions in risk-based screening in Hong Kong.

Key Words: *Breast density; Breast neoplasms; Mammography; Mass screening*

中文摘要

優化香港基於風險的乳癌篩查

錢珮恩、何潔明、林培榮

在香港，乳癌是最常見的癌症，也是女性癌症死亡的第三大原因。過去幾十年來，乳癌發病率大幅增加。2021年，香港政府參考癌症預防及普查專家工作小組的修訂建議，推出基於風險的篩查先導計劃，而其死亡率降低程度尚待評估。本文概述乳癌篩查，簡要討論其背景和最新建議，並重點介紹香港基於風險篩查的補充篩查工具和未來方向。

INTRODUCTION

Female breast cancer had the highest incidence among all cancers diagnosed in women in 2020, with an estimated 2.3 million new cases (11.7%). It accounted for one in four cancer cases and for one in six cancer deaths.[1] The aim of breast cancer screening programme is to reduce breast cancer mortality through early detection and treatment. The World Health Organization recommends

Correspondence: *Dr CPY Chien, Department of Radiology, Queen Mary Hospital, Hong Kong SAR, China*
Email: cpy658@ha.org.hk

Submitted: 13 Apr 2022; Accepted: 5 Sep 2022.

Contributors: All authors designed the study. CPYC acquired and analysed the data and drafted the manuscript. All authors critically revised the manuscript for important intellectual content. All authors had full access to the data, contributed to the study, approved the final version for publication, and take responsibility for its accuracy and integrity.

Conflicts of Interest: All authors have disclosed no conflicts of interest.

Funding/Support: This study received no specific grant from any funding agency in the public, commercial, or not-for-profit sectors.

Data Availability: All data generated or analysed during the present study are available from the corresponding author on reasonable request.

population-based mammography screening biennially for women aged 50 to 69 years at average risk for breast cancer in countries with adequate resources.[2]

Although breast cancer is less common in Asian countries compared to the United States and Europe, its incidence has been increasing substantially over the past decades.[1,3,4] In Hong Kong, breast cancer is the most common cancer and the third leading cause of cancer mortality in women, with age-standardised incidence and mortality rates of 65.5 and 10.2 per 100,000 population, respectively, in 2019.[5] Most Western countries have well-established population-based mammogram screening programmes based on age.[6,7] Our Asian counterparts (i.e., South Korea, Singapore, Taiwan, and Japan) have also introduced screening programmes in the past two decades.[8] In 2021, the Hong Kong Government launched a risk-based pilot screening programme based on the revised recommendations of the Cancer Expert Working Group on Cancer Prevention and Screening (CEWG) under the Centre for Health Protection.[9]

This article provides an overview of breast cancer screening, briefly discusses the background and updated recommendations, and focuses on the supplementary screening tools and future directions in risk-based screening in Hong Kong.

BACKGROUND AND PRINCIPLES OF BREAST CANCER SCREENING

The goal of breast cancer screening is to detect breast cancer at its pre-clinical stage, so that it can be treated early to reduce disease- and treatment-related morbidity and mortality. Evidence has shown that detecting breast cancers at this early stage is associated with better outcomes.[10] The risk of metastasis and death increases with tumour size and number of involved axillary lymph nodes at detection.[11,12]

The 5-year survival rate drops from 86% to 99% in localised and regional disease to 29% in distant disease.[13] Treatment of early cancers requires less extensive breast tissue resection and axillary lymph node dissection, and hence fewer complications and side-effects. It also reduces overall treatment costs and financial burden on the healthcare system. Potential harms, which lead to controversies of effectiveness of screening programmes, include false-positives, overdiagnosis, overtreatment, psychological stress of participants; and lead-time bias which leads to seemingly increased survival.

Careful consideration of the cost-benefit balance, and adherence to the World Health Organization principles outlined by Wilson and Jungner,[14] are important when implementing breast cancer screening programme With numerous randomised controlled trials demonstrating a 20% to 30% decrease in mortality from breast cancer, numerous countries have implemented population-based screening programmes.[15] Most well-established population-based breast cancer screening programmes offer biennial mammography to women aged 40 to 50 years to 69 to 74 years.[16] Subsequent studies with data generated from screening programmes have provided further evidence that screening mammography is beneficial.[17]

UPDATES ON HONG KONG BREAST CANCER SCREENING

In 2010, the CEWG had adopted a simple and rather restrictive set of risk stratification criteria based on the presence of *BRCA1* or *BRCA2* genes, family history, and selected personal risk factors that led to only a small group of high-risk eligible women being screened.[18] For the last few decades, elective screening has been practised in Hong Kong in the private sector. Women attending such screening services are self-referred. The largest self-financed and self-referred mammography screening programme was organised by the Tung Wah Group of Hospitals, which has been offering mammography screening since 1993 with the number of examinations continuing to increase throughout the years.[19]

Recently, there has been a transition from elective screening to a broader risk-based approach. Based on the revised recommendations of the CEWG, the Hong Kong Government has rolled out a risk-based breast cancer screening pilot programme to provide screening services for eligible women over a period of 2 years. A local breast cancer risk stratification model for the Hong Kong Chinese population, developed by The University of Hong Kong based on the identified local risk factors for breast cancer, is employed.[9]

The new CEWG recommendations result in two additional groups of women being recommended for mammographic screening every 2 years. These groups are made up of women at moderate risk with a relevant defined family history, and women aged 44 to 69 with certain combinations of personal risk factors (including a history of breast cancer among first-degree relatives, a prior diagnosis of benign breast disease, nulliparity and late age of first live birth, early age at menarche, high

body mass index, and physical inactivity) putting them at increased risk of breast cancer.[9]

RISK-BASED SCREENING PROGRAMME

Population-based screening programmes based on different age groups have long been implemented in Western countries. They have proven to reduce breast cancer–related mortality effectively.[20] On the other hand, there was increasing evidence in favour of advocating for risk-based breast cancer screening due to potential higher cost-effectiveness in concentrating the resources on screening women with increased risk.[21,22] Some Western countries are also transitioning to risk-based screening approaches that do not rely on age alone.[23,24]

Risk-based programmes are aimed at women who are more likely to benefit, thus reducing the risk of causing harm to women at lower risk, and allow resources to be used more efficiently. In Hong Kong, although the age-standardised incidence rate of breast cancer is rising, it still remains relatively low when compared to Western countries. It is known that performing screening mammography in populations with relatively low disease prevalence would lead to higher false-positive rates and hence unnecessary biopsies, creating potential complications and psychological distress.[25] Therefore, under these circumstances, a personalised risk-based approach may be more cost-effective than universal age-based screening for Hong Kong Chinese women.[26]

The effectiveness of a risk-based screening programme depends much on the accuracy of individual risk estimation. In terms of risk stratification, the Gail model is one of the earliest breast cancer risk assessment tools that has been developed, validated and calibrated to be deployed in different populations.[27,28] More recently, the Breast Cancer Surveillance Consortium model and the Tyrer-Cuzick model have included breast density in risk assessment, which demonstrated modest performance improvement.[29,30] Histories of hyperplasia and lobular carcinoma in situ are also included.[29,30] With more local radiological and biomarker data available, the Hong Kong breast cancer risk stratification model can be improved to cover additional risk factors and identify women with increased risks effectively in the future.

RELATIONSHIP BETWEEN BREAST DENSITY AND BREAST CANCER

Increased mammographic breast density is an independent moderate risk factor for breast cancer. Women with extreme density are 4 to 6 times more likely to develop breast cancer than those with fatty breasts. Furthermore, extreme breast density is a solitary risk factor that puts women into higher lifetime and 10-year risk categories for breast cancer.[31] It is regarded as the same risk category (relative risk of 2.1 to 4) with ductal carcinoma in situ, high endogenous postmenopausal hormonal levels, high-dose radiation to the chest, and two or more first-degree relatives with breast cancer.[32]

Mammography is known to have lower sensitivity in women with dense breasts, including the Chinese population, younger and premenopausal women, and those with genetic predispositions to breast cancer, due to the increased mammographic density masking the radiological features of early breast cancer.[33] Therefore, it leads to more interval cancers and higher cancer stages at diagnosis. In addition, superimposed glandular tissue can also mimic the presence of a lesion, resulting in reduced specificity, increased recall rates, and unnecessary investigations.

SUPPLEMENTARY SCREENING TOOLS IN WOMEN WITH INCREASED RISK OF BREAST CANCER

In view of the associated increased cancer risk and mammographic masking effect in the relatively denser breast tissue in Chinese women, some recommend the use of supplementary screening tools to increase screening sensitivity and specificity.[34] Digital breast tomosynthesis (DBT) generates pseudo–three-dimensional images, which can resolve superimposition of breast tissue, thus increasing lesion visibility and reducing unnecessary recalls due to summation artifacts. It has been shown to have higher sensitivity and specificity compared to traditional digital mammography.[35] Ultrasound has been shown to reduce interval cancer rates for women with dense breasts when added to mammography. However, it is only suggested to be considered as a supplementary tool on a case-by-case basis due to its high false-positive rate.[36]

Breast contrast-enhanced magnetic resonance imaging (MRI) provides physiological parameters related to tumour angiogenesis in addition to anatomical assessment. It has been widely accepted for screening women who are at high risk for breast cancer, such as confirmed carriers of *BRCA1* or *BRCA2* deleterious mutations in genetic testing and those who had radiation therapy to the chest between 10 to 30 years of age for

Hodgkin lymphoma.[9] Kuhl et al[37] found that MRI could identify an additional 15.5 cancers per 1,000 cases in women at average risk of breast cancer. The DENSE (Dense Tissue and Early Breast Neoplasm Screening) trial has shown that using supplemental MRI screening in women with extremely dense breasts resulted in significantly fewer interval cancers than mammography alone.[34] However, due to long imaging time and limited availability, MRI is restricted to screening a limited number of high-risk women. Abbreviated MRI (AB-MRI) is a shortened version of the standard MRI protocol. By retaining a dynamic contrast-enhanced MRI sequence and one to two other sequences (depending on individual institutions), the examination time is shortened to 10 minutes. According to the American College of Radiology Imaging Network EA1141 trial,[38] AB-MRI was superior to DBT in detection of both invasive breast cancer and ductal carcinoma in situ, with 2.4 times higher detection rate in women with dense breasts. The positive predictive values of AB-MRI and DBT were shown to be similar.[38] Current evidence demonstrates that this technique has the potential to supplement mammography screening in women with dense breast tissue and increased risk of breast cancer. The shortened AB-MRI protocol and examination time increase the availability of MRI, allowing more women to be screened. It may potentially be included in the future screening programme.

Contrast-enhanced digital mammography (CEDM) is one of the latest advances in breast imaging. It uses a dual-energy technique performed after intravenous administration of iodinated contrast to identified enhancing lesions. The underlying principle is based on tumour physiology—tumoral angiogenesis increases vascular permeability, resulting in enhancement. Studies have shown that CEDM can improve diagnostic accuracy in evaluation of screening recalls. Initial findings evaluating the application of CEDM in high-risk screening have shown comparable specificity and positive predictive values with MRI. This suggests that CEDM may be useful as an alternative when MRI cannot be performed because of patient contraindication or inaccessibility.[39]

FEATURES OF AN EFFECTIVE SCREENING PROGRAMME

To improve the effectiveness of a risk-based screening programme, accurate risk stratification is essential. Incorporating mammographic breast density in the Hong Kong risk prediction model when more radiological data are available in the future can further enhance the discriminative power of the model to identify women who would benefit from screening.

Diagnostic accuracy depends on interpreter training, skills, and experience. Regular feedback from outcome of screening through assessment, follow-up results and radiological-pathological correlation can enhance the performance of radiologists. Measures such as regular audits and review of interval cancers should be implemented. Double reading is practised in some screening programmes to increase screening performance. Computer-aided detection algorithms can identify areas of abnormal density, morphology, and calcifications and mark them on an overlay image. It is most frequently used as a prompt to radiologists for special consideration during interpretation. Ongoing studies have evaluated it as a surrogate for a second reader.[40] A meta-analysis of five retrospective studies demonstrated better performance in machine learning mammographic breast cancer detection (area under the curve = 0.89) than radiologists (area under the curve = 0.85).[41] Other applications of artificial intelligence in breast cancer screening include lesion characterisation, determination of lesions' malignant probability, and triage of the worklist to streamline workflow.[42,43] A previous study reported that machine learning reduced the number of mammography reads by radiologists by 17% to 91% with 0% to 7% cancers missed.[41] Local regulations, guidelines, and recommendations should be adopted to ensure the quality assurance of mammography screening.

The level of participation and compliance in screening are influenced by personal, socio-economic, and cultural factors. Informed decision-making is important since screening has both positive and negative impact for individuals. Women should be fully informed about the benefits, limitations, and harms under both ethical and legal considerations. Measures can be taken to address the psychological consequences of mammography screening (such as hotlines, follow-up clinics, etc.) to alleviate patients' psychological distress and anxiety. Finally, participation can be influenced by how the screening invitation is made, how access to screening is organised, and how effectively breast cancer awareness is promoted, which are all amendable.

CONCLUSION

The Hong Kong risk-based breast screening programme is in its early phase. Its cost-effectiveness, which depends

on multiple modifiable factors, requires continuous evaluation and improvement. The effectiveness of a risk-based screening programme is determined by the discriminative power of the risk stratification model. Inclusion of individual factors such as breast density, histology results of breast biopsy, and biomarkers may modify it to a more comprehensive model. Personalised screening tailored to individuals' risks and preferences maybe the future direction in Hong Kong and worldwide.

REFERENCES

1. Sung H, Ferlay J, Siegel RL, Laversanne M, Soerjomataram I, Jemal A, et al. Global Cancer Statistics 2020: GLOBOCAN estimates of incidence and mortality worldwide for 36 cancers in 185 countries. CA Cancer J Clin. 2021;71:209-49.
2. World Health Organization. WHO position paper on mammography screening. 2014. Available from: https://www.who.int/publications/i/item/who-position-paper-on-mammography-screening. Accessed 22 Mar 2022.
3. Bray F, McCarron P, Parkin DM. The changing global patterns of female breast cancer incidence and mortality. Breast Cancer Res. 2004;6:229-39.
4. Wong IO, Schooling CM, Cowling BJ, Leung GM. Breast cancer incidence and mortality in a transitioning Chinese population: current and future trends. Br J Cancer. 2015;112:167-70.
5. Hong Kong Cancer Registry, Hospital Authority. Female breast cancer in 2019. Available from: https://www3.ha.org.hk/cancereg/pdf/factsheet/2019/breast_2019.pdf. Accessed 22 Mar 2022.
6. Smith RA, Andrews KS, Brooks D, Fedewa SA, Manassaram-Baptiste D, Saslow D, et al. Cancer screening in the United States, 2018: a review of current American Cancer Society guidelines and current issues in cancer screening. CA Cancer J Clin. 2018;68:297-316.
7. Wübker A. Explaining variations in breast cancer screening across European countries. Eur J Health Econ. 2014;15:497-514.
8. Sitt JC, Lui CY, Sinn LH, Fong JC. Understanding breast cancer screening—past, present, and future. Hong Kong Med J. 2018;24:166-74.
9. Centre for Health Protection, Department of Health, Hong Kong SAR Government. Cancer Expert Working Group on Cancer Prevention and Screening. Recommendations on prevention and screening for breast cancer for health professionals. Available from: https://www.chp.gov.hk/files/pdf/breast_cancer_professional_hp.pdf. Accessed 22 Mar 2022.
10. Eby PR. Evidence to support screening women annually. Radiol Clin North Am. 2017;55:441-56.
11. Colzani E, Liljegren A, Johansson AL, Adolfsson J, Hellborg H, Hall PF, et al. Prognosis of patients with breast cancer: causes of death and effects of time since diagnosis, age, and tumor characteristics. J Clin Oncol. 2011;29:4014-21.
12. Tan LK, Giri D, Hummer AJ, Panageas KS, Brogi E, Norton L, et al. Occult axillary node metastases in breast cancer are prognostically significant: results in 368 node-negative patients with 20-year follow-up. J Clin Oncol. 2008;26:1803-9.
13. National Cancer Institute. Surveillance, Epidemiology, and End Results Program. Cancer stat facts: female breast cancer. Available from: https://seer.cancer.gov/statfacts/html/breast.html. Accessed 22 Mar 2022.
14. Wilson JM, Jungner G. Principles and practice of screening for disease. Geneva, Switzerland: World Health Organization. Public Health Papers No. 34. Available from https://apps.who.int/iris/bitstream/handle/10665/37650/WHO_PHP_34.pdf?sequence=17&isAllowed=y. Accessed 2 Apr 2022.
15. Nelson HD, Cantor A, Humphrey L, Fu R, Pappas M, Daeges M, et al. Screening for breast cancer: a systematic review to update the 2009 U.S. Preventive Services Task Force recommendation. Rockville (MD): Agency for Healthcare Research and Quality; 2016.
16. von Karsa L, Qiao YL, Ramadas K, Keita N, Arrossi S, Dean PB, et al. Screening—implementation. In: Stewart BW, Wild CP, editors. World Cancer Report 2014. Lyon, France: International Agency for Research on Cancer; 2014: 330-6.
17. Myers ER, Moorman P, Gierisch JM, Havrilesky LJ, Grimm LJ, Ghate S, et al. Benefits and harms of breast cancer screening: a systematic review. JAMA 2015;314:1615-34.
18. Centre for Health Protection, Department of Health, Hong Kong SAR Government. Cancer Expert Working Group on Cancer Prevention and Screening. Recommendations on breast cancer screening 2010. Available from: http://www.chp.gov.hk/files/pdf/recommendations_on_breast_cancer_screening_2010.pdf. Accessed 2 Apr 2022.
19. Lui CY, Lam HS, Chan LK, Tam KF, Chan CM, Leung TY, et al. Opportunistic breast cancer screening in Hong Kong; a revisit of the Kwong Wah Hospital experience. Hong Kong Med J. 2007;13:106-13.
20. Sardanelli F, Aase HS, Álvarez M, Azavedo E, Baarslag HJ, Balleyguier C, et al. Position paper on screening for breast cancer by the European Society of Breast Imaging (EUSOBI) and 30 national breast radiology bodies from Austria, Belgium, Bosnia and Herzegovina, Bulgaria, Croatia, Czech Republic, Denmark, Estonia, Finland, France, Germany, Greece, Hungary, Iceland, Ireland, Italy, Israel, Lithuania, Moldova, The Netherlands, Norway, Poland, Portugal, Romania, Serbia, Slovakia, Spain, Sweden, Switzerland and Turkey. Eur Radiol. 2017;27:2737-43.
21. Pashayan N, Morris S, Gilbert FJ, Pharoah PD. Cost-effectiveness and benefit-to-harm ratio of risk-stratified screening for breast cancer: a life-table model. JAMA Oncol. 2018;4:1504-10.
22. Khan SA, Hernandez-Villafuerte KV, Muchadeyi MT, Schlander M. Cost-effectiveness of risk-based breast cancer screening: a systematic review. Int J Cancer. 2021;149:790-810.
23. Kerlikowske K, O'Kane ME, Esserman LJ. Fifty years of age-based screening: time for a new risk-based screening approach. Evid Based Med. 2014;19:183.
24. Allweis TM, Hermann N, Berenstein-Molho R, Guindy M. Personalized screening for breast cancer: rationale, present practices, and future directions. Ann Surg Oncol. 2021;28:4306-17.
25. Nelson HD, Pappas M, Cantor A, Griffin J, Daeges M, Humphrey L. Harms of breast cancer screening: systematic review to update the 2009 U.S. Preventive Services Task Force recommendation. Ann Intern Med. 2016;164:256-67.
26. Wong IO, Tsang JW, Cowling BJ, Leung GM. Optimizing resource allocation for breast cancer prevention and care among Hong Kong Chinese women. Cancer. 2012;118:4394-403.
27. Gail MH, Brinton LA, Byar DP, Corle DK, Green SB, Schairer C, et al. Projecting individualized probabilities of developing breast cancer for white females who are being examined annually. J Natl Cancer Inst. 1989;81:1879-86.
28. Chay WY, Ong WS, Tan PH, Jie Leo NQ, Ho GH, Wong CS, et al. Validation of the Gail model for predicting individual breast cancer risk in a prospective nationwide study of 28,104 Singapore women. Breast Cancer Res. 2012;14:R19.
29. Brentnall AR, Cuzick J, Buist DS, Bowles EJ. Long-term accuracy

of breast cancer risk assessment combining classic risk factors and breast density. JAMA Oncol. 2018;4:e180174.
30. Brentnall AR, Harkness EF, Astley SM, Donnelly LS, Stavrinos P, Sampson S, et al. Mammographic density adds accuracy to both the Tyrer-Cuzick and Gail breast cancer risk models in a prospective UK screening cohort. Breast Cancer Res. 2015;17:147.
31. Harvey JA, Bovbjerg VE. Quantitative assessment of mammographic breast density: relationship with breast cancer risk. Radiology. 2004;230:29-41.
32. American Cancer Society. Breast cancer facts & figures 2019-2020. Atlanta: American Cancer Society, Inc. 2019. Available from: https://www.cancer.org/content/dam/cancer-org/research/cancer-facts-and-statistics/breast-cancer-facts-and-figures/breast-cancer-facts-and-figures-2019-2020.pdf. Accessed 2 Apr 2022.
33. Checka CM, Chun JE, Schnabel FR, Lee J, Toth H. The relationship of mammographic density and age: implications for breast cancer screening. AJR Am J Roentgenol. 2012;198:W292-5.
34. Bakker MF, de Lange SV, Pijnappel RM, Mann RM, Peeters PH, Monninkhof EM, et al. Supplemental MRI screening for women with extremely dense breast tissue. N Engl J Med. 2019;381:2091-102.
35. Østerås BH, Martinsen AC, Gullien R, Skaane P. Digital mammography versus breast tomosynthesis: impact of breast density on diagnostic performance in population-based screening. Radiology. 2019;293:60-8.
36. Berg WA, Rafferty EA, Friedewald SM, Hruska CB, Rahbar H. Screening algorithms in dense breasts: *AJR* Expert Panel Narrative Review. AJR Am J Roentgenol. 2021;216:275-94.
37. Kuhl CK, Strobel K, Bieling H, Leutner C, Schild HH, Schrading S. Supplemental breast MR imaging screening of women with average risk of breast cancer. Radiology. 2017;283:361-70.
38. US National Library of Medicine. Abbreviated breast MRI and digital tomosynthesis mammography in screening women with dense breasts. Available from: https://clinicaltrials.gov/ct2/show/NCT02933489. Accessed 2 Apr 2022.
39. Jochelson MS, Pinker K, Dershaw DD, Hughes M, Gibbons GF, Rahbar K, et al. Comparison of screening CEDM and MRI for women at increased risk for breast cancer: a pilot study. Eur J Radiol. 2017;97:37-43.
40. Gilbert FJ, Astley SM, Gillan MG, Agbaje OF, Wallis MG, James J, et al. Single reading with computer-aided detection for screening mammography. N Engl J Med. 2008;359:1675-84.
41. Hickman SE, Woitek R, Le EP, Im YR, Mouritsen Luxhøj C, Aviles-Rivero AI, et al. Machine learning for workflow applications in screening mammography: systematic review and meta-analysis. Radiology. 2022;302:88-104.
42. Mendelson EB. Artificial intelligence in breast imaging: potentials and limitations. AJR Am J Roentgenol. 2019;212:293-9.
43. Wallis MG. Artificial intelligence for the real world of breast screening. Eur J Radiol. 2021;144:109661.

Hong Kong J Radiol. 2023;26:266-70. Epub 20 Nov 2023 | https://doi.org/10.12809/hkjr2217540

CASE REPORT

Ruptured Cervical Radiculomedullary Artery Mycotic Aneurysm Presenting with Intracranial and Spinal Subarachnoid Haemorrhage: A Case Report

SH Liu[1], NL Chan[2], NR Mahboobani[1], TL Poon[2], WL Poon[1]

[1]Department of Radiology and Imaging, Queen Elizabeth Hospital, Hong Kong SAR, China
[2]Department of Neurosurgery, Queen Elizabeth Hospital, Hong Kong SAR, China

CASE PRESENTATION

A 64-year-old Chinese man with no significant past medical history presented to the Accident and Emergency Department of our institution in December 2021 with a 1-day history of headache and vomiting. He reported no head injury, seizure or loss of consciousness. Physical examination revealed no focal neurological deficit. Non-contrast computed tomography (CT) of the brain showed subarachnoid haemorrhage predominantly in the posterior cranial fossa, extending to the spinal canal at the C3 vertebral level, and to a lesser extent in the basal cisterns and at the inferior frontal regions (Figure 1). CT angiogram of the head and neck arteries revealed a 2-mm arterial-enhancing lesion in the cervical spine canal at the C2/3 vertebral level (Figure 2). It appeared to arise from a branch of the right vertebral artery and was connected to a prominent midline vasculature along the anterior surface of the spinal cord. No intracranial vascular lesion was identified.

Diagnostic cerebral and cervical spine catheter angiography was performed 3 days after admission. On right vertebral artery angiogram, there was a lobulated fusiform aneurysm at the right C4 radiculomedullary artery measuring 7.2 mm in length and 2.5 mm in diameter (Figure 3). This radiculomedullary artery is the dominant supply to the anterior spinal artery in the cervical region and corresponds to the findings on CT angiogram. There was no evidence of arteriovenous shunting. Subsequent magnetic resonance imaging of the spine revealed a contrast-enhancing lesion within the cervical spine canal (Figure 4), corresponding to the CT- and angiography-detected aneurysm. There was no evidence of spinal arteriovenous shunting, vascular malformation or tumours.

The patient developed fever after admission. Initial blood tests showed normal white blood cell count but neutrophilia. Repeated blood tests revealed leucopenia with persistent neutrophilia, thrombocytopenia and elevated C-reactive protein level. Blood culture yielded *Klebsiella pneumoniae* species. The patient was prescribed antibiotics. Echocardiogram showed no evidence of myocardial infarction, endocarditis

Correspondence: *Dr SH Liu, Department of Radiology and Imaging, Queen Elizabeth Hospital, Hong Kong SAR, China*
Email: lsh264@ha.org.hk

Submitted: 23 Feb 2022; Accepted: 11 Aug 2022.

Contributors: SHL, NRM and WLP designed the study. All authors acquired and analysed the data. SHL and NLC drafted the manuscript. NRM, TLP and WLP critically revised the manuscript for important intellectual content. All authors had full access to the data, contributed to the study, approved the final version for publication, and take responsibility for its accuracy and integrity.

Conflicts of Interest: All authors have disclosed no conflicts of interest.

Funding/Support: This study received no specific grant from any funding agency in the public, commercial, or not-for-profit sectors.

Data Availability: All data generated or analysed during the present study are available from the corresponding author on reasonable request.

Ethics Approval: The patient was treated in accordance with the Declaration of Helsinki and provided verbal consent for publication.

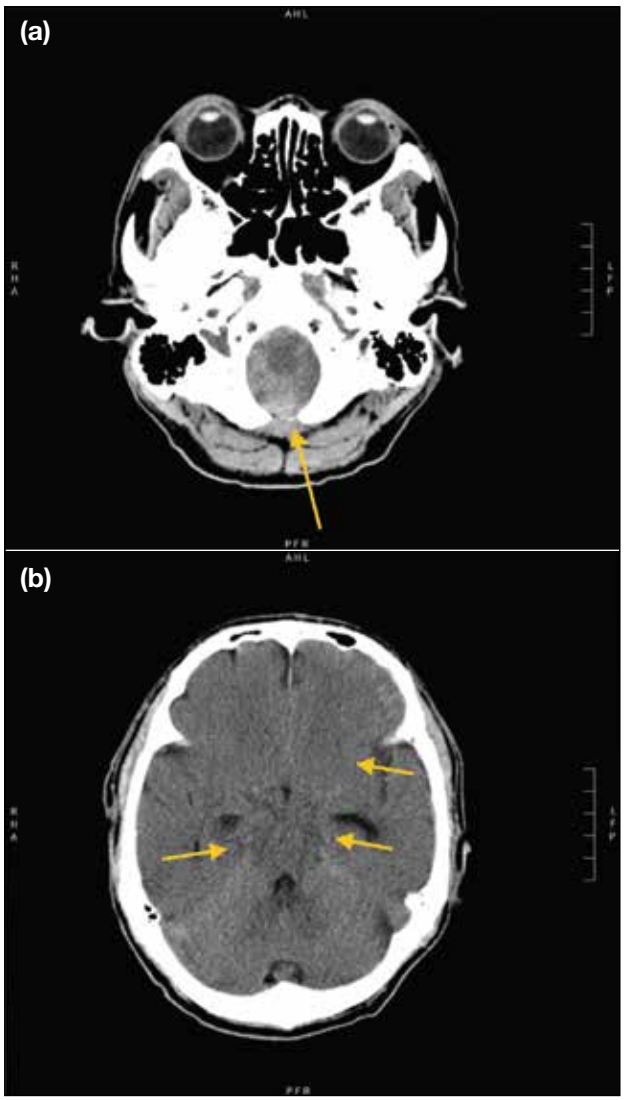

Figure 1. Non-contrast computed tomography of the brain at the level of foramen magnum (a) and basal cisterns (b). Subarachnoid haemorrhage is shown (arrows), predominantly in the posterior cranial fossa, especially at the foramen magnum.

or valvular vegetation. He remained stable with no new neurological signs or symptoms. Laboratory tests showed subsequent normalisation of white blood cell counts, platelet count and C-reactive protein level. Follow-up diagnostic catheter angiography of the right vertebral artery was performed 3 weeks after the first catheter angiography. There was no opacification of the aneurysm, suggesting that it is healed. The right C4 radiculomedullary artery remained patent, with supply to the anterior spinal artery visualised (Figure 5).

With the available clinical history, laboratory test results, and spontaneous occlusion of the aneurysm during antibiotic therapy, the most likely diagnosis for this patient was ruptured mycotic aneurysm at the right C4 radiculomedullary artery. The patient remained stable with neither altered consciousness nor focal neurological deficit. He completed a 6-week course of antibiotics as per the microbiologist's recommendation and was discharged uneventfully.

DISCUSSION

Spinal artery aneurysm is a rare cause of spinal or intracranial subarachnoid haemorrhage. Diagnosis of spinal artery aneurysms can be challenging and is sometimes delayed due to the rarity of the condition. These aneurysms have different morphological features to those of intracranial origin. They are usually fusiform, without a defined neck, and often not related to arterial branching sites.[1] In addition, they are usually associated with underlying vascular lesions such as arteriovenous malformation[2] or fistula.[3] There are also reported cases of association with tumours (e.g., haemangioblastoma),[4] aortic coarctation[2] and Moyamoya disease.[5] Other causes include underlying vasculopathy such as Behçet's disease,[6] Sjögren's syndrome,[7] systemic lupus erythematosus,[8] and pseudoxanthoma elasticum.[9] Mycotic aneurysms, as an alternative consideration, are rarely reported.[1,10]

There is no standardised treatment for ruptured radiculomedullary artery aneurysm due to its rare occurrence and varying aetiology.[11,12] Management should be tailored to each patient and take account of the size of haematoma, size of aneurysm, neurological symptoms, and feasibility and risk of intervention.

Vascular anatomy should be thoroughly evaluated prior to endovascular intervention or surgery. Cross-sectional imaging such as computed tomography or magnetic resonance angiography and catheter angiography can be adopted to delineate the morphology and size of the aneurysm, size of the relevant arteries, and pattern of vascular supply to the relevant segment of the spinal cord.

Dabus et al[13] reported a case of spontaneous thrombosis of a posterior radiculomedullary artery dissecting aneurysm with its parent artery in their case series, of which the patient showed no neurological deterioration on follow-up. This may have been due to the presence of good anastomoses of the radiculopial and radiculomedullary arteries. This emphasises the importance of angiographic evaluation of the arterial supply to the spinal cord. If the

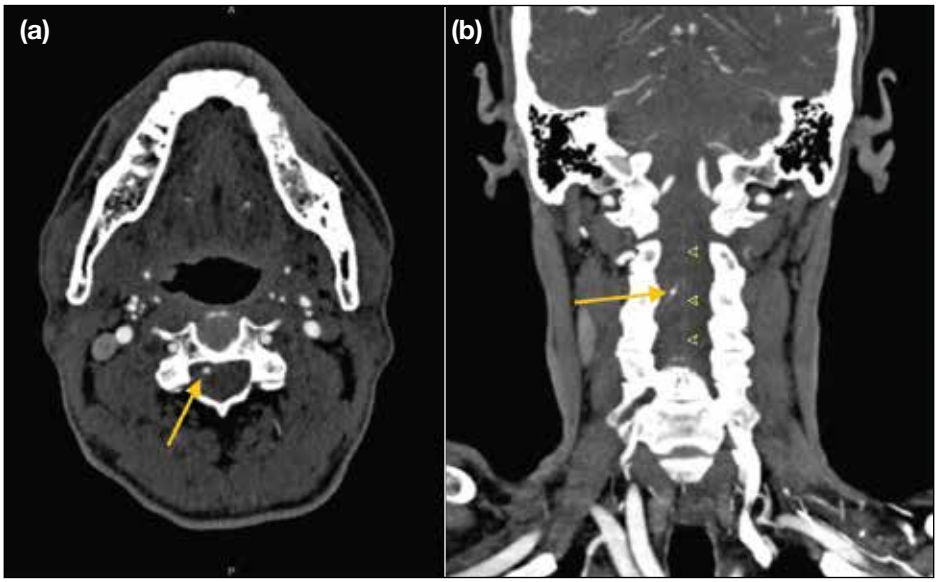

Figure 2. Computed tomography angiogram of the head and neck in axial plane (a) and coronal plane (b) showing tiny arterially enhancing lesion (arrows) in the cervical spinal canal at the C2/3 vertebral level arising from a branch of the right vertebral artery and connecting to the later catheter angiography–confirmed anterior spinal artery (arrowheads in [b]).

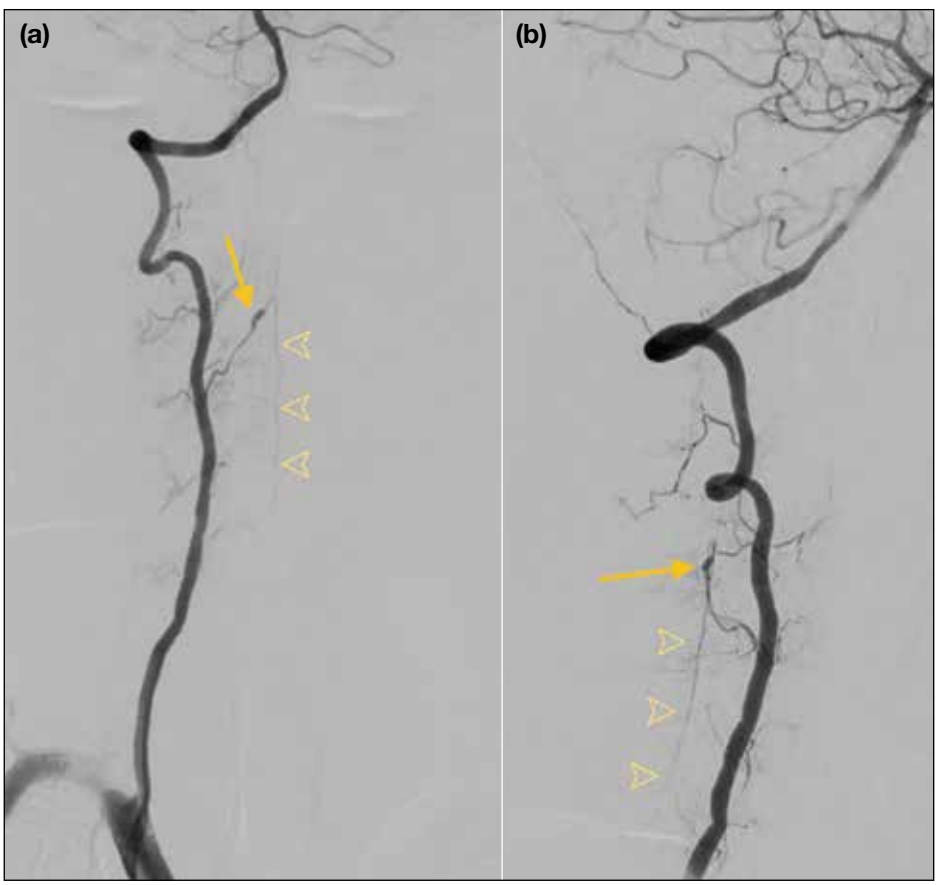

Figure 3. Digital subtraction catheter angiography of the right vertebral artery in anteroposterior projection (a) and lateral projection (b). A lobulated fusiform aneurysm (arrows) is seen at the right C4 radiculomedullary artery, which showed supply to the anterior spinal artery (arrowheads).

culprit artery shows a dominant supply to the relevant segment of cord, thrombosis or inadvertent injury during intervention may jeopardise the spinal cord blood supply. This has to be taken into account when deciding the suitable treatment strategy for each patient.

Endovascular intervention for small fusiform aneurysm without surgical neck at a very small size vessel can be

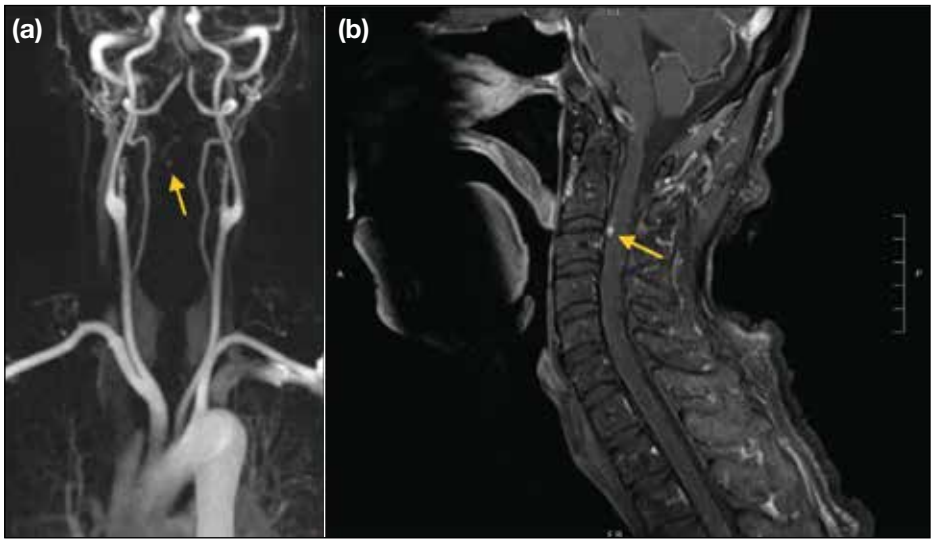

Figure 4. (a) Time-resolved magnetic resonance imaging angiography and (b) post-gadolinium T1-weighted magnetic resonance imaging with fat saturation of the cervical spine. The radiculomedullary aneurysm (arrows) is demonstrated as an enhancing lesion in the spinal canal.

Figure 5. Digital subtraction catheter angiography of the right subclavian artery in anteroposterior projection. Previously noted right C4 radiculomedullary artery aneurysm has healed. Anterior spinal artery is visualised (arrowheads).

technically challenging and carries the potential risk of arterial thrombosis causing spinal ischaemia. In the case of large aneurysm or large haematoma with considerable mass effect, surgery such as clipping or resection may be a better option to reduce compression on the adjacent spinal cord and/or nerve roots.

Cases of resolution or thrombosis of spinal artery aneurysms have been reported,[1,6,7,13-15] either with a conservative approach or with medical treatment when an underlying cause is determined. In cases with small haematoma, minimal or mild neurological symptoms, and technically challenging and high-risk intervention, a conservative approach or medical treatment to target the underlying cause are reasonable options.

In our patient, apart from headache and vomiting, there was no focal neurological deficit. Aetiology was presumed to be a mycotic aneurysm. There was potentially high surgical risk including postoperative neurological deterioration. Medical treatment with antibiotic therapy was adopted.

CONCLUSION

Radiologists should remain alert for spinal artery mycotic aneurysm as a rare cause of subarachnoid haemorrhage. Treatment varies with the size, location and morphology of the aneurysm, vascular anatomy of the spinal arteries, presenting symptoms, and risk of intervention including potential neurological deterioration. Decision for intervention should be based on the balance of

risks and benefits. In patients with mild symptoms and high surgical risk, medical treatment with antibiotics is a reasonable treatment choice. Follow-up imaging including catheter angiography should be considered to monitor progress and guide further management.

REFERENCES

1. Berlis A, Scheufler KM, Schmahl C, Rauer S, Götz F, Schumacher M. Solitary spinal artery aneurysms as a rare source of spinal subarachnoid hemorrhage: potential etiology and treatment strategy. ANJR Am J Neuroradiol. 2005;26:405-10.
2. Rengachary SS, Duke DA, Tsai FY, Kragel PJ. Spinal arterial aneurysm: case report. Neurosurgery. 1993;33:125-9; discussion 129-30.
3. Malek AM, Halbach VV, Phatouros CC, Higashida RT, Dowd CF, Wachhorst S, et al. Spinal dural arteriovenous fistula with an associated feeding artery aneurysm: case report. Neurosurgery. 1999;44:877-80.
4. Berlis A, Schumacher M, Spreer J, Neumann HP, van Velthoven V. Subarachnoid haemorrhage due to cervical spinal cord haemangioblastomas in a patient with von Hippel-Lindau disease. Acta Neurochir (Wien). 2003;145:1009-13.
5. Walz DM, Woldenberg RF, Setton A. Pseudoaneurysm of the anterior spinal artery in a patient with Moyamoya: an unusual cause of subarachnoid hemorrhage. AJNR Am J Neuroradiol. 2006;27:1576-8.
6. Bahar S, Coban O, Gürvit IH, Akman-Demir G, Gökyiğit A. Spontaneous dissection of the extracranial vertebral artery with spinal subarachnoid haemorrhage in a patient with Behçet's disease. Neuroradiology. 1993;35:352-4.
7. Klingler JH, Gläsker S, Shah MJ, Van Velthoven V. Rupture of a spinal artery aneurysm attributable to exacerbated Sjögren syndrome: case report. Neurosurgery. 2009;64:E1010-1; discussion E1011.
8. Fody EP, Netsky MG, Mrak RE. Subarachnoid spinal hemorrhage in a case of systemic lupus erythematosus. Arch Neurol. 1980;37:173-4.
9. Kito K, Kobayashi N, Mori N, Kohno H. Ruptured aneurysm of the anterior spinal artery associated with pseudoxanthoma elasticum. Case report. J Neurosurg. 1983;58:126-8.
10. Nakamura H, Kim P, Kanaya H, Kurokawa R, Murata H, Matsuda H. Spinal subarachnoid hemorrhage caused by a mycotic aneurysm of the radiculomedullary artery: a case report and review of literature. NMC Case Rep J. 2015;2:49-52.
11. Crobeddu E, Pilloni G, Zenga F, Cossandi C, Garbossa D, Lanotte M. Dissecting aneurysm of the L1 radiculomedullary artery associated with subarachnoid hemorrhage: a case report. J Neurol Surg A Cent Eur Neurosurg. 2022;83:99-103.
12. van Es AC, Brouwer PA, Willems PW. Management considerations in ruptured isolated radiculopial artery aneurysms. A report of two cases and literature review. Interv Neuroradiol. 2013;19:60-6.
13. Dabus G, Tosello RT, Pereira BJ, Linfante I, Piske RL. Dissecting spinal aneurysms: conservative management as a therapeutic option. J Neurointerv Surg. 2018;10:451-4.
14. Yang TK. A ruptured aneurysm in the branch of the anterior spinal artery. J Cerebrovasc Endovasc Neurosurg. 2013;15:26-9.
15. Longatti P, Sgubin D, Di Paola F. Bleeding spinal artery aneurysms. J Neurosurg Spine. 2008;8:574-8.

Hong Kong J Radiol. 2023;26:271-82. Epub 7 Dec 2023 | https://doi.org/10.12809/hkjr2217644

PICTORIAL ESSAY

Breast Ductography: A Hidden Diagnostic Gem for Patients with Abnormal Nipple Discharge

FFY Wan[1], EPY Fung[2], KM Kwok[2], KM Wong[2], LW Lo[2], WS Mak[2], WP Cheung[2]

[1]Department of Radiology and Imaging, Queen Elizabeth Hospital, Hong Kong SAR, China
[2]Department of Diagnostic and Interventional Radiology, Kwong Wah Hospital, Hong Kong SAR, China

INTRODUCTION

Nipple discharge is one of the commonest breast disease symptoms[1] and it can be physiological or pathological. Physiological nipple discharge typically involves multiple ducts in both breasts. Its common causes include pregnancy, lactation, endocrine disorders, and side-effects from medications.[2] Nipple discharge is considered pathological when it is unilateral single-duct discharge that is spontaneous, bloody, serous, or clear, with or without an associated palpable mass. The commonest aetiology is intraductal papilloma, which is seen in approximately 35% to 48% of patients, followed by ductal ectasia, which is the cause in 17% to 36% of patients.[1] Malignancy, most commonly ductal carcinoma in situ (DCIS), is found in 5% to 15% of patients.[3]

Breast ductography is a valuable investigation for assessment of single-duct nipple discharge. It involves administration of iodinated contrast into the duct, followed by mammographic examination. Ductography can unveil the cause of nipple discharge, including duct ectasia and fibrocystic changes. In the presence of filling defects suggestive of tumour, ductography assists in subsequent surgical planning by localising the abnormalities. The aim of this pictorial review is to illustrate the techniques for a successful examination and classical radiological findings of pathologies detected by ductography.

TECHIQUES FOR PERFORMING DUCTOGRAPHY

Indications and Contraindications

Pathological nipple discharge (PND) from single duct is the indication for ductography. The discharge must be observed during the examination so that the discharging duct can be appropriately identified and cannulated. Ductography is not recommended in lactating women or patients with active mastitis. Allergic reactions to the contrast injected into the ductal system are rarely reported. Nonetheless, patients with a history of mild or moderate allergic reactions to iodinated contrast should still be premedicated with steroids. Patients with a history

Correspondence: *Dr FFY Wan, Department of Radiology and Imaging, Queen Elizabeth Hospital, Hong Kong SAR, China*
Email: wfy471@ha.org.hk

Submitted: 1 Oct 2022; Accepted: 28 Nov 2022.

Contributors: All authors designed the study, acquired and analysed the data, drafted the manuscript, and critically revised the manuscript for important intellectual content. All authors had full access to the data, contributed to the study, approved the final version for publication, and take responsibility for its accuracy and integrity.

Conflicts of Interest: All authors have disclosed no conflicts of interest.

Funding/Support: This study received no specific grant from any funding agency in the public, commercial, or not-for-profit sectors.

Data Availability: All data generated or analysed during the present study are available from the corresponding author on reasonable request.

Ethics Approval: Ethics approval has been obtained from the Kowloon Central Cluster/Kowloon East Cluster Research Ethics Committee of Hospital Authority, Hong Kong (Ref No.: IRB-2022-176). The requirement for informed consent from patients was waived by the Committee due to retrospective nature of the study.

of severe allergic reactions (e.g., anaphylaxis) should not undergo ductography and alternative investigation such as magnetic resonance imaging (MRI) should be considered.[3]

Patient Preparation Prior to the Examination

Patient preparation is crucial for a successful examination. Patients should be reminded not to squeeze the nipple 1 day prior to the procedure. This ensures that adequate discharge is available on the day of examination for localisation and cannulation of the discharging duct orifice. Similar to mammography, patients should avoid applying deodorant, talcum powder, or lotion in their axillae or on their breasts, since these substances may masquerade as microcalcifications on mammography.

Review of Relevant Imaging

Before the examination, any recent breast imaging, including mammography and ultrasound, should be reviewed for any suspicious findings. If not recently performed, mammography with craniocaudal (CC) and mediolateral (ML) views should be performed for reference prior to duct cannulation.

Discharging Duct Cannulation and Contrast Injection

In our centre, the contrast injection system consists of a 30-gauge Jabczenski cannula (Cook Medical, Bloomington [IN], United States) with right-angled tip connected via small-volume extension tubing to a 1-mL syringe filled with 350 mg/mL non-ionic iodinated contrast material (Figure 1). The use of non-diluted contrast is advised for optimal ductal opacification. The extension tubing and cannula should be properly primed with contrast, and any air bubbles should be expelled from the system to avoid artefacts.

Depending on the location of the duct opening, the patient is placed in the sitting or oblique supine position with the ipsilateral arm resting comfortably on an arm rest (Figure 2). The nipple is cleansed to remove any dried secretions and given a sterile prep. Gentle pressure is applied in the periareolar region to elicit nipple discharge. Identification of the 'trigger point', i.e., the area which repeatedly produces nipple discharge when compressed, is helpful. Once nipple discharge is elicited, it is prudent to confirm that the discharge comes from a single pore since ductography is not the appropriate investigation for multi-pore discharge. In case of difficulty in localising the discharging pore, 'spreading' the nipple with the fingers on the adjacent skin can help visualise the

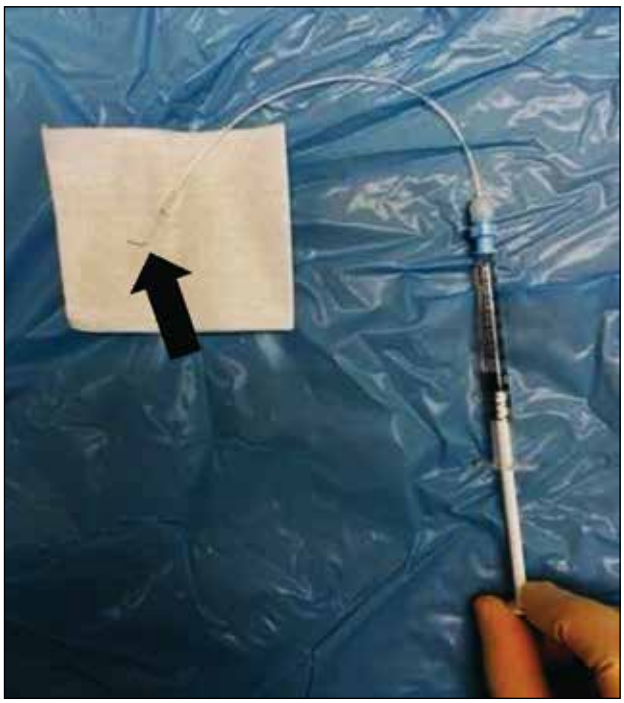

Figure 1. A 30-gauge Jabczenski cannula used for ductography. The right-angled tip (arrow) facilitates easy taping of the device in situ after cannulation.

Figure 2. Patient positioning: sitting or oblique supine position with the ipsilateral arm resting comfortably on an arm rest.

discharging orifice. With careful inspection, the orifice of the discharging duct may appear relatively patulous and slightly erythematous. Once the location of the discharging orifice is confirmed, the nipple is stabilised between the thumb and the index finger with gentle elevation (Figure 3). The tip of the cannula is placed with application of gentle downward guidance (Figure 4). In case of difficulty in cannulating the discharging duct, gentle probing with careful rotation or angulation along the pore may result in successful cannulation. If the most superficial part of the orifice is cannulated but resistance is encountered during further insertion, it is advised to maintain gentle pressure with careful rotation or angulation; forceful cannulation should always be avoided due to risk of ductal perforation.

Figure 3. Stabilising and gently elevating the nipple to facilitate cannulation of the discharging duct.

Figure 4. Placing the tip of the cannula into the orifice of the discharging duct with application of gentle downward guidance.

After successful cannulation, the cannula should be held in position against the nipple. Approximately 0.2 to 0.4 mL of non-ionic contrast is introduced by slow and gentle injection until contrast reflux, high resistance, or pain occurs. Small lesions may be obscured if too much contrast is injected; it is therefore recommended to begin with small amounts. Because the ducts are fragile, pain or a burning sensation may indicate duct perforation or contrast extravasation. Either symptom is an indication to stop further contrast injection. The cannula position is maintained in place by taping it onto the skin (Figure 5), which is facilitated by the right-angled tip of the cannula. This renders further contrast injection feasible and reduces contrast leakage upon subsequent breast compression for mammographic acquisition.

Mammographic Acquisition

The contrast injection system should be held in place and can be secured by taping the syringe and extension tubing onto the patient's chest (Figure 6). Attention should be paid when transferring the patient to the mammography department to prevent the cannula from slipping out.

Mammograms with CC and ML views are subsequently performed. An additional magnification view is useful for detecting faint or subtle microcalcifications associated with the abnormal ductal system. One

Figure 5. Maintaining the cannula in place by taping it onto the skin.

Figure 6. Securing the contrast injection system in place by taping the syringe and extension tubing onto the patient's chest.

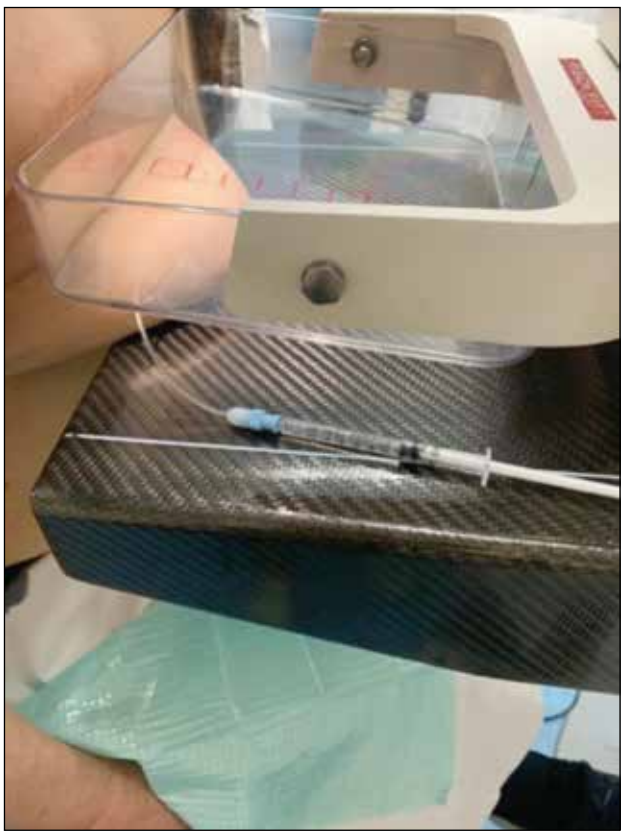

Figure 7. During mammographic acquisition, avoid overlapping of the syringe or extension tubing with the breast parenchyma to avoid abnormalities being obscured.

suggestion when performing mammography is to avoid overlapping of the syringe or extension tubing with breast parenchyma during mammographic acquisition to avoid abnormalities being obscured (Figure 7). If there is significant superimposition of the opacified ducts, a standard ML oblique view or a rolled CC view can be considered. Spot compression views can also be acquired if needed.

Supplementary Ultrasound

After the mammographic examination, supplementary ultrasound is performed with particular attention to any retroareolar or ductal abnormalities and areas with corresponding mammographic abnormalities. It is helpful to perform ultrasound first with the cannula still in situ. The advantage of doing so is that the discharging ductal system may still be distended by the contrast, making any intraductal lesions more conspicuous, and the relationship of the distended ducts and adjacent lesions may be better delineated. Afterwards, the cannula can be removed and the retroareolar region can be scrutinised again.

Because the orifices on the nipple can be closely related and there may be communication between different ducts, this renders the possibility of cannulating the wrong duct, resulting in suboptimal assessment of the ductal system harbouring the pathology. This highlights the importance of careful identification and precise cannulation of the discharging orifice.

Patient Selection

A total of 125 consecutive patients referred to our institution for ductography from January 2016 to July 2022 were reviewed. The procedure was not performed in 20 patients with no nipple discharge during the examination (16.0%) and in five patients with discharge from multiple ducts (4.0%). The examination could not be completed in five patients with failed cannulation (4.0%), two patients with resistance on contrast injection (1.6%), and six patients with contrast extravasation (4.8%). Among patients who completed the procedure, intraductal papilloma (24.1%) was the commonest pathology, followed by duct ectasia (21.8%), DCIS (10.3%), fibrocystic change (4.6%), duct adenoma (1.1%), and invasive carcinoma (1.1%). The rest

(36.8%) had no abnormal findings. Cases with variable normal and pathological ductographic appearances were selected for demonstration.

Imaging Findings

Normal Ductographic Appearances

A normal duct arborises from a single-entry point on the nipple into smaller ducts extending peripherally. Normal ducts are thin and smooth-walled with no filling defects or wall irregularities. Normal ductograms may show variability in ductal calibre, branching patterns, and parenchymal distribution as shown in Figure 8. However, the significance of different branching patterns, extent of ductal distribution, and ductal calibres is unknown.

Lobular blush is caused by contrast filling the lobular portion of the terminal duct lobular unit and is a finding of no clinical significance (Figure 9). It occurs when the ductal system has reached its maximum pressure and there is risk of extravasation with additional contrast administration.

Air bubbles can occasionally be seen within the ducts. Their round morphology and change in position between radiographs are usually sufficient for differentiating them from genuine lesions (Figure 10).

Extravasation

In the event of contrast extravasation (Figure 11), patients usually complain of pain or a burning sensation, but some may be asymptomatic. Common causes include administration of too much contrast material, forceful contrast administration, or too-vigorous manipulation of the cannula causing wall perforation. Infrequently, malignancy causing destruction of ductal wall integrity may lead to extravasation. Since the presence of extravasation may obscure the underlying pathology, the procedure should be rescheduled 7 to 14 days later.

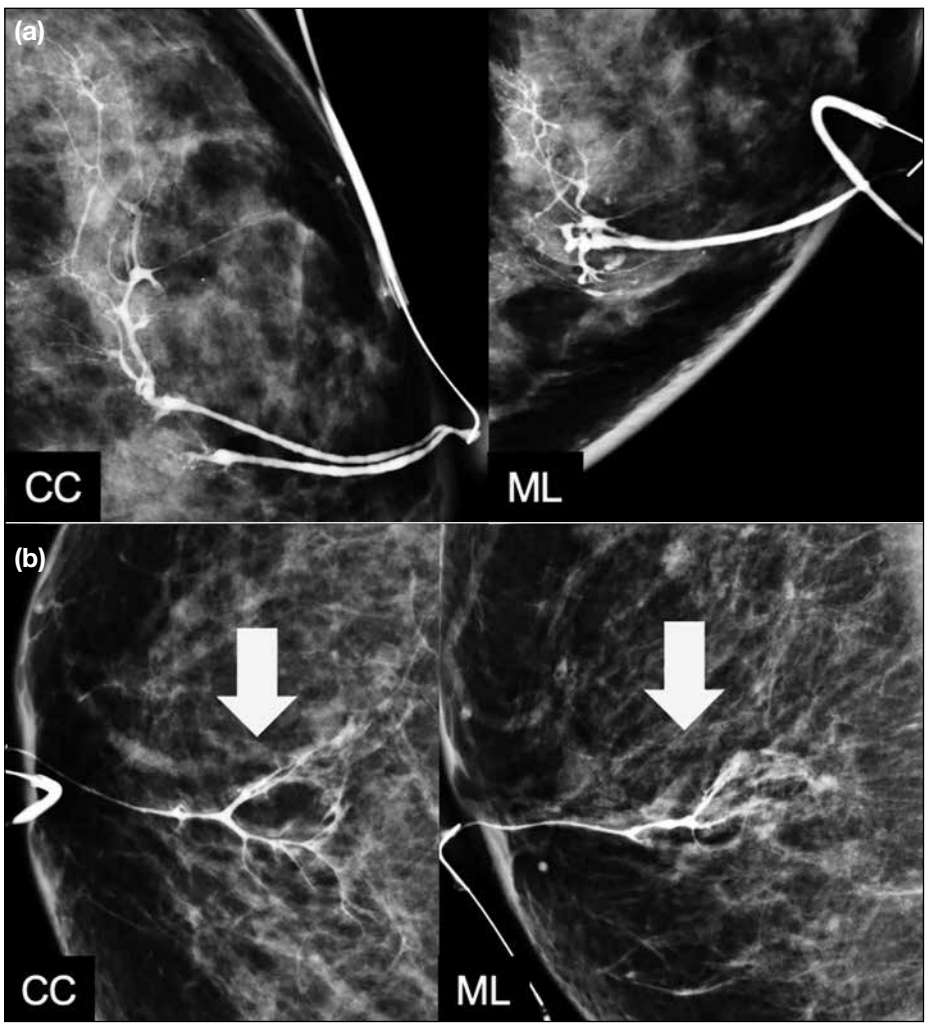

Figure 8. Variable appearances of normal ductograms with craniocaudal (CC) and mediolateral (ML) views. (a) Normal ductal calibre with normal branching and parenchymal distribution. (b) Relatively attenuated ductal calibre with less branching and limited parenchymal distribution.

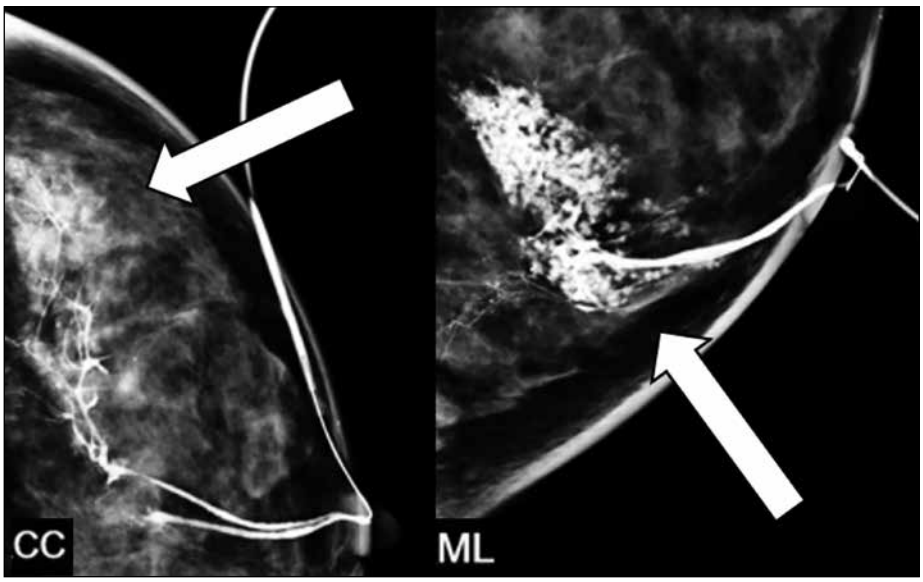

Figure 9. Ductography with craniocaudal (CC) and mediolateral (ML) views. Lobular blush (arrows) due to contrast filled the lobular portion of the terminal duct lobular unit, which is a normal finding.

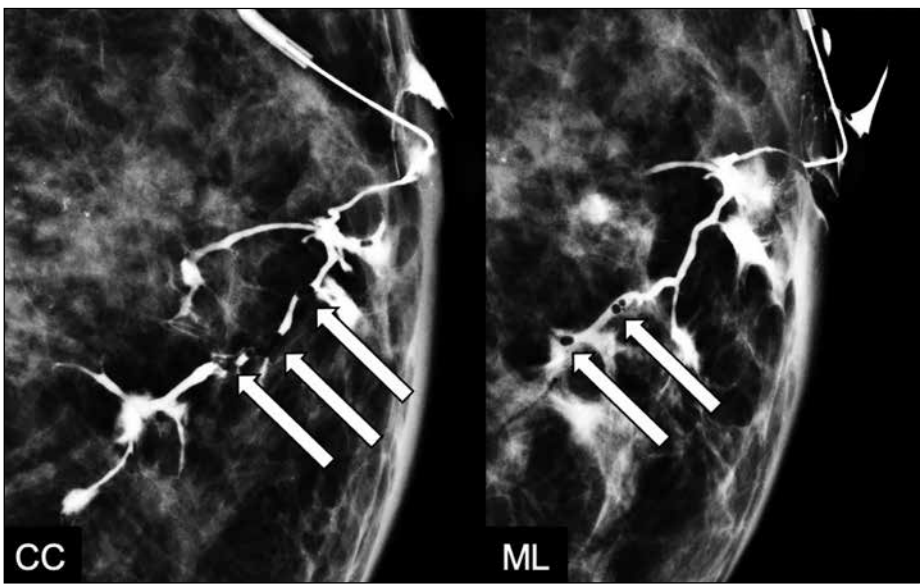

Figure 10. Ductography with craniocaudal (CC) and mediolateral (ML) views. Air bubbles seen as well-defined filling defects within the ducts, characteristically shifting in position between radiographs (arrows).

Duct Ectasia

Duct ectasia refers to non-specific dilatation of mammary ducts and is defined as ductal calibre more than 3 times the width of the cannula.[4] It can cause both physiological and PND. Ductography typically demonstrates a dilated ductal system without intraductal filling defects, ductal wall irregularities, ductal obstruction, or periductal contrast extravasation (Figure 12).

Fibrocystic Change

Fibrocystic change is benign alteration in the terminal ductal lobular unit with or without associated fibrosis. As one of the primary components of fibrocystic change, cysts develop from progressive lobular distension. Cysts communicating with ducts could lead to nipple discharge by decompression of cyst fluid into ducts. Ductography shows normal ducts communicating with cysts (Figure 13).

Intraductal Papilloma

Papillomas are benign masses of breast duct epithelium with a fibrovascular stalk attached to the duct wall. They may be single or multiple and may extend along the ducts. When large, they can appear to be encysted

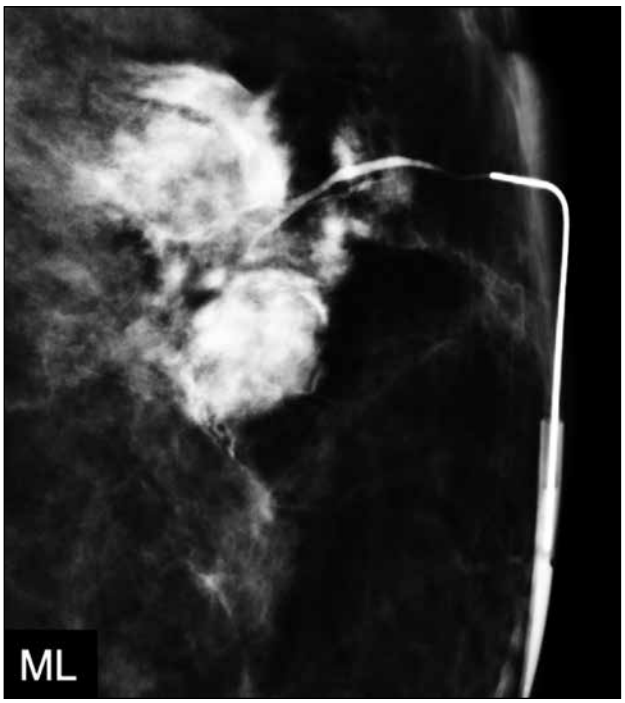

Figure 11. Ductography with mediolateral (ML) view. Contrast extravasation obscured the ductal system, rendering suboptimal assessment.

and multilobulated. This is the commonest cause of spontaneous unilateral single-orifice nipple discharge, accounting for 35% to 48% of cases.[1] The mammogram is frequently negative and ductography could be useful for its detection. Ductographic findings include single intraductal filling defects, multiple intraductal filling defects, ductal wall irregularities, and ductal obstruction (Figure 14a, 14b, 14c, and 14d, respectively). Rarely, contrast may be seen to accumulate within the cystic component of the mass which communicates with the duct (Figure 14e). Although these findings can be non-specific and seen in other entities, malignancy in particular, ductography is still useful in assessing the number, extent and location of the abnormalities. Surgical excision of papillomas with atypia is widely accepted with an upgrade rate to malignancy ranging from 21% to 38%.[2] However, the management of asymptomatic papillomas without atypia is more controversial, with an upgrade rate to malignancy of 2% to 12%.[2] Although some clinicians still recommend surgical excision of all papillary lesions, ultrasound-guided vacuum-assisted excision has been proven to be a safe and effective alternative with high rate of successful lesion removal.[5]

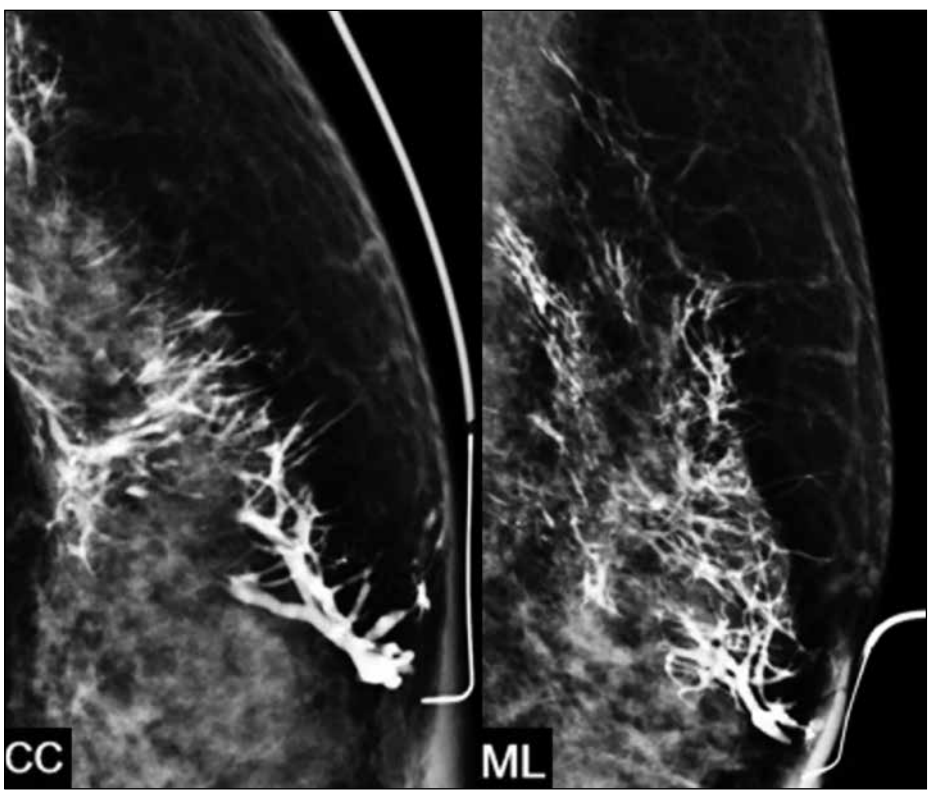

Figure 12. Ductography with craniocaudal (CC) and mediolateral (ML) views showing a dilated ductal system without filling defects, wall irregularities, obstruction or extravasation, suggestive of duct ectasia.

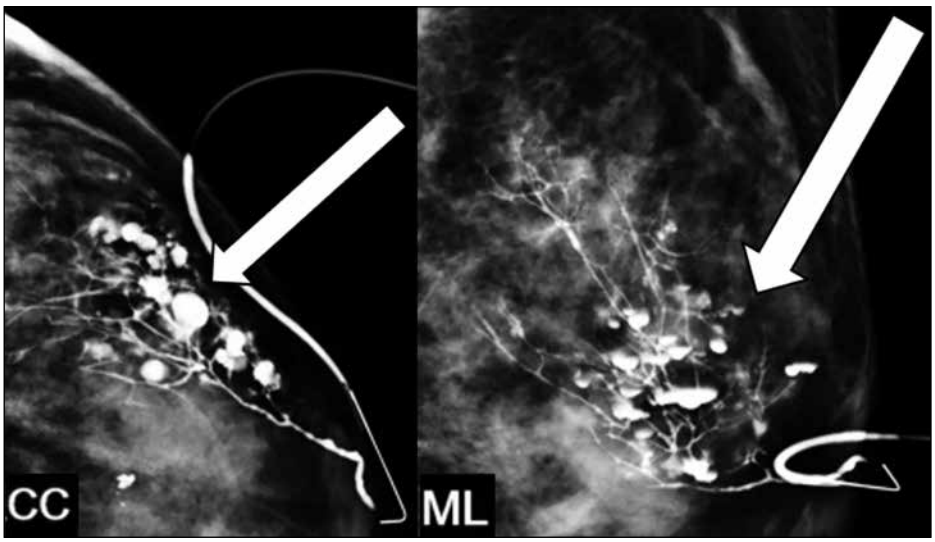

Figure 13. Ductography with craniocaudal (CC) and mediolateral (ML) views showing multiple cysts communicating with the ductal system (arrows) and the ductal system is otherwise normal, compatible with fibrocystic change.

Ductal Carcinoma In Situ

Cancer is found in 5% to 15% of patients with PND, the commonest type being DCIS. Up to 12% of patients with DCIS present with nipple discharge.[6] Ductographic findings of malignancy, most commonly DCIS, may mimic those of intraductal papillomas, including filling defects, abrupt ductal termination, ductal wall irregularities, and periductal contrast extravasation (Figure 15). Histological assessment would be helpful in differentiation of malignancy from other benign entities including papillomas.

Duct Adenoma

Duct adenomas are uncommon benign glandular tumours which usually fill and distend the ductal lumen. They are usually single, occasionally multiple, nodular lesions occupying medium- and large-sized breast ducts but not major subareolar ducts. Because of their location, they more commonly present as palpable lumps, unlike intraductal papillomas which are more likely associated with nipple discharge. Figure 16 illustrates a rare case of duct adenoma presenting with nipple discharge.

DISCUSSION

In patients with PND, mammography and ultrasound are first-line investigations for women who are ≥ 30 years of age.[1] Mammographic abnormalities were found to be positive in 50% to 90% of patients with breast cancer and in < 50% of patients with intraductal papilloma.[7] Mammography often fails to demonstrate lesions that are small, lack calcifications, or are located entirely within the duct.[8] Nevertheless, it is still a crucial initial imaging modality. DCIS is the commonest malignancy associated with PND and it may present as suspicious microcalcifications on mammography. Underlying invasive cancer may also present as mass or architectural distortion. Mammography may be complementary to ultrasound in women < 30 years of age if they are *BRCA*-positive or have other gene mutation predisposing to breast cancer. In particular, it should be considered in women < 30 years of age who present with suspicious masses on ultrasound. This is because mammography can detect any calcifications associated with the mass or the ducts. If present, the extent, pattern, and morphology of the calcifications are best assessed on mammography.[2]

Apart from mammography, ultrasound also plays an important role in the initial evaluation of PND. Ultrasound can identify sub-centimetre ductal abnormalities and associated ductal changes which are occult on mammography, especially in dense breasts. In a study, ultrasound examination in patients with PND but negative mammographic findings led to detection of malignancy in 15% of cases.[9]

If no abnormality explaining the nipple discharge can be detected on both mammography and ultrasound, ductography is usually the next step in imaging examinations in our centre. The value of ductography as a second-line investigation is controversial. It is an invasive examination, although it is actually rather minimally invasive. Despite the possible events of contrast extravasation and ductal perforation, these are minor complications with no reported long-term

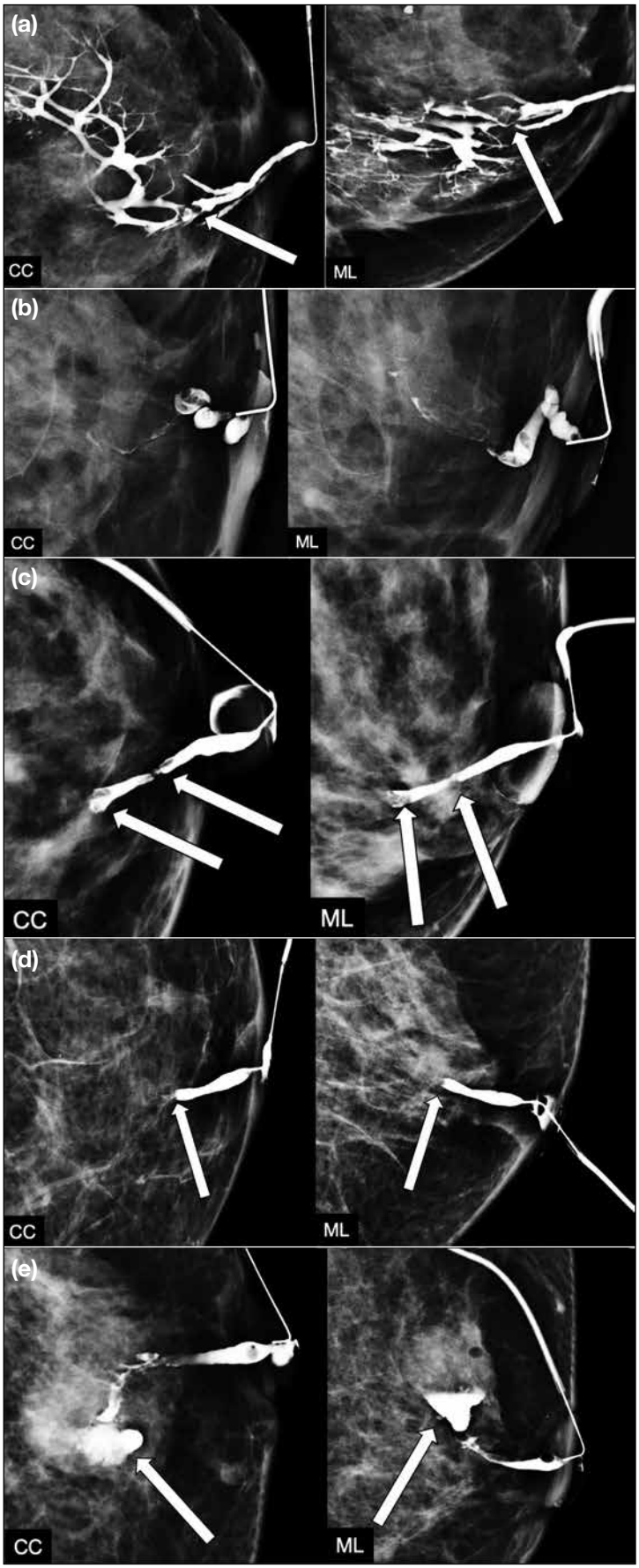

Figure 14. Mammography with craniocaudal (CC) and mediolateral (ML) views showing ductographic appearances of pathologically proven intraductal papillomas: (a) single intraductal filling defect (arrows); (b) multiple intraductal filling defects; (c) ductal wall irregularities (arrows); (d) ductal obstruction (arrows); and (e) contrast accumulation within the cystic component of the mass communicating with the mammary duct (arrows).

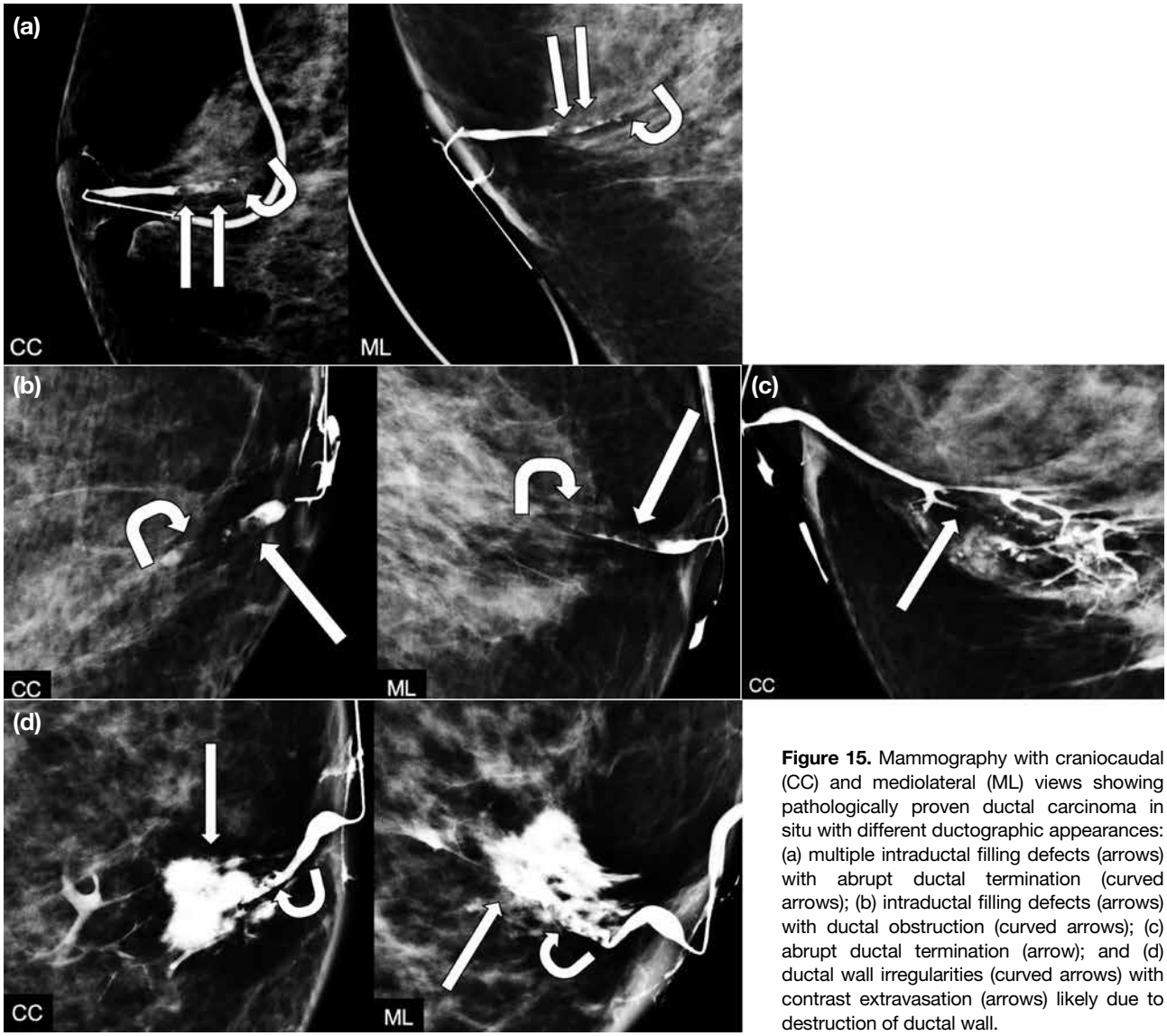

Figure 15. Mammography with craniocaudal (CC) and mediolateral (ML) views showing pathologically proven ductal carcinoma in situ with different ductographic appearances: (a) multiple intraductal filling defects (arrows) with abrupt ductal termination (curved arrows); (b) intraductal filling defects (arrows) with ductal obstruction (curved arrows); (c) abrupt ductal termination (arrow); and (d) ductal wall irregularities (curved arrows) with contrast extravasation (arrows) likely due to destruction of ductal wall.

consequences. The primary goal of ductography is to localise intraductal lesions and assist in surgical planning. Since there is considerable overlap in ductographic findings of papillary lesions and malignancy, histological correlation is usually required to ascertain the benign or malignant nature of an intraductal abnormality.[1]

Ductography is more sensitive than mammography and ultrasound but has lower specificity than those two modalities.[1] In cases of negative findings with conventional imaging, ductography has been shown to localise 76% of otherwise occult high-risk and malignant lesions.[9] However, a negative ductographic examination cannot be used to exclude the possibility of underlying malignancy, with a false negative rate reported to be 20% to 30%.[9]

The management approach for evaluating PND is evolving. Because of its high sensitivity in detecting breast malignancy and its capability for biopsy, breast MRI has emerged as the most sensitive modality in detecting malignancy. Contrast-enhanced breast MRI has been proposed for investigation when conventional imaging modalities have failed to identify the underlying cause of PND. It offers an alternative means when ductography is not performed due to risk of iodinated contrast reaction, failure to cannulate the duct, or patients' preference. MRI can enable detection of

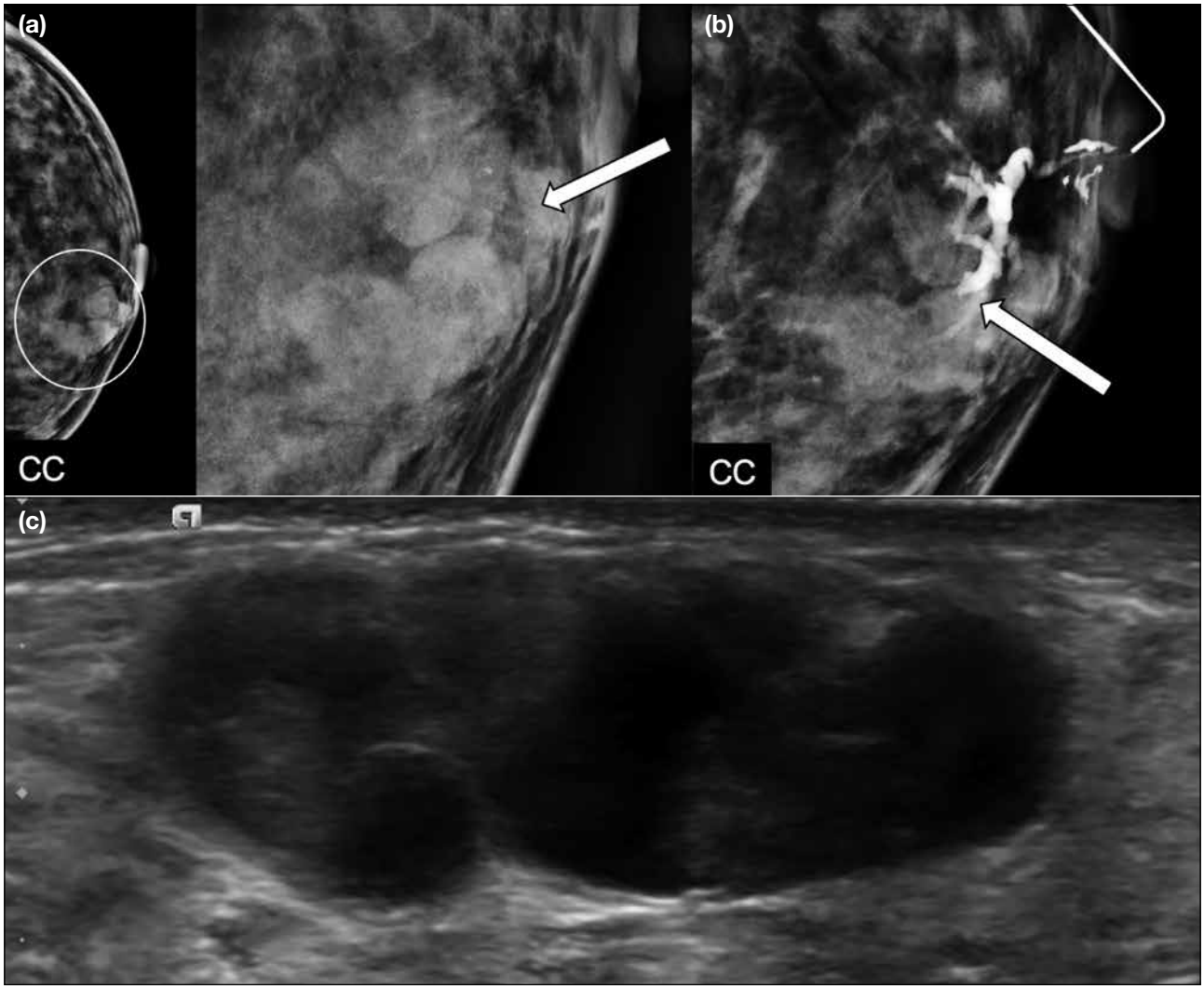

Figure 16. Histologically proven duct adenoma of the breast: (a) preliminary craniocaudal (CC) mammogram with additional spot compression view before ductogram showing an oval isodense mass at the inner part of left breast (circle) with partially obscured margins, associated with amorphous microcalcifications (arrow); (b) CC ductogram showing mildly prominent subareolar ducts and abrupt termination of the ductal system (arrow) near the mass; and (c) subsequent ultrasound demonstrated a mixed solid-cystic mass at 9 to 12 o'clock position of the periareolar region of the left breast.

lesions in peripheral ducts that are beyond the area normally encompassed by ductography or targeted ultrasound. In contrast to ductography, which only detects abnormalities in discharging ducts, MRI allows evaluation of the entire ductal system at the same time and enables identification of additional cancers in both the ipsilateral and contralateral breast. With increasing availability of MRI scanners and growing experience in MRI interpretation, there have been more reports showing the high sensitivity and negative predictive value of MRI for breast cancer. The European Society of Mastology guidelines evaluated 10 papers on the use of MRI in PND and concluded that there is still insufficient evidence to support routine use of MRI for these patients.[10] Its relatively high cost and poor accessibility in less developed countries, as well as patient factors (e.g., claustrophobia, severe obesity, and implantable devices not compatible with MRI examination), could be possible causes of its limited use in many departments. Nonetheless, patients with persistent symptoms after unremarkable or failed ductographic examination may benefit from MRI. Furthermore, it is recommended to perform MRI in *BRCA* mutation carriers and other high-risk patients to minimise radiation exposure.

A new area of research involves MR ductography with use of a three-dimensional heavily T2-weighted fat-suppressed sequence. It is non-invasive and does not require use of contrast. The discharging duct is often dilated with fluid and can be seen on heavily T2-weighted images. The presence of intraluminal filling defects, ductal wall irregularities, or ductal obstruction can be assessed. Compared with conventional ductography, MR ductography can show the distal part of a duct obstructed by an intraductal mass. On the other hand, it cannot reveal a non-dilated duct. According to a feasibility study involving 21 patients,[11] the indirect MR ductography sequence did not show significantly better performance when compared with conventional ductography. More large-scale studies with refinement of the sequence or fusion imaging with contrast-enhanced MRI could potentially be a fruitful area of research.

Apart from MRI, the addition of digital breast tomosynthesis (DBT) to conventional ductography has been investigated as a technique in the evaluation of PND. This three-dimensional reconstruction can provide sectional images from different projection angles, thus reducing overlap of the ductal system and tissue superimposition. Retrospective studies have compared the diagnostic performance of DBT-ductography and digital ductography, revealing higher sensitivity for DBT-ductography without compromise in specificity.[12,13] A recent prospective study by Tao et al[14] evaluated 128 patients with PND and concluded that DBT-ductography increases the sensitivity and specificity of lesion detection by enhancing the image quality without significant increase in the radiation dose. Further studies may be helpful in validating and generalising the findings of DBT-ductography in patients with PND.

Surgical duct excision has been the standard of care to exclude underlying malignancy. There has been increasing trend in adopting surveillance for patients with unremarkable findings on combined assessment using mammogram, ultrasound and ductograpohy.[2] Despite being the reference standard, microdochectomy cannot detect all malignancies, especially those located far from the nipple. Sanders and Daigle[15] examined the role of MRI as an alternative to microdochectomy. Among the 85 patients who underwent MRI prior to duct excision, eight malignant lesions (9.4%) were detected and seven out of these eight malignancies (87.5%) were identified on MRI. The authors proposed that a negative MRI study may obviate the need for microdochectomy in most patients.

CONCLUSION

Ductography is a practical, valuable, and cost-effective procedure in the diagnosis of intraductal lesions. Gaining familiarity with the procedure and including it in the evaluation of patients with PND may facilitate management for these patients. If ductography is technically unfeasible, MRI should be considered as an ancillary tool to investigate for the possible causes.

REFERENCES

1. Lee SJ, Trikha S, Moy L, Baron P, diFlorio RM, Green ED, et al. ACR Appropriateness Criteria® evaluation of nipple discharge. J Am Coll Radiol. 2017;14(5S):S138-53.
2. Gupta D, Mendelson EB, Karst I. Nipple discharge: current clinical and imaging evaluation. AJR Am J Roentgenol. 2021;216:330-9.
3. Patel BK, Falcon S, Drukteinis J. Management of nipple discharge and the associated imaging findings. Am J Med. 2015;128:353-60.
4. Cardenosa G. Clinical breast imaging: the essentials. Pennsylvania (PA): Wolters Kluwer; 2014: 381.
5. Chau CM, Fung EP, Wong CW, Kwok KM, Leung AY, Wong LK, et al. Ultrasound-guided vacuum-assisted excision of papillary breast lesions as an alternative to surgical excision: 7-year experience. Hong Kong J Radiol. 2020;23:253-60.
6. Barreau B, de Mascarel I, Feuga C, MacGrogan G, Dilhuydy MH, Picot V, et al. Mammography of ductal carcinoma in situ of the breast: review of 909 cases with radiographic-pathologic correlations. Eur J Radiol. 2005;54:55-61.
7. Orel SG, Dougherty CS, Reynolds C, Czerniecki BJ, Siegelman ES, Schnall MD. MR imaging in patients with nipple discharge: initial experience. Radiology. 2000;216:248-54.
8. Yoon JH, Yoon H, Kim EK, Moon HJ, Park YV, Kim MJ. Ultrasonographic evaluation of women with pathologic nipple discharge. Ultrasonography. 2017;36:310-20.
9. Morrogh M, Morris EA, Liberman L, Borgen PI, King TA. The predictive value of ductography and magnetic resonance imaging in the management of nipple discharge. Ann Surg Oncol. 2007;14:3369-77.
10. Sardanelli F, Boetes C, Borisch B, Decker T, Federico M, Gilbert FJ, et al. Magnetic resonance imaging of the breast: recommendations from the EUSOMA working group. Eur J Cancer. 2010;46:1296-316.
11. Nicholson BT, Harvey JA, Patrie JT, Mugler JP 3rd. 3D-MR ductography and contrast-enhanced MR mammography in patients with suspicious nipple discharge: a feasibility study. Breast J. 2015;21:352-62.
12. Moschetta M, De Ruvo V, Drago A, Troiano N, Paolicelli S, Rubini G, et al. DBT-galactography: a promising tool for improving the diagnostic workup of nipple discharge. Eur Radiol Exp. 2020;4:40.
13. Lee JY, Jang M, Kim SM, Yun BL. Galactography using digital breast tomosynthesis for the evaluation of pathologic nipple discharge: a comparison with 2D synthetic digital mammography. J Korean Soc Breast Screen. 2019;16:60-9.
14. Tao J, Liao H, Liu Y, Peng Q, Zhu W, Peng S, et al. Evaluation of breast galactography using digital breast tomosynthesis: a clinical exploratory study. Diagnostics (Basel). 2021;11:2060.
15. Sanders LM, Daigle M. The rightful role of MRI after negative conventional imaging in the management of bloody nipple discharge. Breast J. 2016;22:209-12.

Hong Kong J Radiol. 2023;26:283-92. Epub 30 Nov 2023 | https://doi.org/10.12809/hkjr2217566

PICTORIAL ESSAY

Mimics of Pituitary and Pineal Germ Cell Tumours on Imaging: A Pictorial Essay

CC Huang[1,2]

[1]*Department of Radiology, MacKay Memorial Hospital, Taipei, Taiwan*
[2]*Department of Medicine, MacKay Medical College, New Taipei City, Taiwan*

INTRODUCTION

Intracranial germ cell tumours (GCTs) comprise 0.4% to 9.4% of primary intracranial neoplasms and intracranial germinoma accounts for 50% to 70% of all intracranial GCTs.[1,2] They are characteristically located in the suprasellar and pineal regions. Apart from GCTs, other diseases are also found in the suprasellar and pineal regions.

In this pictorial essay, mimickers of intracranial GCTs are illustrated. These GCT mimics are based on a retrospective analysis of 313 consecutive cases collected over 29 years at a single hospital with a tentative or initial diagnosis of GCT but proven to be otherwise on histology.

GERM CELL TUMOURS

The most common locations of GCTs are the pineal gland and suprasellar regions. The levels of some oncoproteins may elevate in the serum or cerebrospinal fluid (CSF), including alpha-fetoprotein, beta-hCG, and placental alkaline phosphatase, depending on the tumour types.[3] Germinoma and teratoma are the most common and the second most common types of intracranial GCTs, respectively. Approximately 90% of intracranial germinoma patients are diagnosed before the age of 20 years.[2] The two most common locations of intracranial germinoma are the pineal region (37%-65%) and the suprasellar region (25%-49%), with approximately 8% of cases showing bifocal involvement in these two locations.[3,4] The male-to-female ratio is 1.88:1 in the suprasellar region; the ratio is even higher for pineal germinomas.[1] Tumour location, size, and resultant endocrine dysfunction are the main causes of clinical symptoms and signs in germinoma. The prodrome in suprasellar lesions can last from months to years, longer

Correspondence: *Dr CC Huang, Department of Radiology, MacKay Memorial Hospital, Taipei, Taiwan*
Email: hcc.5306@mmh.org.tw

Submitted: 15 Apr 2022; Accepted: 23 Oct 2022.

Contributor: The author designed the study, acquired the data, analysed the data, drafted the manuscript, and critically revised the manuscript for important intellectual content. The author had full access to the data, contributed to the study, approved the final version for publication, and takes responsibility for its accuracy and integrity.

Conflicts of Interest: The author has disclosed no conflicts of interest.

Funding/Support: This study received no specific grant from any funding agency in the public, commercial, or not-for-profit sectors.

Data Availability: All data generated or analysed during the present study are available from the corresponding author on reasonable request.

Ethics Approval: All procedures were conducted in accordance with the ethical standards of the institutional research committee and the Declaration of Helsinki. All patients were consented for the imaging examination in this study.

Acknowledgement: The author expresses thanks to the Division of Neuroradiology, Hospital of the University of Pennsylvania for their assistance during the study.

than that in pineal lesions. In suprasellar germinomas, symptoms related to diabetes insipidus often occur first, followed by other endocrine dysfunctions. As the tumour grows, visual impairment may occur due to compression of the optic chiasm; obstructive hydrocephalus is also possible if the drainage of CSF is affected. In pineal germinomas, the aqueduct and dorsal midbrain can be affected, resulting in obstructive hydrocephalus, diplopia, and Parinaud's syndrome. Other symptoms due to tumour dissemination or metastasis can develop.[4] Computed tomography (CT) of the head seldom shows calcification of the germinoma, but when located in the pineal region, it can enlarge and engulf the pineal calcification. In magnetic resonance imaging (MRI), germinoma usually presents as iso- to hyperintense to grey matter on T1-weighted and T2-weighted images, with marked enhancement and cyst formation, and hydrocephalus, as well as water restriction on diffusion-weighted imaging (DWI). Dissemination via the CSF and invasion of adjacent brain parenchyma also commonly occur.[3,4] Because of the risk of CSF seeding, imaging evaluation should include the entire neuroaxis; however, even with extensive involvement, the prognosis of germinomas is good because of the radiosensitive nature of these tumours.[3] The prognosis of teratoma varies, depending on the histological findings. Some clues to the diagnosis of germinoma have been proposed, such as engulfment of the pineal calcification and bifocal involvement with normal alpha-fetoprotein level in the serum and CSF. Nonetheless, surgical confirmation is usually required.[3,4] In our cases, there are typical instances of engulfment of the pineal calcification, doublet lesions, and also infiltrative lesions involving both frontal lateral ventricular walls (Figure 1). However, nongerminomatous GCTs can also demonstrate bifocal involvement.[1,2]

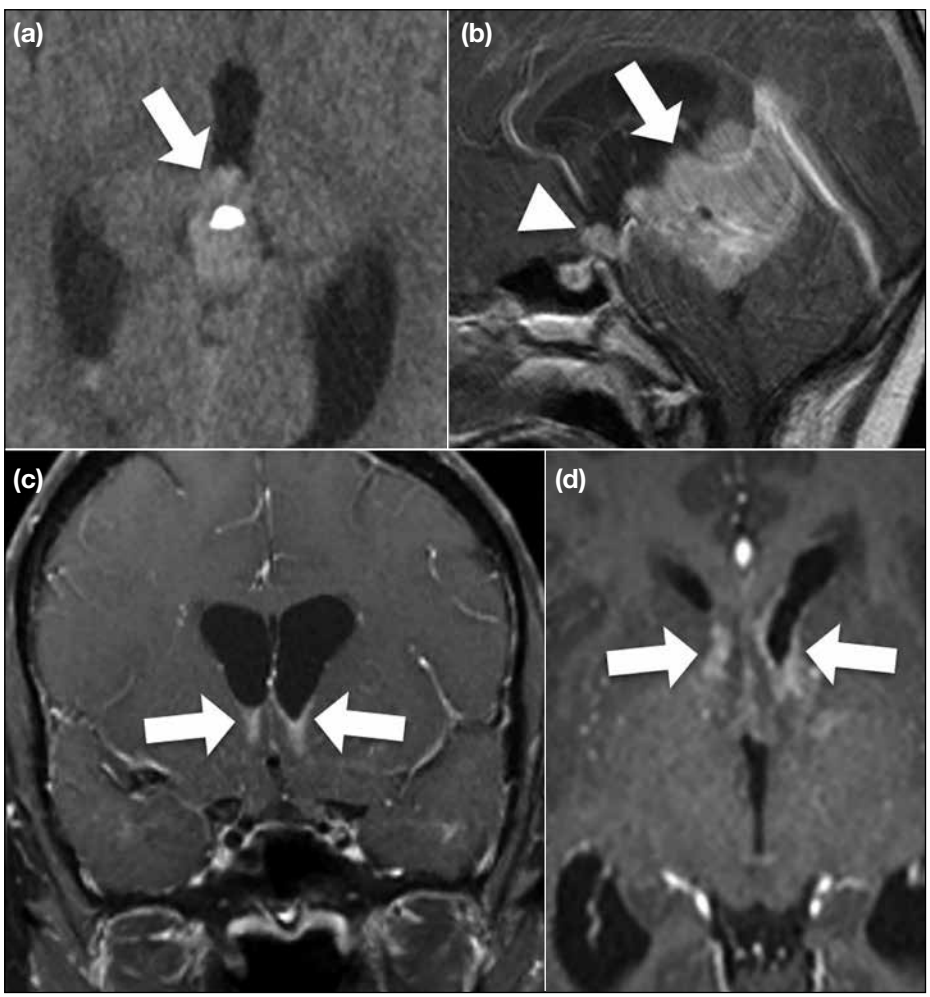

Figure 1. Germinoma. Case 1 (a) showing engulfment of the pineal calcification by a pineal germinoma (arrow) on axial nonenhanced computed tomography image. Case 2 (b) showing doublet germinoma lesions with a larger pineal component (arrow) and a smaller suprasellar component (arrowhead) on enhanced sagittal T1-weighted fat-suppressed image. Case 3 showing a rare presentation of a germinoma with bilateral enhancing frontal horn wall infiltration (arrows) on coronal (c) and axial (d) T1-weighted fat-suppressed images.

MIMICS OF SUPRASELLAR GERM CELL TUMOURS

Craniopharyngioma

Approximately 1.2% to 4.0% of paediatric brain tumours are craniopharyngiomas, which are commonly located in the sellar and suprasellar regions.[5] The adamantinomatous type is more common in childhood. Imaging features include calcifications and cystic components, which are found in our case (Figure 2).

Glial Cell Tumour

When located in the suprasellar region, the glial cell

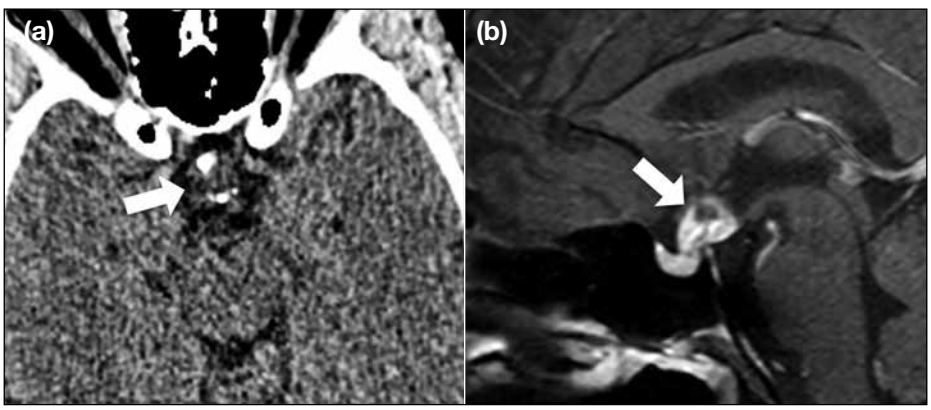

Figure 2. Adamantinomatous craniopharyngioma. Calcification is identified in the suprasellar tumour (arrow) on axial nonenhanced computed tomography (a) with strongly enhancing soft tissue and cystic portions of the tumour (arrow) on sagittal T1-weighted fat-suppressed image (b).

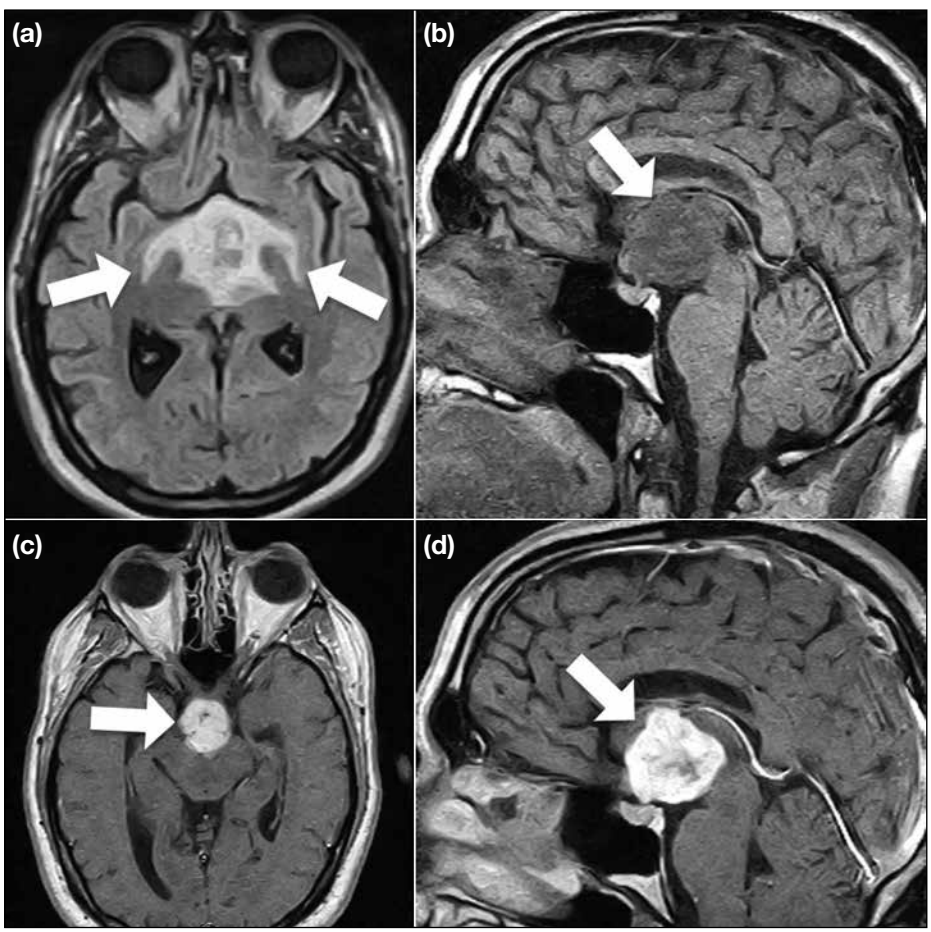

Figure 3. Glial cell tumour. The case displays suprasellar oedematous infiltration along both optic tracts (arrows) on nonenhanced axial T2-weighted fluid-attenuated inversion recovery image (a). The main tumour portion (arrows) is located in the suprasellar and retrochiasmatic region, with heterogeneous iso- to hypointensity on sagittal unenhanced T1-weighted image (b) and strong heterogeneous enhancement on the axial (c) and sagittal (d) T1-weighted enhanced images.

tumour is commonly referred to as an optic pathway glioma. These cases are usually diagnosed at 4 to 5 years of age.[6] Imaging findings include involvement along the course of optic pathway with variable enhancement and cystic components as well as calcifications. Sometimes, oedema in the optic pathway near the tumour is a diagnostic clue (Figure 3).[7]

Lymphocytic Hypophysitis

Lymphocytic hypophysitis is an autoimmune inflammatory disease with lymphocytic infiltration involving the pituitary gland, stalk, and hypothalamus, which can affect adults and children of both sexes.[8] Possible common symptoms include headache, hyper or hypofunction of pituitary gland, and diabetes insipidus.[8] Depending on disease involvement, typical imaging findings are strong enhancement and enlargement of the pituitary gland, stalk, and hypothalamus. Sometimes, loss of the neurohypophyseal bright spot is noted (Figure 4).[8] Delayed enhancement of the whole pituitary gland due to this disease is also described in the literature.[8] Repeated imaging studies are sometimes necessary because lesions might be found months after an initial normal imaging study.[8]

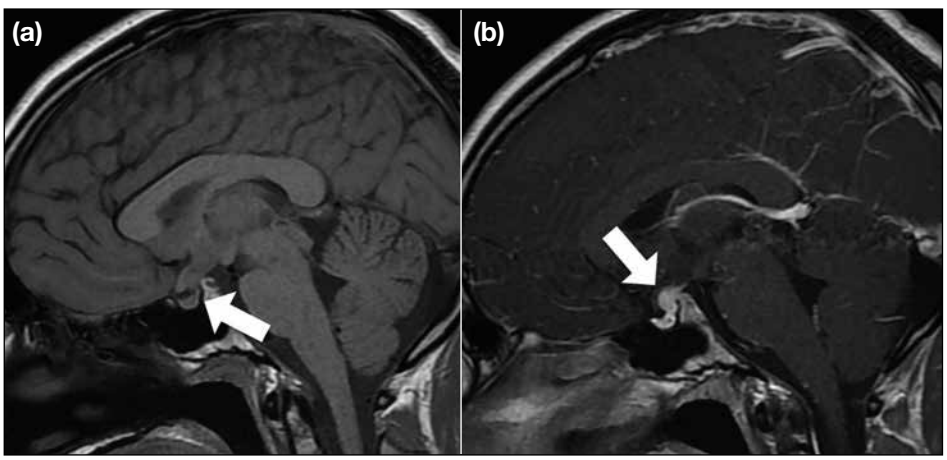

Figure 4. Lymphocytic hypophysitis. The case demonstrates the lesion presenting as thickening of the pituitary stalk with tapering in the sella; there is loss of the normal bright signal (arrow) in the neurohypophysis on sagittal T1-weighted image (a). Marked enhancement of the lesion (arrow) is found on enhanced sagittal T1-weighted image (b).

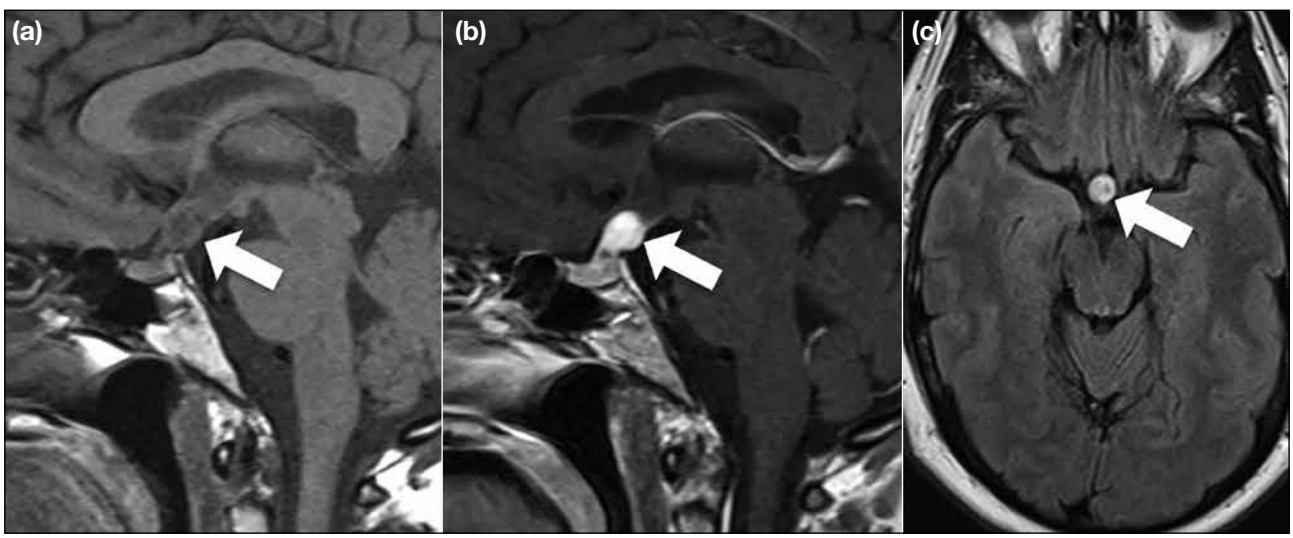

Figure 5. Pituicytoma. This case shows a well-defined iso- to hypointense suprasellar lesion (arrow) on sagittal T1-weighted image before contrast injection (a) and the lesion (arrow) is strongly enhanced after contrast injection (b). The lesion is iso- to hyperintense (arrow) on axial T2-weighted fluid-attenuated inversion recovery image (c).

Pituicytoma

Pituicytomas are rare benign tumours originating from a type of glial cell, the pituicyte, in the neurohypophysis and pituitary stalk. They usually affect adults with a slight male predominance.[9] The imaging presentation of pituicytoma is nonspecific but it usually presents as a well-defined homogeneously or heterogeneously enhancing solid mass in the sellar or suprasellar region (Figure 5). Calcification, adjacent bony changes, or necrosis are absent, but cystic portions sometimes can be identified.[9]

Pituitary adenoma

Pituitary adenoma is more common in adults but can be found in children.[7] It may display signal intensities similar to those of the adjacent normal pituitary gland on pre-contrast MRI and relatively less enhancement on

Figure 6. Pituitary adenoma. The tumour (arrow) involves the sellar and suprasellar regions and has marginal calcification and diffuse hyperdensity on nonenhanced axial computed tomography image (a). On axial T2-weighted image (b), the tumour (arrow) is mainly iso- to hyperintense, with focal hypointensity, possibly due to haemorrhage. The tumour (arrows) enhances heterogeneously in sagittal (c) and coronal (d) contrast-enhanced T1-weighted fat-suppressed images.

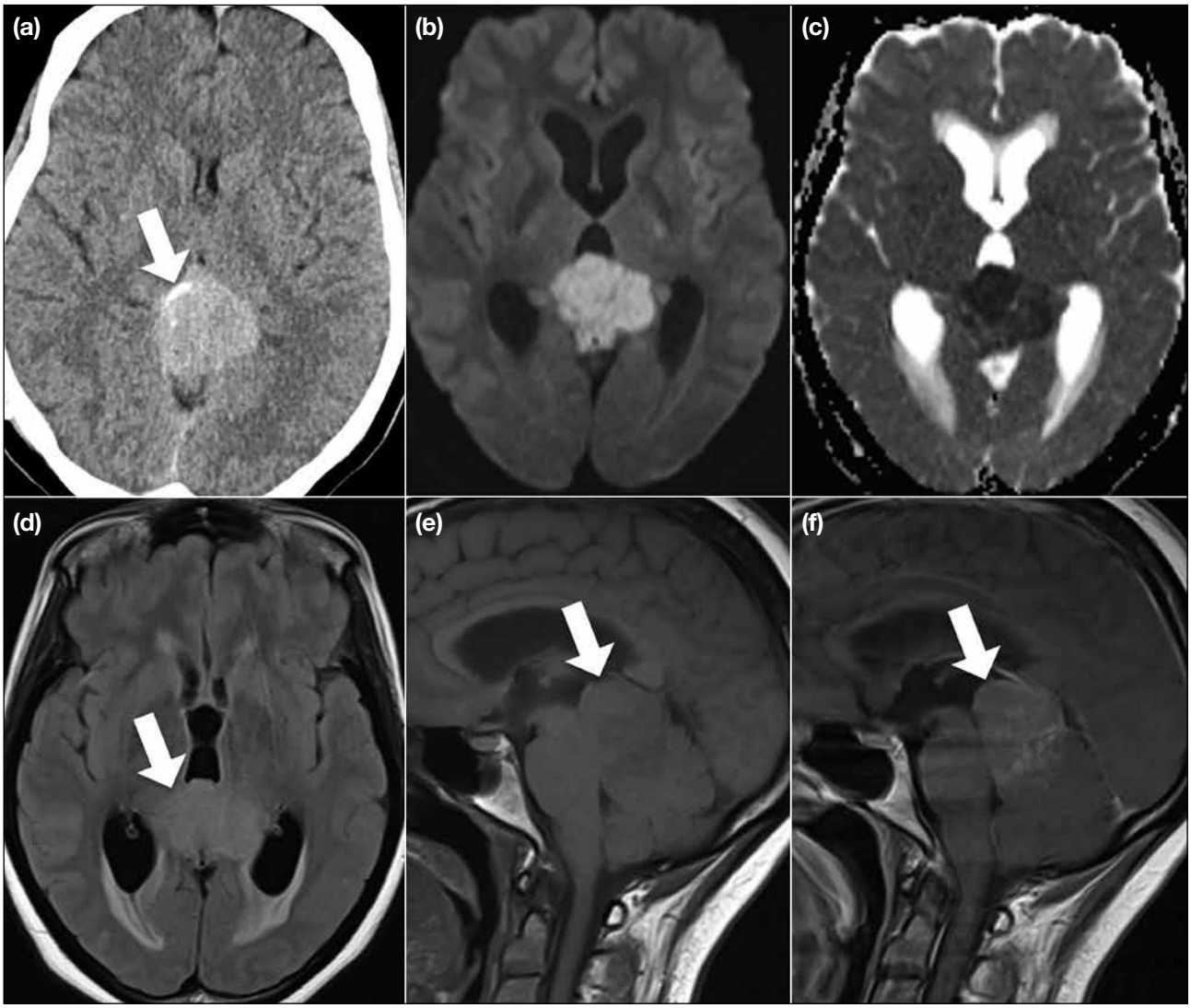

Figure 7. Primitive neuroectodermal tumour. The tumour is hyperdense on nonenhanced axial computed tomography image with displacement of the pineal calcification (arrow) from the midline by the tumour (a). Water restriction is noted on diffusion-weighted imaging (b) and apparent diffusion coefficient (c) images. The tumour (arrows) is iso- to hyperintense on axial T2-weighted fluid-attenuated inversion recovery image (d) and heterogeneously hypointense with heterogeneous enhancement on sagittal T1-weighted images (e and f).

enhanced MRI. Cystic components, calcification, and haemorrhage may be visible (Figure 6). The tumours can display suprasellar or parasellar extension. Dynamic contrast-enhanced MRI is useful to detect a relatively hypointense microadenoma in its early enhancement phase.[10]

MIMICS OF PINEAL GERM CELL TUMOURS

Primitive Neuroectodermal Tumour

The primitive neuroectodermal tumour of the pineal gland is also known as a pineoblastoma, which is a highly malignant tumour and accounts for 40% of pineal parenchymal tumours. The diagnosis of pineoblastoma peaks before the age of 20 but can be at any age.[3] The tumour is usually > 3 cm and the pineal calcification, if present, is displaced from the midline by the tumour. Because of its high cellularity, pineoblastomas are hyperdense on CT and show water restriction on DWI (Figure 7). Heterogeneous enhancement and obstructive hydrocephalus are present and CSF dissemination is common.[3]

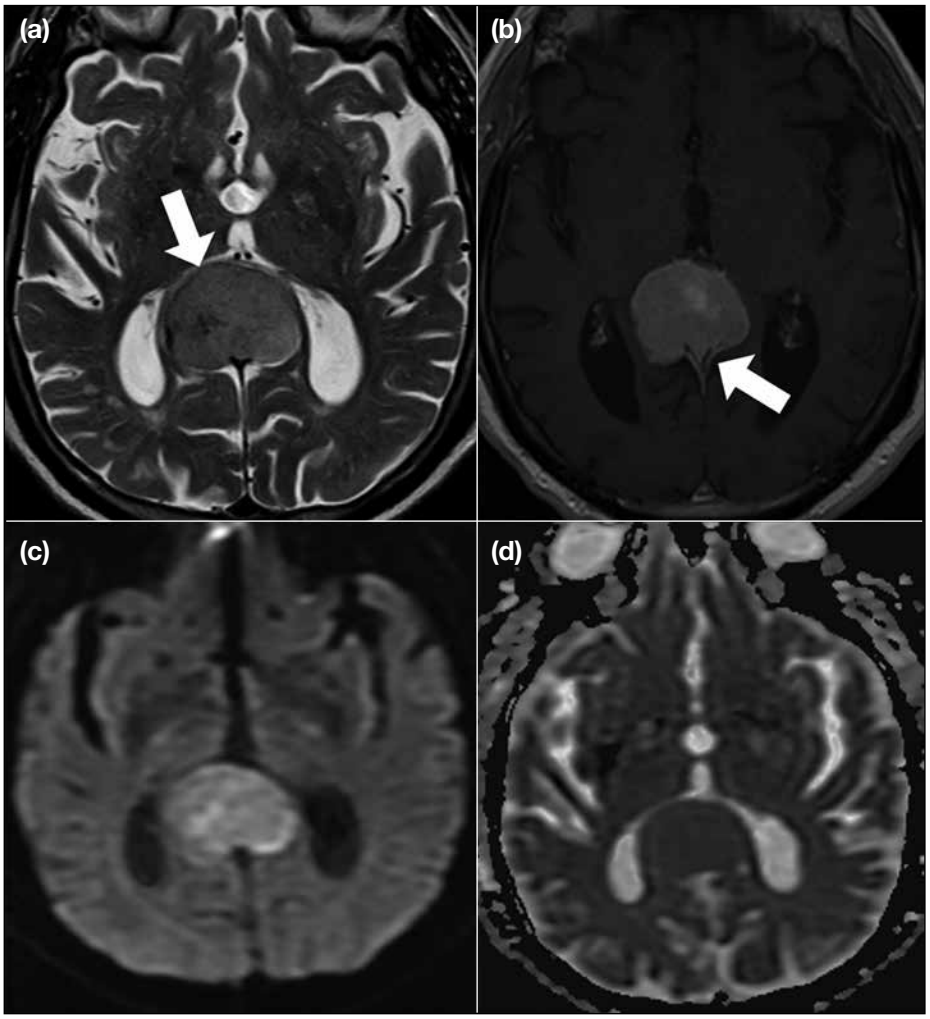

Figure 8. Meningioma. There is a well-defined hyperintense tumour (arrow) with minimal hypointensity on T2-weighted image in the pineal region (a). Strong enhancement with a small dural tail (arrow) is found on enhanced axial T1-weighted image (b). Mild water restriction is noted on diffusion-weighted imaging (c) and apparent diffusion coefficient image (d).

Meningioma

Pineal region meningiomas are uncommon, accounting for 6.2% of all pineal tumours and 0.3% of all intracranial meningiomas.[11] Because of the highly cellular nature, meningioma shows hyperdensity on CT and water restriction on DWI (Figure 8). Strong enhancement is noted. Calcifications and a dural tail are sometimes present.[3]

Pineal Cyst

Pineal cysts can be found radiographically in 23% of patients, with a female predominance. Although they can be found at all ages, they are most commonly identified in adults. Typically, the lesion is < 15 mm; larger lesions may show intracystic haemorrhage.[3,12] The imaging findings are typically well-defined cystic lesions with water signal intensity inside. Sometimes the cystic portion shows hyperintensity on fluid-attenuated inversion recovery images because of the proteinaceous contents. Wall enhancement can be found and rarely, and enhancement of the suspected cystic part has been reported and was present in our case (Figure 9). The likely mechanism is passive diffusion of the contrast into the cyst.[3,13]

Papillary Tumour of the Pineal Region

Papillary tumour of the pineal region is a rare neuroepithelial tumour located in the pineal region. It can affect children and adults without sex difference.[3] On imaging studies, this tumour is described as a well-

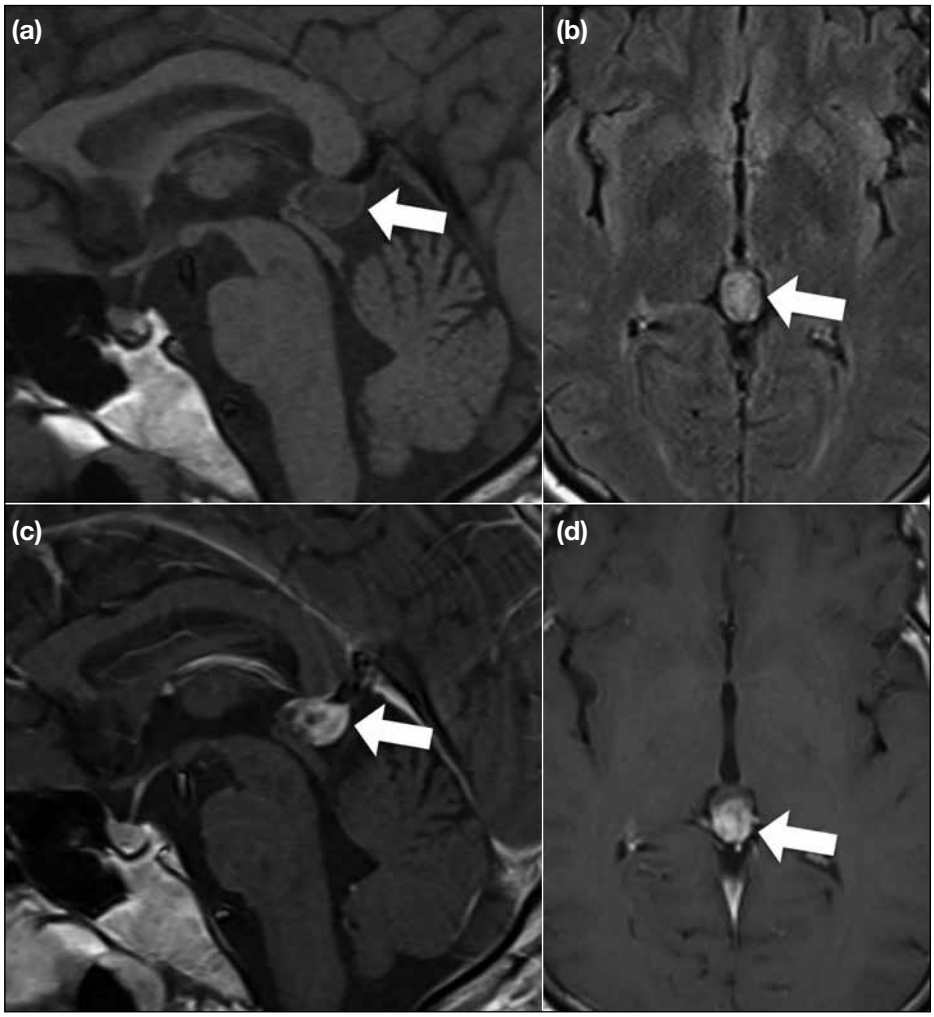

Figure 9. Pineal cyst. The case shows a pineal lesion (arrows) with heterogeneous hypointensity on sagittal T1-weighted image (a) and hyperintensity on axial T2-weighted fluid-attenuated inversion recovery image (b). About two-thirds of the lesion (arrows) enhances on sagittal (c) and axial (d) T1-weighted images.

defined enhancing lesion with possible cystic portions. Usually, there is absence of fat, haemorrhage, melanin or calcification. Sometimes, there is T1 signal hyperintensity in the lesion (Figure 10), which is considered to be due to proteinaceous content.[3] One of our cases shows calcification at the lesion site (Figure 10), but it could be just due to normal pineal calcification considering the old age of the patient.

Pineal Parenchymal Tumours

Pineal parenchymal tumour of intermediate differentiation accounts for about 20% of all pineal parenchymal tumours and can be found at any age with a slight female predominance.[3] Imaging findings are variable and may be indistinguishable from pineocytoma or pineoblastoma. Usually, this tumour presents as a lobulated heterogeneously enhancing lesion, sometimes with a cystic component. Pineal calcification can be displaced to the periphery by the tumour. Because of its high cellularity, it can show hyperdensity on CT and water restriction on DWI (Figure 11). Local invasion is reported in approximately 80% of cases.[3,14]

CONCLUSION

This pictorial essay suggests that the presence of doublet lesions in both the suprasellar and pineal regions, although less common, might be a useful clue for intracranial germinomas. However, imaging diagnosis for single germinomas in either the suprasellar or pineal region remains challenging because of the overlapping imaging presentations of intracranial germinomas and their mimics. When the mimics are also frequently observed

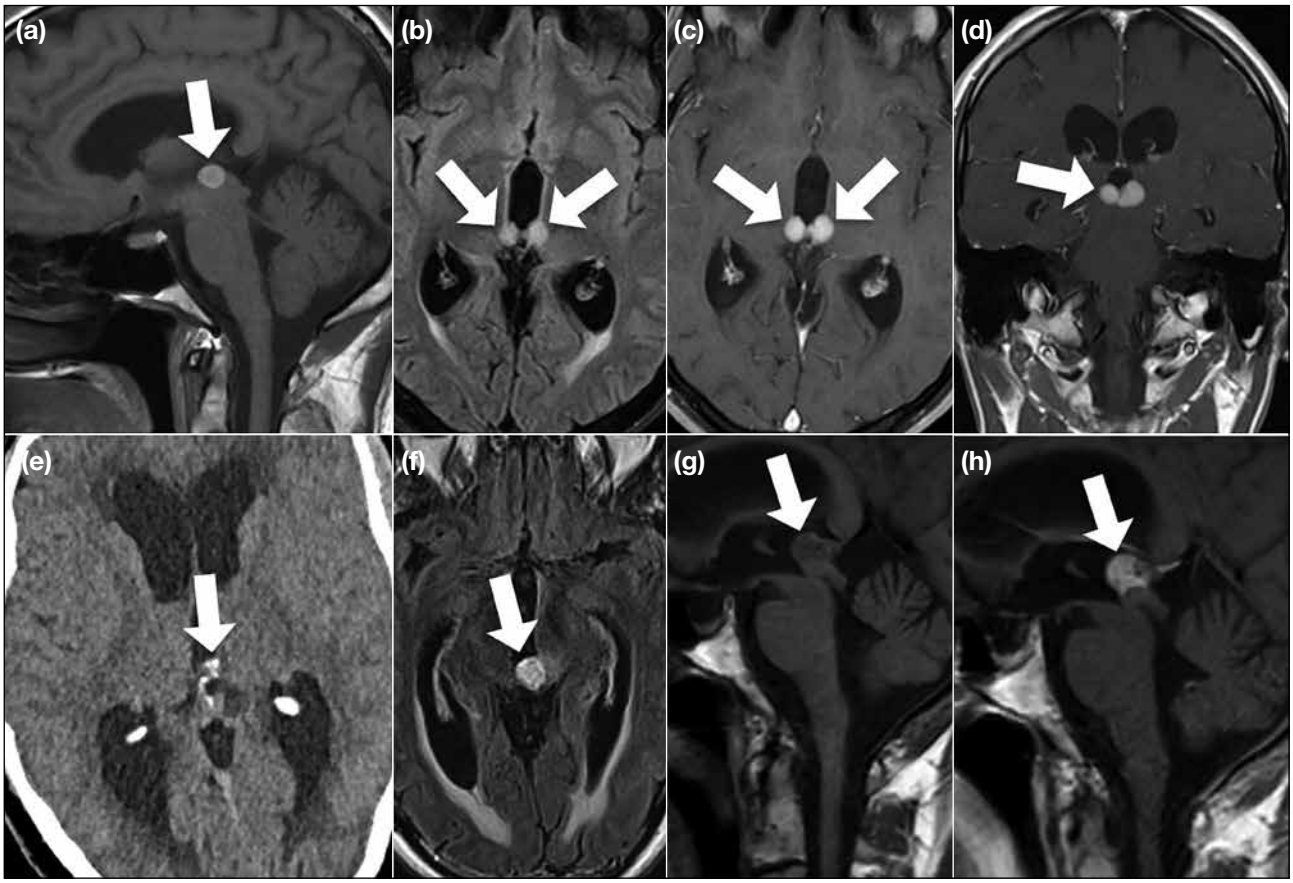

Figure 10. Papillary tumour of the pineal region. Case 1 shows a well-defined bilobulated hyperintense lesion (arrows) in the posterior commissure on sagittal T1-weighted image (a), which is hyperintense on axial T2-weighted fluid-attenuated inversion recovery image (b) and homogeneously enhancing on enhanced axial (c) and coronal (d) T1-weighted images. Case 2 shows a hypodense pineal tumour with probable displacement of the pineal calcification (arrows) to the margin of the gland on the nonenhanced axial computed tomography image (e). The tumour (arrows) is heterogeneously hyperintense on T2-weighted fluid-attenuated inversion recovery image (f) and heterogeneously hypointense on unenhanced (g) and enhancing on contrast-enhanced (h) sagittal T1-weighted images.

in children or young adults, such as craniopharyngioma and glial cell tumour in the suprasellar region and primitive neuroectodermal tumour in the pineal region, the diagnosis becomes even more difficult.

Imaging diagnosis of intracranial GCTs is challenging due to their diverse presentation and overlapping appearance with other diseases. The phenomenon of doublet lesions in the suprasellar and pineal regions may be a clue to diagnose germinoma but is uncommon and might also happen in other tumours.

REFERENCES

1. Jennings MT, Gelman R, Hochberg F. Intracranial germ-cell tumors: natural history and pathogenesis. J Neurosurg. 1985;63:155-67.
2. Echevarría ME, Fangusaro J, Goldman S. Pediatric central nervous system germ cell tumors: a review. Oncologist. 2008;13:690-9.
3. Smith AB, Rushing EJ, Smirniotopoulos JG. From the archives of the AFIP: lesions of the pineal region: radiologic-pathologic correlation. Radiographics. 2010;30:2001-20.
4. Osorio DS, Allen JC. Management of CNS germinoma. CNS Oncol. 2015;4:273-9.
5. Müller HL. Childhood craniopharyngioma — current concepts in diagnosis, therapy and follow-up. Nat Rev Endocrinol. 2010;6:609-18.
6. Aihara Y, Chiba K, Eguchi S, Amano K, Kawamata T. Pediatric optic pathway/hypothalamic glioma. Neurol Med Chir (Tokyo). 2018;58:1-9.
7. McCrea HJ, George E, Settler A, Schwartz TH, Greenfield JP. Pediatric suprasellar tumors. J Child Neurol. 2016;31:1367-76.
8. Rivera JA. Lymphocytic hypophysitis: disease spectrum and approach to diagnosis and therapy. Pituitary. 2006;9:35-45.
9. Yang X, Liu X, Li W, Chen D. Pituicytoma: a report of three cases and literature review. Oncol Lett. 2016;12:3417-22.
10. Kucharczyk W, Bishop JE, Plewes DB, Keller MA, George S. Detection of pituitary microadenomas: comparison of dynamic

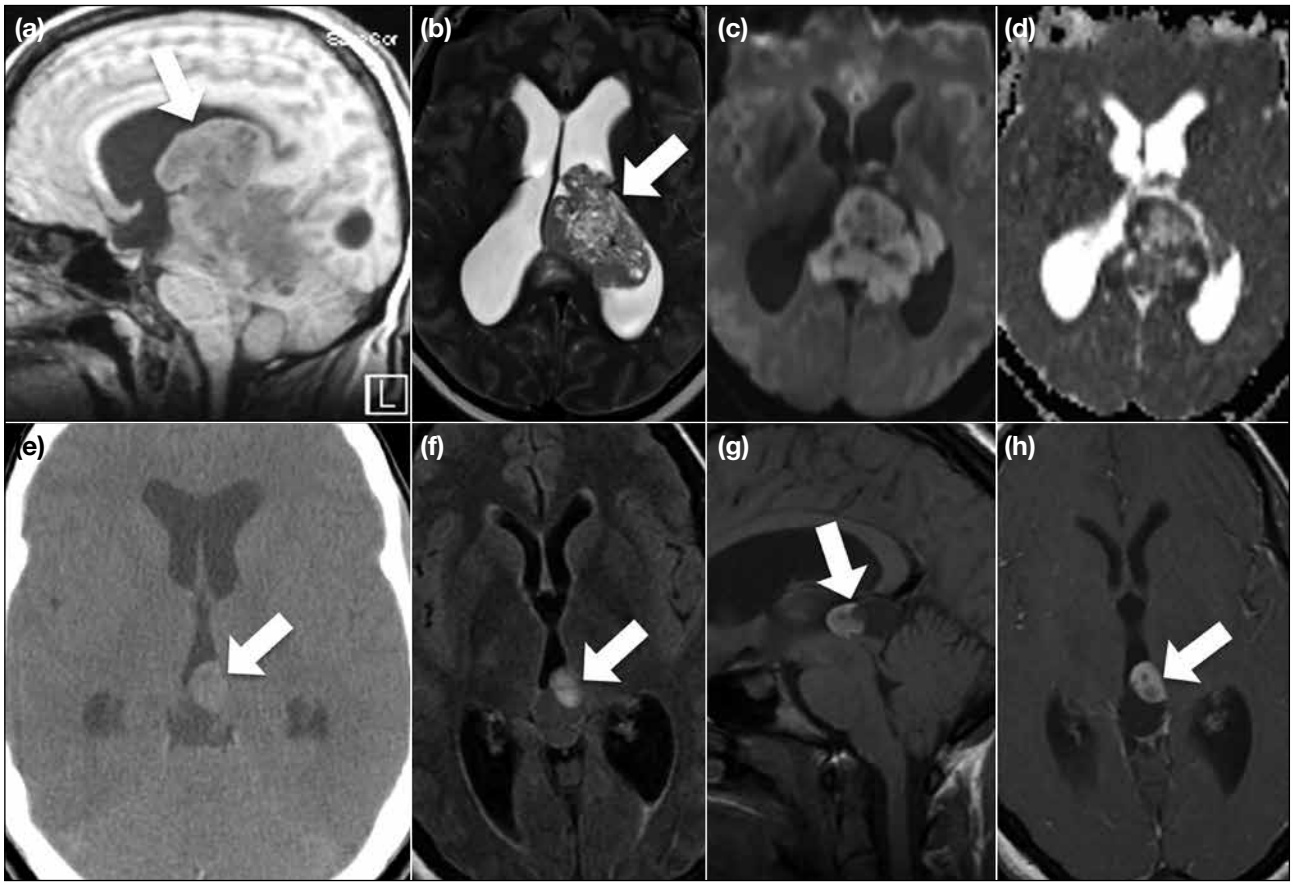

Figure 11. Large pineal parenchymal tumour of intermediate differentiation. Case 1 shows a large lobulated tumour (arrows in [a] and [b]) in the pineal region with extension into the left lateral ventricle and invasion of the adjacent corpus callosum. It is iso- to hypointense on sagittal T1-weighted image (a), with heterogeneous signals on axial T2-weighted image (b). Diffusion-weighted imaging (c) shows water restriction and apparent diffusion coefficient image (d). Case 2 displays a heterogeneously hyperdense tumour (arrows in [e] to [h]) in the pineal region on nonenhanced axial computed tomography image (e), with hypointense and hyperintense parts on the axial T2-weighted fluid-attenuated inversion recovery image (f). There are hypo-, iso-, and hyperintense portions on nonenhanced sagittal T1-weighted image (g) and some enhancement on axial T1-weighted image (h).

keyhole fast spin-echo, unenhanced, and conventional contrast-enhanced MR imaging. AJR Am J Roentgenol. 1994;163:671-9.
11. Konovalov AN, Spallone A, Pitzkhelauri DI. Meningioma of the pineal region: a surgical series of 10 cases. J Neurosurg. 1996;85:586-90.
12. Richardson JK, Hirsch CS. Sudden, unexpected death due to "pineal apoplexy". Am J Forensic Med Pathol. 1986;7:64-8.
13. Pu Y, Mahankali S, Hou J, Li J, Lancaster JL, Gao JH, et al. High prevalence of pineal cysts in healthy adults demonstrated by high-resolution, noncontrast brain MR imaging. AJNR Am J Neuroradiol. 2007;28:1706-9.
14. Yoon DJ, Park J, Lezama LM, Heller GD. Pineal parenchymal tumour of intermediate differentiation: a rare differential diagnosis of pineal region tumours. BJR Case Rep. 2016;2:20150371.

AUTHOR INDEX FOR VOLUME 26

ACKNOWLEDGEMENT OF JOURNAL REVIEWERS

The Editor-in-Chief and the Members of the Editorial Board of the *Hong Kong Journal of Radiology* wish to express their gratitude to the following experts whose service on the Journal Reviewer Panel ensured the quality of accepted manuscripts in Volume 26 of the Journal:

Dr CC Chan
Dr JPK Chan
Dr VSH Chan
Dr YL Chan
Dr HC Cheng
Dr JHM Cheng
Dr KK Cheng
Dr CY Cheung
Dr FY Cheung
Dr KK Cheung
Dr KH Chin
Dr JLF Chiu
Dr CY Chu
Dr PY Chu
Prof W Chu
Dr WP Chu
Dr ASL Fung
Dr EPY Fung
Dr HS Fung
Dr KKF Fung
Dr YW Hon
Dr JWY Hui
Dr TL Kwan
Dr HC Lam
Dr HS Lam
Dr SHY Lam
Dr CC Law
Dr GKY Lee
Dr KH Lee
Dr VHF Lee
Dr AKC Leung
Dr ST Leung
Dr WS Li
Dr MY Lim
Dr LW Lo
Dr SSW Lo
Dr C Ng
Prof RKC Ngan
Dr NY Pan
Dr MH So
Dr GKF Tam
Dr CB Tan
Dr CSL Tong
Dr MMP Tong
Dr SC Tsai
Dr KH Tsang
Dr JWC Wai
Dr KH Wong
Dr LKM Wong
Dr SM Wong
Dr T Wong
Dr SM Yu
Dr MK Yuen

CATEGORIES OF PAPERS

Hong Kong Journal of Radiology publishes various categories of articles. Each category serves a distinct purpose and is judged by different criteria.

EDITORIAL

Commissioned article presenting the author's opinion on a topical subject or an article published in the current issue. Unsolicited Editorials are not accepted.

Format: An abstract is not required. The text is limited to 1000 words, with a maximum of 1 table or figure, and up to 10 references.

REVIEW ARTICLE

Systematic reviews or meta-analyses of recent developments in a specific topic. Scoping reviews of the literature that identify area(s) for future research will also be considered. No new information is described, and no subjective opinion or personal experiences are expressed.

Format: A structured abstract of ≤ 250 words; headings should include: Objective(s), Methods, Results, Conclusion. The text is limited to 5000 words, with a maximum of 20 tables and figures (total), and up to 60 references.

ORIGINAL ARTICLE

Provides new information based on original research. Includes prospective studies with in-depth statistical analysis, unique retrospective observations of a disease or disorder, and studies of novel applications of an interventional procedure or treatment method.

Format: A structured abstract of ≤ 250 words; headings should include: Objective(s), Methods, Results, Conclusion. The text is limited to 3500 words, with a maximum of 20 tables and figures (total), and up to 50 references.

PERSPECTIVE

Narrative review articles discussing recent developments in a specific topic. No new information is described; may include subjective opinion or personal experiences.

Format: An unstructured abstract of ≤ 250 words. The text is limited to 2500 words, with a maximum of 20 tables and figures (total), and up to 60 references.

PICTORIAL ESSAY

Teaching exercise with message in the figures and legends. Emphasis is on quality of the illustrations and clinical relevance of the message.

Format: An abstract is not required. The text is limited to 2500 words, with a maximum of 20 tables and figures (total), and up to 15 references.

CASE REPORT

Brief discussion of a case with unique features not previously described. Additional cases (case series) may be added to augment the discussion. The discussion should be succinct and focus on a specific message.

Format: An abstract is not required. The text is limited to 1500 words, with a maximum of 8 tables and figures (total), and up to 15 references.

BRIEF COMMUNICATION

This includes post-meeting commentary, update on new imaging or therapeutic advances, brief description of a specific technique or procedure or new equipment. Teaching exercise aimed at describing a certain radiological or radiotherapeutic technique for trainees and practising radiologists is also welcome.

Format: An abstract is not required. The text is limited to 1500 words, with a maximum of 8 tables and figures (total), and up to 15 references.

LETTER TO THE EDITOR

Short letter on any matter of interest to journal readers, including comments on an article that has previously appeared in the journal. The authors of the article commented on would be invited to reply.

Format: An abstract is not required. The text is limited to 500 words, with up to 5 references. Figures and tables are permitted only exceptionally.

INFORMATION FOR AUTHORS

Aims and Scope

Hong Kong Journal of Radiology is the official peer-reviewed academic journal of the Hong Kong College of Radiologists. It is a multidisciplinary journal covering research work pertaining to the science and practice of the component specialties of the College. The journal publishes various categories of papers, including Reviews, Original Articles, Perspectives, Pictorial Essays, Case Reports, Brief Communications, and Letters to the Editor. Manuscripts will be subject to rigorous peer review. *HKJR* adheres to the Recommendations for the Conduct, Reporting, Editing, and Publication of Scholarly Work in Medical Journals of the International Committee of Medical Journal Editors (ICMJE; www.icmje.org), and the Core Practices of the Committee on Publication Ethics (COPE; publicationethics.org/).

Journal Policies

Reporting Guidelines: *HKJR* recommends the use of reporting guidelines in the preparation of manuscripts, such as those advocated by the EQUATOR Network (eg, CONSORT for randomised trials).

Funding: Any sponsor(s) of the research involved, along with grant number(s) should be provided.

Conflicts of interest: All authors must provide a statement reporting any conflicts of interest. Where none exist, please state 'The authors have no conflicts of interest to declare.'

Ethics: All studies must be conducted in accordance with the Declaration of Helsinki. For studies involving humans, a statement must be included in the manuscript that provides the name of the review board and approval number (or waiver). A statement on patient/guardian consent must also be included. For studies involving animals, appropriate ethics approval is required, and this should be stated in the manuscript.

Submission: Manuscripts should be submitted online via HKAMedTrack (www.hkamedtrack.org/hkjr). Manuscripts must be unpublished works that are not under consideration by another publication.

Copyright: On acceptance of an article by the journal, the corresponding author will be asked to transfer copyright of the article to the College.

Editing: Accepted manuscripts will be copyedited according to journal style. Authors are responsible for all statements made in their work, including changes made by the copy editor.

Proofs and Reprints: The corresponding author will receive page proofs, which should be proofread and returned promptly. Corrections are limited to printer's errors — no substantial author's changes will be made without charge. Quotes for extra copies of reprints are available at the Editorial Office.

Manuscript Preparation

In general, manuscripts should be prepared following the 'IMRaD' structure as recommended by the ICMJE. Please provide a **blinded** manuscript and separate title page in Word format (.doc or .docx). Manuscripts must be written in English. For accepted manuscripts, an abstract in Traditional Chinese will also be required.

Authors: Provide the full name, qualifications (maximum of two), and affiliation (where the study was conducted) for all authors. The authors' names in Chinese characters, if available, should also be provided. **The corresponding author**, on behalf of the authors, is responsible for all contact with the journal. Provide the full name, postal address, telephone and fax numbers, and email address of the corresponding author.

Title: Concisely convey the main topic of the study. Avoid obvious terms such as "a study of" or "novel". If appropriate, please include the study design in the title (eg, 'randomised controlled trial', 'systematic review', 'case report'). An abbreviated title of <45 characters is also required.

Abstract: For article types requiring an abstract, this should provide a complete summary of the article, including the aims/purpose, main methods, key results, and conclusions. Abbreviations and clinical or technical jargon should be avoided. Please refer to the Categories of Papers for details.

Key Words: Five relevant index terms should be provided, selected from the Medical Subject Headings (MeSH; www.ncbi.nlm.nih.gov/mesh).

Tables: Submit tables on separate pages in as simple a format as possible. They should be numbered and concisely titled. Abbreviations should be defined in footnotes.

Figures: Restricted to the minimum necessary to support the textual material. Illustrations should be submitted as separate files (.jpg format, ≥350-dpi resolution). All figures should be numbered with a legend to indicate the anatomical area and pathological condition shown. All symbols and abbreviations should be defined in the legend. Please ensure that legends and illustrations correspond.

References: Should be numbered in the order in which they are first cited in the text. Each reference citation should be in superscript Arabic numerals after full-stops and commas. In the reference list, include the complete title, and names and initials of all authors.

Acknowledgement(s): Any individuals who contributed substantially to the study but does not qualify for inclusion as an author should be acknowledged. Written permission from acknowledged individuals is required.

Please refer to the *HKJR* website for further guidance:
http://www.hkjr.org/page/information-authors

The Hong Kong Society of Diagnostic Radiologists Trust Fund

Hong Kong Society of Diagnostic Radiologists Research Grant

The Hong Kong Society of Diagnostic Radiologists (HKSDR) was founded in 1977 to promote interflow of professional knowledge in diagnostic radiology and to foster close contact among doctors working in the field of diagnostic radiology. The HKSDR Trust Fund was established in 1985.

Taking into account the rapid progress in imaging technology and thus the need to promote research to advance our knowledge and to serve our patients better, the Trust Fund offers three awards of up to HK$17,000 each and is open to application.

The application should be made by the principal investigator of the research project related to the scientific or clinical aspects of diagnostic radiology to be conducted in Hong Kong. The principal investigator should be a trainee/specialist in the field of diagnostic radiology. He/she has to be a registered medical practitioner in Hong Kong.

Application and enquiry can be directed to:

Dr. Lam Chiu Ying Flora, Hon Secretary of Trust Fund Working Group
c/o Ms. HY Ng, Department of Diagnostic & Interventional Radiology
Kwong Wah Hospital
25 Waterloo Road, Yaumatei, Kowloon, Hong Kong.
Tel: (852) 3517 5189